

# NOVEL METHOD TO MEASURE ABRASION OF SOLID TYRES

B. A. Y. Chathura

(118301X)



University of Moratuwa, Sri Lanka.  
Electronic Theses & Dissertations  
[www.lib.mrt.ac.lk](http://www.lib.mrt.ac.lk)

Thesis submitted in partial fulfillment of the requirements for the degree Master of  
Engineering

Department of Mechanical Engineering.

University of Moratuwa  
Sri Lanka

February 2016

## DECLARATION

I declare that this is my own work and this thesis/dissertation2 does not incorporate without acknowledgement any material previously submitted for a Degree or Diploma in any other University or institute of higher learning and to the best of my knowledge and belief it does not contain any material previously published or written by another person except where the acknowledgement is made in the text.

Also, I hereby grant to University of Moratuwa the non-exclusive right to reproduce and distribute my thesis/dissertation, in whole or in part in print, electronic or other medium. I retain the right to use this content in whole or part in future works (such as articles or books).

Signature:

Date:



University of Moratuwa, Sri Lanka.  
Electronic Theses & Dissertations  
[www.lib.mrt.ac.lk](http://www.lib.mrt.ac.lk)

The supervisors should certify the thesis/dissertation with the following declaration.

The above candidate has carried out research for the Masters/MPhil/PhD thesis/ Dissertation under my supervision.

Signature of the supervisor:

Date

## ABSTRACT

Peripheral velocity, load, floor surface and type of rubber compounds are the key determinants considered when selecting solid tyres. These factors also determine the life of the tyres. However, there is no accepted method to measure tyre wear against the factors mentioned above. At present, lifespan of tyres is determined through field tests where the tyres are used in different industries and collecting data on tyre life in terms of running hours. Another method is to use a drum-type apparatus with bonded abrasive paper or abrasive particles between the tyre and the drum. The limitations of these methods include the time requirement and inaccuracies in data to enable accurate analysis of tyre life. As a result, the tyre manufacturers find it difficult to specify the tyre life with adequate degree of certainty to the customers. This gives rise to a need for a standard method to assure the life of tyres, especially solid tyres, for the benefit of the customers and to conduct tests to help improve tyre performance. The proposed apparatus has the facility to change the operating speed, surface and the load. The overall designed length, width and height of the machine are respectively 3000 mm, 1150 mm and 3350 mm. The computer-based simulation results for design evaluation suggest that the stress and strain are within allowable limits under typical loading conditions. Then a scale down prototype was constructed and three samples which were manufactured from three different compounds were tested for measure rubber abrasion and temperature. Results showed high abrasion resistance compound according to DIN 53516 had low wearing and low heat build up compound according to drum testing results had low temperature. Construction and testing of the apparatus are proposed as future work to complete the work.

Keywords: tyre life, testing, apparatus

## ACKNOWLEDGMENT

Manufacturing Systems Engineering is a rapid advancing area, which combines scientific theory and technology to develop new manufacturing methods. The theories and design help to open new doors to think differently and get innovative ideas to improve new products.

First I thank Dr. H. K. G. Punchihewa, the supervisor of this research, for his guidance and co-operation and I also thank Dr.R. A. R. C. Gopura, Coordinator of Manufacturing Systems Engineering Master degree. I also thank to then head of the department Dr. V. P. C. Dassaayake. A special thanks goes out to Dr. W.K. Mampearachchi and transportation engineering division in the Department of Civil Engineering for helping to identify running surfaces friction, and his enthusiastic support and motivation extended towards me in completing this report.

I thank all the other staff members of the Department of Mechanical Engineering for their assistance during the Master degree program



University of Moratuwa, Sri Lanka.  
Electronic Theses & Dissertations  
[www.lib.mrt.ac.lk](http://www.lib.mrt.ac.lk)



## Table of content `

<b>1</b>	<b>INTRODUCTION.....</b>	<b>1</b>
	1.1. Introduction to research project .....	1
	1.2. Aim and objectives.....	2
	1.3. Methodology .....	2
	1.4. Introduction to chapters.....	3
<b>2</b>	<b>TYRE ABRASION .....</b>	<b>4</b>
	2.1 Tyre characteristic .....	4
	2.2 Tyre abrasion.....	8
	2.2.1 Initiation of abrasion .....	12
	2.2.2 Abrasion patterns .....	13
	2.2.3 Smearing and the effect of antioxidants.....	14
	2.3 Road characteristics .....	16
	2.3.1 Longitudinal frictional forces.....	21
	2.3.2 Lateral frictional forces .....	25
	2.3.3 Combined braking and cornering.....	26
	2.3.4 Friction mechanisms .....	27
	2.3.5 Factors affecting available pavement friction .....	28
	2.3.6 Pavement surface characteristics.....	29
	2.3.7 Pavement surface texture .....	33
	2.3.8 Friction and texture measurement methods .....	37
	2.4 Tyre abuses.....	40
<b>3</b>	<b>SPECIFIC SOLID TYRES .....</b>	<b>44</b>
	3.1. Solid resilience tyres .....	44
	3.1.1. Tyre construction .....	45
	3.2. Press on band tyres.....	47
<b>4</b>	<b>TESTING METHODS .....</b>	<b>49</b>
	4.1 Abrasion testing of rubber compound.....	49
	4.2 Tyre field testing .....	50
	4.3 Drum testing.....	50



4.4	Tyre wear life tester .....	52
4.5	Advances in indoor tire tread wear simulation .....	54
4.6	Measurement and modelling of tyre forces on a low coefficient surface	60
4.7	A versatile flat track tire testing machine .....	68
4.8	Abrasive wear amount estimate for 3D patterned tire utilising frictional dynamic rolling analysis .....	73
4.9	Tread wear and footprint geometrical characters of truck bus radial tires	82
<b>5</b>	<b>TYRE FIELD TESTIG RESULTS .....</b>	<b>88</b>
5.1	Tyre test in-house under observation .....	88
5.2	Tyre test at outside under random observation .....	89
5.3	Tyre drum testing results.....	92
<b>6</b>	<b>DESIGN .....</b>	<b>94</b>
6.1	Design Tree .....	94
6.2	Design requirements.....	96
6.3	Design features.....	97
6.4	Component design and selection.....	98
6.5	Detailed design.....	106
6.6	Design evaluation.....	108
6.7	Abrasion tester 2D drawing. ....	112
<b>7</b>	<b>PROTOTYPE TESTING .....</b>	<b>113</b>
7.1	Introduction of machine .....	113
7.2	Testing procedure.....	114
7.3	Results.....	114
7.4	Analysis on abrasion of tyre materials .....	118
<b>8</b>	<b>DISCUSSION .....</b>	<b>119</b>
<b>9</b>	<b>CONCLUSION AND FUTURE WORK .....</b>	<b>121</b>
<b>10</b>	<b>REFERENCE .....</b>	<b>122</b>



## LIST OF FIGURES

Figure 2.1: Conventional pneumatic tyre structure .....	6
Figure 2.2: Radial tyre structure .....	7
Figure 2.3: Solid tyre structure .....	9
Figure 2.4: Factors affecting the tyre wear .....	10
Figure 2.5: Schematic diagram of the friction and wear mechanisms in rubber-like materials .....	10
Figure 2.6: Broad correlations of friction and wear .....	12
Figure 2.7: Initiation of abrasion .....	13
Figure 2.8: Cross-sections through abrasion pattern .....	14
Figure 2.9: Energy index of abrasion .....	16
Figure 2.10: Frictional heating .....	16
Figure 2.31: Frictional force components due to adhesion .....	18
Figure 2.32: Hysteresis in rubber .....	19
Figure 2.33: Loading and unloading of tyre rubber in the contact patch .....	19
Figure 2.34: Simplified diagram of forces acting on a rotating wheel .....	21
Figure 2.35: Rolling resistance force with a free-rolling tire .....	24
Figure 2.36: Forces and moments of a constant-braked wheel .....	24
Figure 2.37: Pavement friction versus tire slip .....	25
Figure 2.38: Dynamics of a vehicle traveling around a constant radius curve at a constant speed .....	26
Figure 2.39: Brake ( $F_x$ ) and lateral ( $F_y$ ) forces as a function of longitudinal slip .....	27
Figure 2.310: Lateral force versus longitudinal force at constant slip angles .....	28
Figure 2.311: Key mechanisms of pavement–tire friction .....	28
Figure 2.312: Micro-texture versus macro-texture .....	31
Figure 2.313: Effect of water film thickness on pavement friction.....	33
Figure 2.314: Simplified illustrations of the various texture ranges ....	35

Figure 2.315: Texture wavelength influence on pavement– tire interactions .....	36
Figure 2.316: Effect of micro-texture and macro- texture on pavement–tire friction .....	36
Figure 3.1.1: Solid tyre construction .....	46
Figure 4.1.1: DIN abrasion tester .....	51
Figure 4.3.1: Drum testing machine .....	52
Figure 4.4.1: Tyre wear life tester .....	54
Figure 4.5.1: Advance tyre wear simulation graph.....	56
Figure 4.5.2: Advance tyre wear simulation results .....	57
Figure 4.5.3: Vehicle mechanics programmed equation .....	58
Figure 4.5.4: Feature of indoor test wear equipment .....	60
Figure 4.5.5: The effect of altering the steering curves produces higher wear rates .....	61
Figure 4.5.6: The tread loss profiles for the base load .....	61
Figure 4.6.1: Peak Longitudinal Coefficient of Friction 1.....	63
Figure 4.6.2: Peak Longitudinal Coefficient of Friction 2 .....	64
Figure 4.6.3: Tire Test at CALSPAN .....	65
Figure 4.6.4: Lateral Forces at 30 mph Dry .....	66
Figure 4.6.5: Lateral Forces at 30 mph Wet .....	66
Figure 4.6.6: Lateral Forces at 45 mph Wet .....	67
Figure 4.6.7: Lateral Forces at 60 mph Wet .....	67
Figure 4.6.8: Lateral Forces at 75 mph Wet .....	68
Figure 4.7.1: Dynamic tire testing machine .....	70
Figure 4.7.2: Central mechanism .....	71
Figure 4.7.3: Three dimensional sensor and braking system .....	72
Figure 4.7.4: Lateral movement system .....	73
Figure 4.8.1: Illustration: (a) indoor wear test equipment and (b) acceleration history for generating drive files .....	75
Figure 4.8.2: Schematic representation of blade abrader .....	76
Figure 4.8.3: Material modeling of tire:(a)material composition and(b)modeling of belt layers .....	78

Figure 4.8.4: Tire FEM meshes .....	79
Figure 4.8.5: Representation: (a) driving modes and (b) vehicle acceleration histogram .....	80
Figure 4.8.6: A simulation tire model .....	81
Figure 4.9.1: Examples of problem tires .....	85
Figure 4.9.2: Sample tire, tire static loaded test machine .....	85
Figure 4.9.3: Load vs. contact area coefficient .....	87
Figure 4.9.4: Load vs. tread contact length .....	87
Figure 5.1: Tyre abrasion life base on volume loss .....	90
Figure 6.1: Chain and sprocket .....	100
Figure 6.2: Conveyor belt .....	101
Figure 6.3: Vibration model .....	103
Figure 6.4: Schematic diagram of the forces acting on the tyre in the test machine .....	108
Figure 6.5: Outward appearance of the abrasion testing apparatus ...	108
Figure 6.6: Von Misses stress and displacement distribution in machine elements .....	110
Figure 7.1: Front view of machine.....	114
Figure 7.2: End view of machine .....	114
Figure 7.3: Weight loss as percentage from final weight for all samples ....	116
Figure 7.4: Heat build up of samples .....	116
Figure 7.5: Comparison between new test and DIN test.....	116
Figure 7.6: Test surface of cement .....	117
Figure 7.7: Sample after test and before test .....	117
Figure 7.8: Sample A .....	118
Figure 7.9: Sample B .....	118
Figure 7.10: Sample C .....	118

## LIST OF TABLE

Table 2.31: Friction measurements and crash rates .....	21
Table 2.32: Factors affecting available pavement friction .....	29
Table 2.41: Tyre claim against tyre sizes .....	41
Table 2.42: Tyre claim against country basis .....	41
Table 2.43: Claim tyre production date and raw material .....	42
Table 3.1.1: Solid tyre technical specification .....	46
Table 3.2.1: Press on band technical specification .....	47
Table 4.1.1: DIN abrasion tester specification .....	49
Table 4.4.1: Tyre wear life tester results .....	53
Table 4.4.2: Surface roughness .....	53
Table 4.6.1: Tires for CALSPAN Testing .....	64
Table 4.7.1: Output variables .....	69
Table 4.7.2: Input variables .....	70
Table 4.8.1: Loading condition and driving mode .....	82
Table 4.9.1: Details of the three tires .....	84
Table 4.9.2: Statistics of feedback information .....	85
Table 5.1: In-house field test analyses data .....	89
Table 5.2: Test results against tyre brand and running hours .....	92
Table 5.5: Drum testing tyre results for 18x7-8 .....	93
Table 6.1: Summary of parameters used for the static study .....	116
Table 7.1: Proto testing details.....	122
Table 7.2: Comparison of new test results and DIN test results.....	122

## **LIST OF ABBREVIATIONS**

ESC - Electronic Stability and Control

NADS - National Advanced Driving Simulator

POB - Press on band

PLC - Programmable Logic Controller

SIT - Contour or clip of solid tyres

SPEC - Specification

SRT - Solid resilience tyre

STD - Standard solid tyre

TRC - Transportation Research Center



University of Moratuwa, Sri Lanka.  
Electronic Theses & Dissertations  
[www.lib.mrt.ac.lk](http://www.lib.mrt.ac.lk)

# CHAPTER 1

## 1. INTRODUCTION

### 1.1. Introduction to research project

Abrasion properties of solid tyre treads determine their lifespan [1],[3]. The lifespan is affected by the peripheral velocity of the tyres, loads which the tyres are subjected to, roughness of the surfaces on which the tyres are used and the environment where the tyres are used [1],[3],[4]. The driving pattern also plays a role in determining the tyre life [3],[5]. Adhesive wear removal of material caused by high transient adhesion, i.e. welding; abrasive wear - caused by cutting-rupture action of sharp angular asperities on the sliding counter face or as third bodies, i.e. particles, erosive wear - cutting-rupture action of particles in a liquid stream; corrosive wear - from direct chemical surface attack; fatigue wear caused by rapid or gradual material property changes that give rise to cracks and with their growth, loss of material are considered to be the main tyre wear mechanisms [1],[3],[4],[6]. Study of wear mechanisms is important to select material for solid tyres and manufacturers need to understand the behavior of tyres under different conditions in order for them to assure the tyre life for their customers and to improve abrasion properties of tyres to increase their lifespan.

Lifespan of tyres is determined through field tests and obtaining feedback on performance [2],[6]. Here, the tyres are used in different environments and data is collected on tyre wear patterns and tyre life in terms of running hours. The main limitations of this method are the time taken to obtain data and the reliability of feedback. Another method being used is to use a drum type apparatus with bonded abrasive paper [5],[7]. The tyres are mounted and rotated at different speeds allowing to roll on the drum surface with abrasive paper. The varied surface roughness values are accommodated by changing the grit size of the abrasive paper. Using this apparatus, data on tyre wear is collected to assess the tyre life. A variant of the drum type apparatus is also used for the same purpose where abrasive particles between the tyre and the drum are used instead of abrasive paper [8],[9]. The



limitations of these methods include inaccuracies in data due to non-uniform application of abrasive material between the tyre surface and the drum and their inability to simulate the actual environmental conditions during the tests to enable accurate evaluation of tyre life. Further, these methods are expensive.

## 1.2. Aim and objectives

Considering the requirements that emerged from the analysis of limitations of the existing methods, the aim of the research was to develop an apparatus to assure solid tyre life using a standard testing procedure. The apparatus would also enable the study of relationship between different wear mechanisms and tyre life in order to understand about tyre wear to help improve tyre performance. The objectives were

- To study the methods that can induce tyre wear,
- To determine the design features for an apparatus for simulating tyre wear,
- To design the apparatus and
- Finally to evaluate it.

## 1.3.



University of Moratuwa, Sri Lanka.  
Electronic Theses & Dissertations  
www.lib.mrt.ac.lk

## Methodology

As the first step, parameters that affect tyre life were explored and the design requirements were identified. Possible mechanisms that could be used in the development of an apparatus were then studied with respect to design features that need to be present in the apparatus. The design features were then mapped against the design requirements using an axiomatic design approach [10]. A design tree [10] was also constructed to help analyses the alternative solutions. The suitability of each solution was qualitatively evaluated and the unsuitable options were omitted. Afterwards, conceptual models for the apparatus were developed and a viable model was selected for detailed design. The selected conceptual model was designed with the aid of solid modeling using SolidWorks® 2011. Finally, computer based simulations were conducted using the same solid modelling package to evaluate the design. The test load acting on each component was calculated based on the

internationally approved standard values stated in the literature [10],[11]. This test load and the standard material specification was given as the input for the Solid Works software. Von Misses stress and strain distributions were calculated and the designed elements were graphically analyzed. Design features were updated whenever needed during the detailed design phase. After that a scaled down prototype was fabricated and testing was performed to validate detail design.

#### **1.4. Introduction to chapters**

In Chapter 1 include aim and objective and methodology of project there in Chapter 2 includes tyre characteristic that is different type of tyres available in market although in this project mainly focus on solid tyres further in this chapter include tyre wearing methods with road characteristic through road characteristic discussed about longitudinal and lateral friction forces and friction mechanism, factors effected to that surface texture and measurement methods. In Chapter 3 include loading capacity and specification about solid tyres, Chapter 4 includes all currently available testing method which should be used to test abrasion of tyres. The field test results that is actual tyre testing in different territory had include in Chapter 5, in Chapter 6 include detail design of testing machine with all relevant drawings, in Chapter 7 include detail about prototype testing machine with testing results, finally Chapter 8 include discussion of this report.



University of Moratuwa, Sri Lanka  
Electronic Theses & Dissertations  
www.lib.mrt.ac.lk

## CHAPTER 2

### 2. TYRE ABRASION

#### 2.1 Tyre characteristic

The tread is the part of the tire that comes in contact with the road surface. The portion that is in contact with the road at a given instant in time is the contact patch. The tread is a thick rubber, or rubber/composite compound formulated to provide an appropriate level of traction that does not wear away too quickly. The tread pattern is characterized by the geometrical shape of the grooves, lugs, voids and sipes. Grooves run circumferentially around the tire, and are needed to channel away water. Lugs are that portion of the tread design that contacts the road surface. Voids are spaces between lugs that allow the lugs to flex and evacuate water. Tread patterns feature non-symmetrical (or non-uniform) lug sizes circumferentially to minimize noise levels at discrete frequencies. Sipes are valleys cut across the tire, usually perpendicular to the grooves, which allow the water from the grooves to escape to the sides in an effort to prevent hydroplaning.

Regardless of the design or application of the tire, all tires must fulfill a fundamental set of functions that is:

- Provide load-carrying capacity.
- Provide cushioning and dampening.
- Transmit driving and braking torque.
- Provide cornering force.
- Provide dimensional stability.
- Resist abrasion.
- Generate steering response.
- Have low rolling resistance.
- Provide minimum noise and minimum vibration.
- Be durable throughout the expected life span.

Treads are often designed to meet specific product marketing positions. High performance tires have small void ratios to provide more rubber in contact with

the road for higher traction, but may be compounded with softer rubber that provides better traction, but wears quickly. Mud and snow (M&S) tires are designed with higher void ratios to channel away rain and mud, while providing better gripping performance. Specialized tires will always work better than general/all purpose/all weather tires when being used in the conditions the specialized tires are designed for.

**Basically tyres can be categorize into different groups**

1. Pneumatic tyres: this is common tyres that should be used in cars, trucks bus ect, even although this consider as pneumatic tyre this can also be used liquid nitrogen and develop gel compound used for inside filling purpose.
  - a. Conventional tyres: this is most common type and cheap compare with other pneumatic categories basic construction listed below mostly buses, lorries, three wheelers, tractors and trailers and motorbikes are used this type of tyres

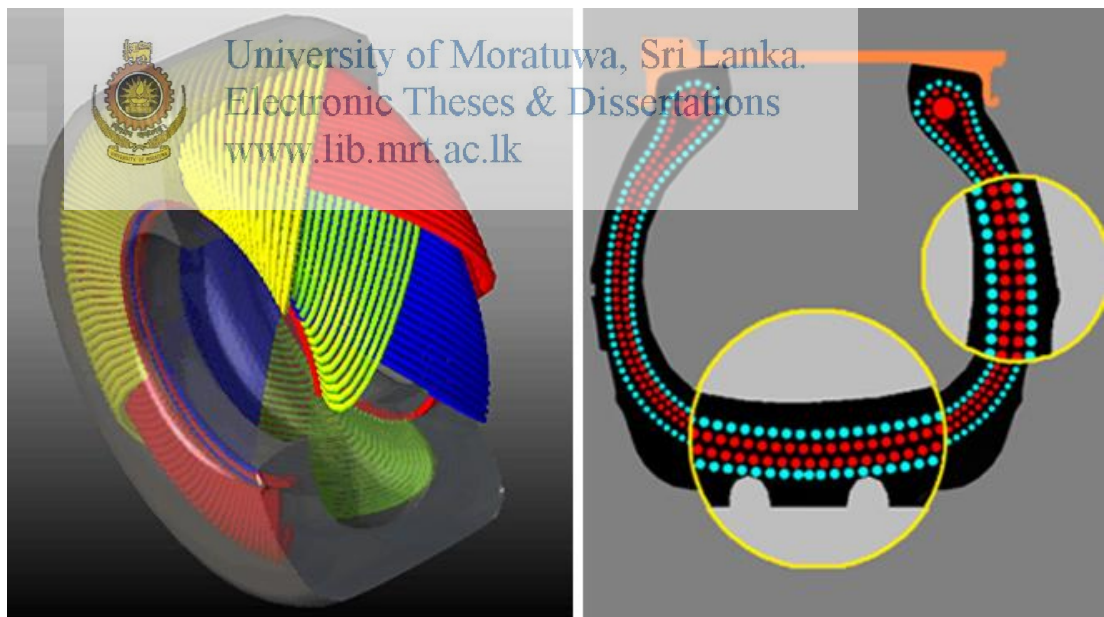


Figure 2.1 Conventional pneumatic tyre structure [11]

- b. Radial tyres: In the Radial design, Polyester cords are laid in and overlapped at 90 degrees to the centerline of the tire and then steel mesh belts are

added. The Radial design prevents the point of contact (where the rubber meets the road) from deforming, unlike the Bias Ply, which does deform under load [11].

- There are a number of benefits to the Radial design for the trailer operator.  
Softer, smoother, quieter ride
- Improved fuel economy
- Flat, wider footprint for better tire wear
- Runs cooler than a bias ply, minimizing risk of a blowout on the highway
- Longer tire life
- Better tracking – Improved sway control

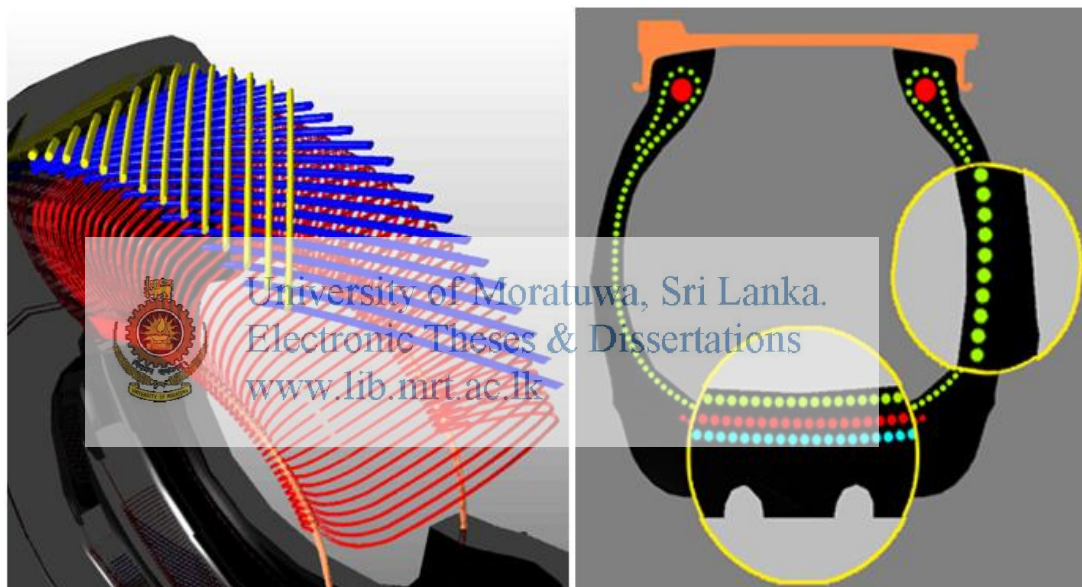



Figure 2.2 Radial tyre structure [11]

- c. Radial tubeless tyres: tubeless tyres as the name suggested, are tyres without tube. The tyre built in a way that it can contain the air by itself. It does not require a tube within it. The tyre has a chloro-butyl lining on its inside which is airtight. Together with the air tight joint between the tyre and the wheel, the membrane form a container that holds the air for the tyre. During high speed cruises, the temperature within the tyre rises significantly. This in turn increases the pressure on the tyre tube. An ordinary tyre is fairly vulnerable under such circumstances. Any protrusion into the tyre which at

other times will cause a routine puncture, due to such heat, causes the tube to burst like a balloon. The air escapes fast as the only air tight component in the tyre is the tube. Sometimes the air escape with so much force that it tears the tyre as well. This may casue the driver to lose control of the vehicle which at a high speed can be fatal. The tubeless tyre is better suited to hold air than a much thinner tube. In case of a protrusion, the air escape only through the hole that cause the puncture, which is plugged by the very thing that caused the puncture, and hence escapes at a slow pace giving the much required safety. As tubeless tyres contain the air themselves, they provide much more efficient dissipation of heat. This is enhanced if the wheels are made of alloys rather than the conventional ones.

2. Solid tyres: this is tyre that consist complete rubber they are extremely stable, puncture resistant, and maintenance free. Solid tyres have a high load capacity and are extremely economical. This makes them ideal for forklift trucks, airport vehicles, heavy-duty transport vehicles, platform trucks, and other industrial vehicles.

 University of Moratuwa, Sri Lanka.  
Electronic Theses & Dissertations  
www.lib.mrt.ac.lk

These tyres are commonly used at airports and seaports, logistics centers, and industrial applications. Industries where a clean environment is of paramount importance (e.g. the food and pharmaceutical industry) can use the non-marking version (Clean Solid Tires). They are also highly stable, puncture-resistant and have a long service life [11]. But additionally, they are especially designed for minimum floor marking in a clean industrial environment. Basically there two types of tyres that solid resilience tyre (SRT) and Press on band tyre (POB) the main deference between these two are SRT is consist only rubber although POB tyres had steel and bonded with rubber.





Figure 2.3 Solid tyre structure [11]

2.2 Tyre abrasion


 University of Moratuwa, Sri Lanka.  
 Electronic Theses & Dissertations  
[www.lib.mrt.ac.lk](http://www.lib.mrt.ac.lk)

This project is mainly considered tyre abrasion of solid tyres because testing and research were very limited in this regards and this should be very important to Sri Lanka that is more than 60% of world market solid tyres were manufactured in Sri Lanka.

Wear prediction is of great importance because of the cost of testing actual rubber articles. Laboratory studies of rubber abrasion aim at least to assist in the selection of materials. Although the studies show how for certain arrangements the rate of abrasion can be predicted, the wear of rubber articles in practice is beset with complications. For example, the wear of a road tyre brings into play its gross deformation properties just as much as the actual abrasion resistance of the rubber tread. Road topography, dust, water and other contaminants complicate matters further.

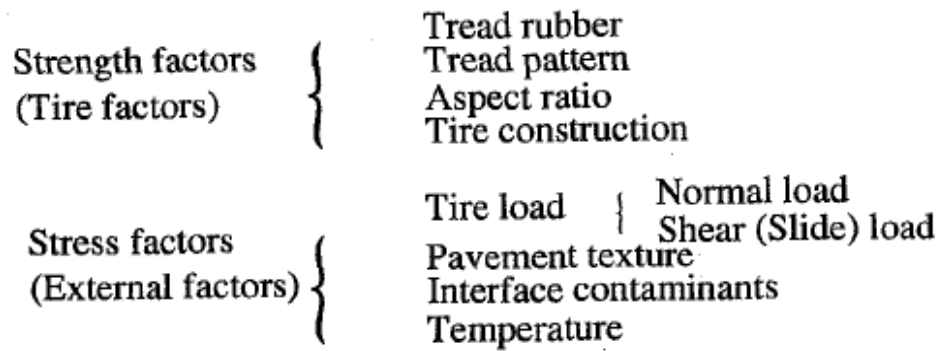


Figure 2.4: Factors affecting the tyre wear [8]

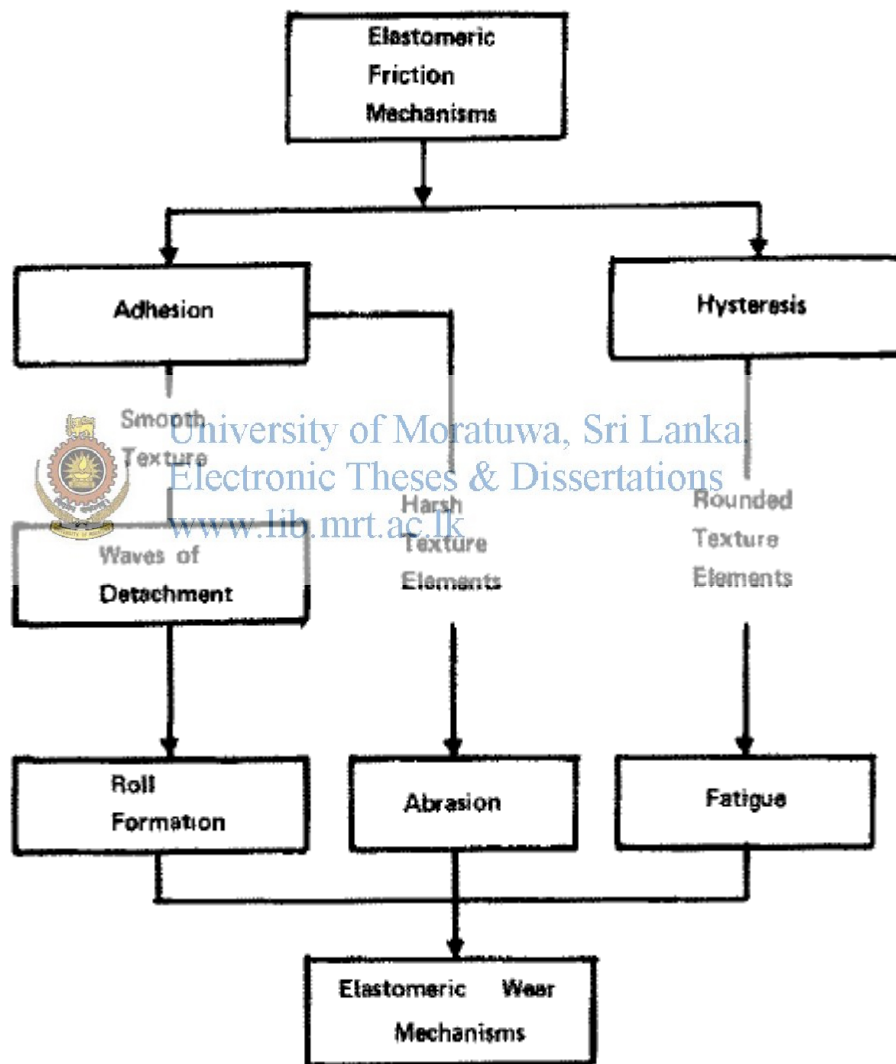


Figure 2.5: Schematic diagram of the friction and wear mechanisms in rubber-like materials [12]



The surface effect is having its origin as a molecular kinetic stick-slip action between rubber and the underlying surface, whereas the hysteresis factor is a bulk phenomenon within the body of the rubber slider. It is seen that, depending on the surface conditions, adhesion and hysteresis give rise to several distinct wear effects. Thus on a perfectly smooth texture adhesion may give rise to wear by roll formation in cases where the tear strength of the particular rubber is low. A more common experience occurs on harsh textures where the adhesion mechanism gives rise to abrasive or cutting wear. Should the nature of the surface texture of the substrate be such that its asperities are smooth and rounded rather than harsh, the hysteresis mechanism of friction gives rise to fatigue wear [12].

That is the fatigue mechanism is relatively mild in intensity but continuous, where as the abrasive wear phenomenon is severe and usually of short duration. For example a rolling un-braked tyre exhibits the fatigue mechanism because of the repeated and cyclic loading and unloading of discrete asperities in the road surface if the latter are smooth and rounded. Under wet conditions and with severe braking the same tyre will experience locked wheel sliding, and on this particular surface hysteresis friction will then induce a more severe form of the fatigue wear mechanism [12].

In contrast, locked wheel sliding of a tyre on a dry harsh texture causes severe and perhaps irreversible abrasive wear resulting in local overheating and the production of rubber wear fragments. Fatigue wear is also present in the latter case but it is of such minor proportions as to be negligible. We see then that the various mechanisms of friction and wear occur in different combinations when a tyre is subjected to braking, driving, free rolling and cornering manoeuvres.

Consider next the relation between frictions and wear as depicted in Fig. 2.6. Here the energy index of abrasion (defined as the ratio of worn rubber layer thickness to the work of friction) for various tread rubbers is plotted as a wear factor against the corresponding measured coefficient of friction. It is seen that the fatigue mechanism

for frictional coefficients of less than unity produces comparatively little wear, whereas severe abrasive wear (on harsh rough surfaces) or roll formation (on smooth substrates) correspond to frictional coefficients greater than 1.25 [12].

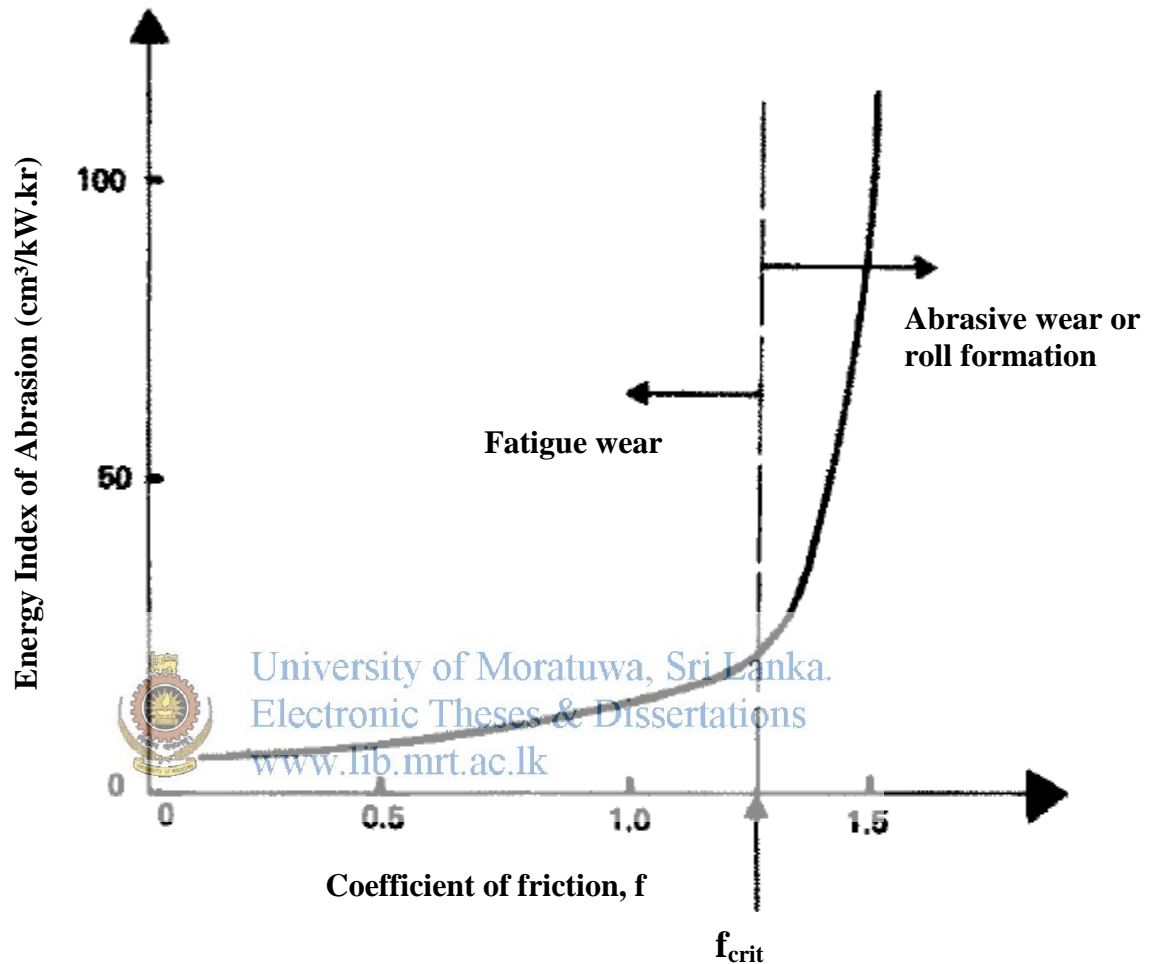


Figure 2.6: Broad correlations of friction and wear [12].

The vehicle characterization is critical to the process since both wear rate and various forms of uneven and irregular wear are strongly dependent on vehicle suspension/steering characteristics and on dynamic load transfer behavior. The characterization process involves mapping the vehicle over a practical range of acceleration, deceleration and cornering maneuvers. This mapping can be carried out by use of a computational vehicle model or by experimental testing of an actual vehicle. The proposed tyre testing method distinctly capture different wearing pattern on different surfaces as well as different speeds and loads.

### 2.2.1 Initiation of abrasion

In the absence of any serious chemical decomposition the abrasion process initially results in the removal of small rubber particles just a few microns in size, leaving pits



Figure 2.7 (Soft polyisoprene hemisphere ( $R = 18.5$  mm) sliding against glass at a speed of  $1 \text{ mms}^{-1}$  under an applied load of  $0.2$  N. High friction ( $\sim 2$ ) is accompanied by the transfer of particles of approximate diameter  $8 \text{ }\mu\text{m}$  to the glass plate [13].

With continued rubbing, larger pieces of rubber of the order of  $0.1$  mm are removed. Although most weight loss is attributable to the larger pieces, it is thought that the detachment of the smaller particles initiates the abrasion process.

The small particles have a characteristic size of  $1-5 \text{ }\mu\text{m}$ , but whether this relates to a structural unit in the rubber compound or is determined by localized stresses is not known. Other suggestions are that mechanical rupture to produce the particles relates to flaws in the rubber, including dirt, or voids that cavitate leading to internal subsurface failure.

Micro tearing seen for optically smooth rubber hemispheres slid against a glass plate may relate to the initiation process. Photomicrographs of the contact zone were taken in reflected white light through the glass plate. With increasing sliding speed, characteristic Schallamach waves were seen to merge into semi static gross ridges owing to surface buckling. All contact was concentrated on the crests of the ridges. In the wake of the ridges, distinct wear debris could be seen transferred to the glass surface. Globbs of debris were typically 2-15  $\mu\text{m}$  in size regardless of rubber type (Hardness 40-60 IRHD). The transfer process was more obvious in the case of a soft (23 IRHD) polyisoprene hemisphere. Here ridges appear distorted by rubber stuck to the glass, with ligaments being pulled out of the rubber surface (Figure. 2.7) owing to high traction forces. The observed contact ridges are possibly the precursor of abrasion patterns [13].

### 2.2.2 Abrasion patterns

Unidirectional abrasion of rubber often results in surface patterns characterized by ridges one after another at right angles to the sliding direction (Figure 2.8.a).

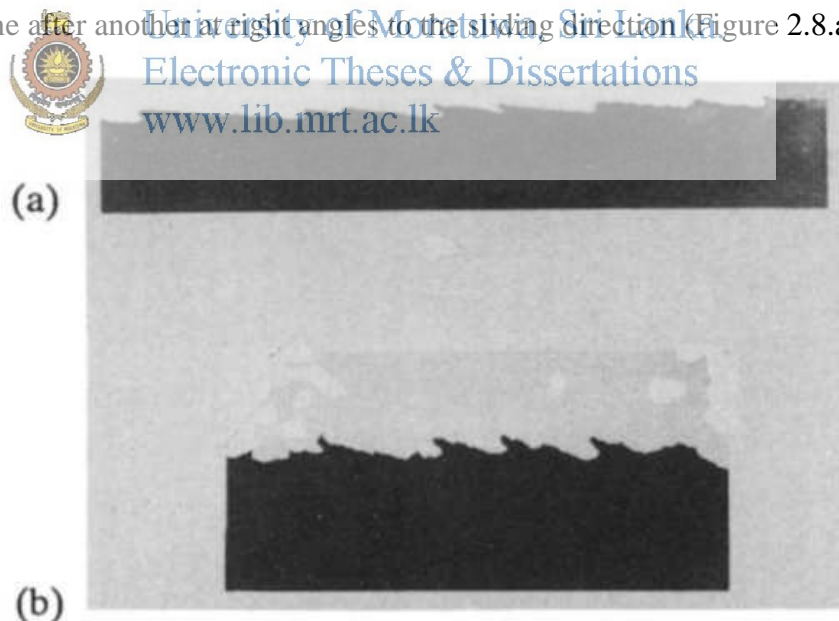


Figure 2.8 Cross-sections through abrasion pattern on (a) unfilled NR and (b) a worn tyre tread [13].

A cross section reveals that the ridge shape is asymmetric, the steep side of the ridges facing the direction of attack. From time to time the crests detach to produce large

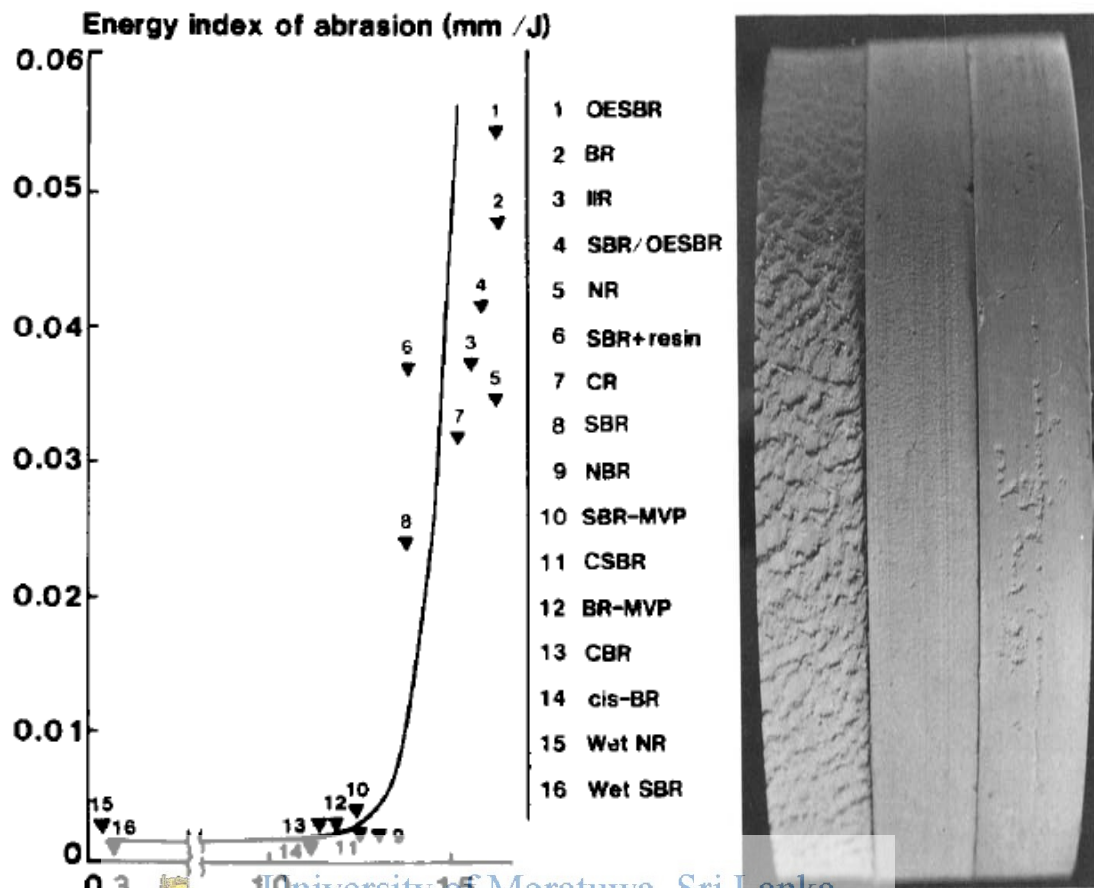
pieces of debris. The ridge height and the spacing increase with increasing severity of abrasion. The formation of such an abrasion pattern is characteristic of a low modulus elastomer sliding with high friction against a counterface. On sharp tracks the abrasion pattern is replaced by score lines parallel to the direction of motion if the modulus of the elastomer is sufficiently high or the friction is reduced by the presence of a lubricant (Figure. 2.8.b). If the direction of sliding is continuously changed, the pattern of ridges does not form and the abrasion rate is lower. A finer-scale roughness results (microns rather than millimetres). This is termed “intrinsic” abrasion [13].

### 2.2.3 Smearing and the effect of antioxidants

It is well known that for some conditions the surface of rubber becomes tacky during abrasion experiments, drum testing of tyres and sometimes even for tyres on the road. It has been suggested that either exudation of low molecular weight additives or degradation of the polymer to a material of low molecular weight could be responsible. Degradation might result from either the material or mechanical stress, At high sliding speeds, such as skidding of a vehicle on locked wheels, frictional heating certainly [13]



University of Moratuwa, Sri Lanka  
Electronic Theses & Dissertations  
www.lib.mrt.ac.lk



University of Moratuwa, Sri Lanka.  
Electronic Theses & Dissertations  
www.lib.mrt.ac.lk

Figure 2.9 [13]

Figure 2.10 [13]

The relationship between abrasion and the coefficient of friction of rubbers tested on a ribbed metal surface at pressure  $p = 0.63 \text{ kgfcm}^{-2}$ : 1, Europrene 1712 (oil-extended styrene-butadiene); 2, SKB; 3, butyl rubber; 4, combination of Europrene 1500 and Europrene 1712 (1:1); 5, NR; 6, SKS-30ARK with resins (15 parts of urea formaldehyde and 12 parts of epoxyamine 89 added to latex); 7, Nairit; 8, Europrene 1500; 9, SKN-26; 10, SKS-25-MVP-5; 11, SKS-30-1; 12, SKMVP- 15; 13, SKD-1; 14, SKD; 15, NR with water as a lubricant; 16, Europrene 1500 with water as a lubricant [13].

Effect of lubricants on abrasion of SBR gum by a vertical blade (direction of abrasion is from top to bottom, the test pieces are 12.5 mm wide and 63.5 mm in diameter, the blade is aligned normal to the direction of abrasion and is loaded to  $463 \text{ Nm}^{-1}$ ). From left to right: no lubricant, wear rate  $22.9 \text{ pm cycle}$ ,  $F/h = 748 \text{ Nm}^{-1}$ ;

soapy water lubricant, wear rate 0.4 pm cycle,  $F/h=543 \text{ Nm}^{-1}$ , wear rate 0.04 pm cycle,  $F/h=465 \text{ Nm}^{-1}$  [13].

Abrasion of rubber can be even more sensitive to detailed conditions than friction. For example, a lubricant may cause a small decrease in frictional force but a dramatic decrease in abrasion. It appears that the main cause of abrasion is tearing or fatigue under the action of high local stresses caused by friction.

In the case of fatigue, such as that occurs under mild abrasion conditions, the presence of oxygen decreases abrasion resistance in a manner reminiscent of the influence of oxygen on the cyclic growth of cracks in the rubber. Antioxidants can be used to, at least, partially restore the abrasion and crack growth resistance. Smearing may also occur and this has been ascribed to mechano-oxidative degradation of susceptible rubbers such as NR, SBR or EPDM. It appears to be a complication rather than a basic mechanism of abrasion [13]. In this research project the main focus had been on changing the tyre compound, lug pattern, speed, load and working floor how can be change to suit better customer requirement of tyre.

### 2.3



University of Moratuwa, Sri Lanka.  
Electronic Theses & Dissertations  
[www.lib.mrt.ac.lk](http://www.lib.mrt.ac.lk)

The most definitive method of determining the behavior of a tire is to examine its performance when subjected to road testing. Proving ground testing allows all types of tires such as passenger car, truck, earthmover solid tyres, and farm to be tested under closely monitored conditions. An industry proving ground will generally have the following test tracks and road courses available:

- High-speed tracks, either circular or oval.
- Interstate highway simulation.
- Gravel and unimproved roads.
- Cobblestone.
- Cutting, chipping, and tearing courses.
- Wet and dry skid pads, serpentine and slalom courses for aesthetics, and handling tests.
- Tethered tracks for farm tire durability.



- Glass roads for footprint monitoring.

For example, the 7250-acre Goodyear Proving Grounds in Texas contains a 5-mile high-speed circle, 8 miles of simulated interstate highway, gravel and rock courses for a range of tire type testing, skid pads with spray equipment, and a glass road facility for tire footprint observations and evaluation of water dispersion [14].

The classical laws of friction can be summarised as:

1. Friction is a property of two contacting surfaces. It does not make sense to discuss friction as if it were a material property.
2. Frictional force is linearly proportional to normal force and can be defined using a coefficient of friction (frictional force/normal force).
3. The coefficient of friction is independent of contact area between the two surfaces.
4. The static coefficient of friction (stiction) is greater than the kinetic (sliding) coefficient of friction.
5. The coefficient of friction is independent of sliding speed.

A detailed treatment of this subject with regard to tyres is given by Moore (1975), where it is shown that the above laws are flawed, or limited in certain [15].

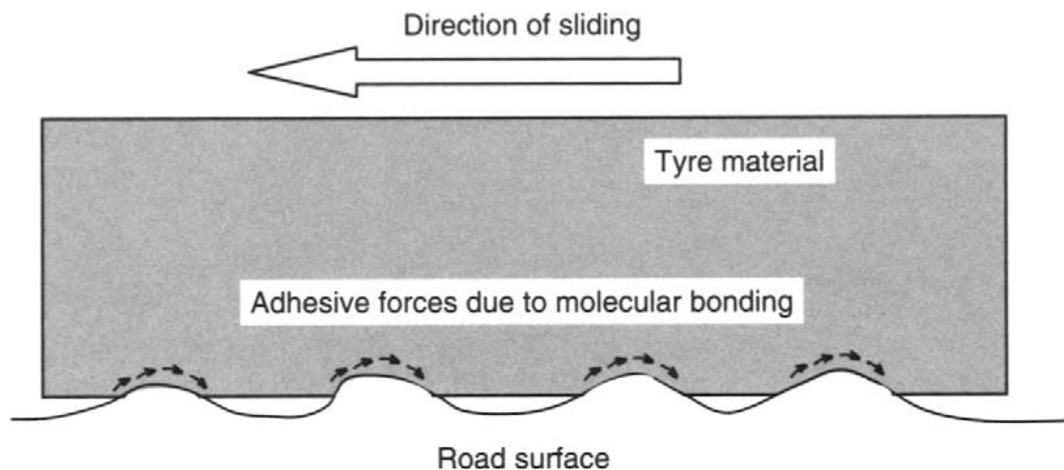


Figure 2.31: Frictional force components due to adhesion [15].



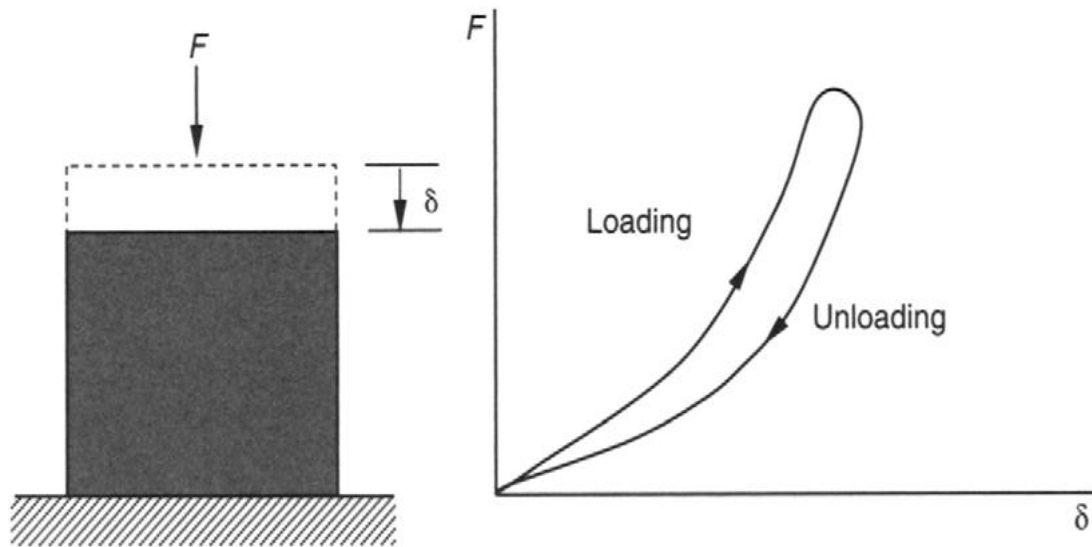


Figure 2.32: Hysteresis in rubber [15].

In order to understand the hysteresis mechanism considers a block of rubber subjected to an increasing and then a decreasing load as shown in Figure 2.32. As the rubber is loaded and unloaded it can be seen that for a given displacement the force  $F$  is greater during the loading phase than the unloading phase[15].

If this continue to consider the situation where a non-rotating tyre is sliding over a non-smooth surface with a coefficient of friction assumed to be zero it can be seen from Figure 2.33 that an element of rubber in the contact patch will be subject to continuous compressive loading and unloading.

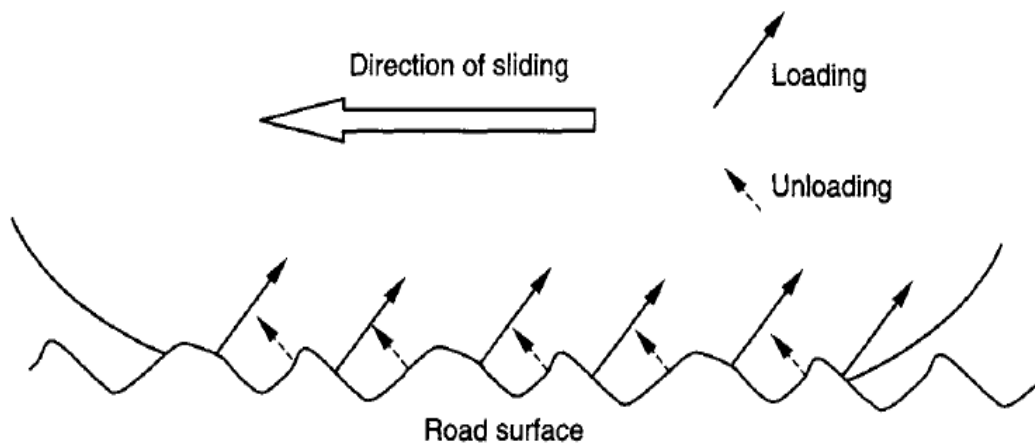


Figure 2.33: Loading and unloading of tyre rubber in the contact patch [15].

In the idealized situation of no friction as the tyre slides over the irregular road surface compressive forces normal to the surface are generated as the rubber is loaded and unloaded. Due to the hysteresis in the rubber the sum of the loaded forces is greater than the sum of the unloaded forces resulting in, for example here, a resultant braking force opposing the direction of sliding [15].

Pavement friction design is basically a process of selecting the right combination of pavement surface micro-texture and macro-texture to optimize available pavement friction for a given design situation. For both asphalt and concrete surfaces, micro-texture is defined by the surface aggregate material properties. The important aggregate properties that influence short- and long-term micro-texture are [16].

- Mineralogical and petrographic properties.
  - ❖ Aggregate composition/structure and mineral hardness.
- Physical and geometrical properties.
  - ❖ Angularity, shape, and texture.
- Mechanical properties.
  - ❖ Abrasion/wear resistance.
  - ❖ Polish characteristics.
- Durability properties.
  - ❖ Soundness



University of Moratuwa, Sri Lanka.  
Electronic Theses & Dissertations  
www.lib.mru.ac.lk

Several test methods are available for characterizing aggregate frictional properties. The extent of aggregate testing and characterization required as part of the friction design process will vary from agency to agency, based on the types of aggregates available, the variability of aggregate properties, the quality and historical performance of available aggregates, and the anticipated applications (e.g., mix types, roadway functional class). Since laboratory material testing does not guarantee friction performance in the field, it is essential that testing be used in conjunction with field performance history to identify acceptable aggregate types

A comprehensive evaluation of friction measurements and crash rates revealed that increasing pavement friction does reduce crash rates significantly, as summarized below.[16]

Table 2.31: Friction measurements and crash rates [14].

Friction Interval	Crash rate (injuries per million vehicle km)
< 0.15	0.80
0.15 - 0.24	0.55
0.25 - 0.34	0.25
0.35 - 0.44	0.20

**Pavement friction:**

Pavement friction is the force that resists the relative motion between a vehicle tire and a pavement surface. This resistive force, illustrated in figure 2.34, is generated as the tire rolls or slides over the pavement surface.

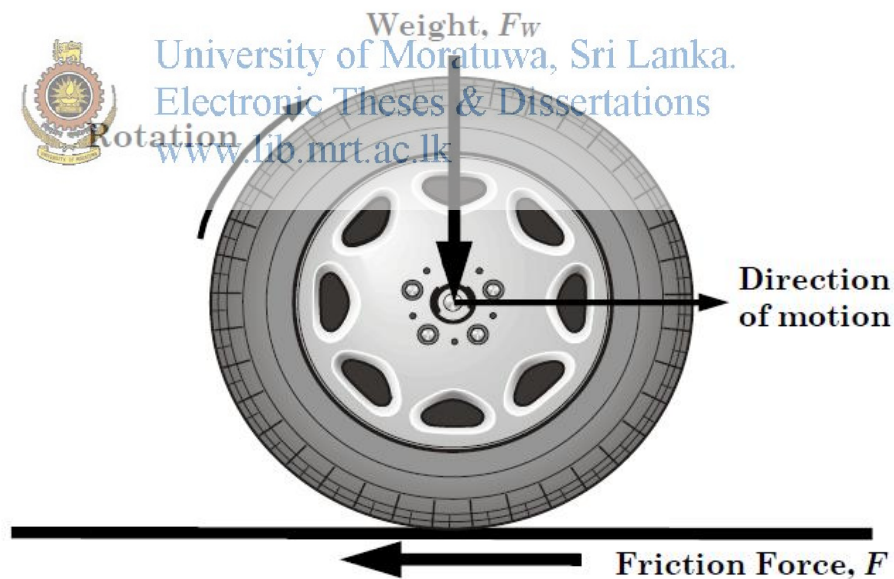


Figure 2.34: Simplified diagram of forces acting on a rotating wheel[16]

The resistive force, characterized using the non-dimensional friction coefficient,  $\mu$ , is the ratio of the tangential friction force ( $F$ ) between the tire tread rubber and the

horizontal traveled surface to the perpendicular force or vertical load (FW) and is computed using equation 1.

$$\mu = \frac{F}{FW} \quad \text{-----} \quad 1$$

Pavement friction plays a vital role in keeping vehicles on the road, as it gives drivers the ability to control/maneuver their vehicles in a safe manner, in both the longitudinal and lateral directions. It is a key input for highway geometric design, as it is used in determining the adequacy of the minimum stopping sight distance, minimum horizontal radius, minimum radius of crest vertical curves, and maximum super-elevation in horizontal curves. Generally speaking, the higher the friction available at the pavement– tire interface, the more control the driver has over the vehicle [16].

### 2.3.1 Longitudinal frictional forces

Longitudinal frictional forces occur between a rolling pneumatic tire (in the longitudinal direction) and the road surface when operating in the free rolling or constant-braked mode. In the free-rolling mode (no braking), the relative speed between the tire circumference and the pavement referred to as the slip speed is zero. In the constant-braked mode, the slip speed increases from zero to a potential maximum of the speed of the vehicle. The following mathematical relationship explains slip speed (Meyer, 1982) [16].

$$S = V - V_p = V - (0.68 \times \omega \times r) \quad \text{-----} \quad 2$$

Where: S = Slip speed, mi/hr.

V = Vehicle speed, mi/hr.

V<sub>p</sub> = Average peripheral speed of the tire, mi/hr.

ω = Angular velocity of the tire, radians/sec.

r = Average radius of the tire, ft.

Again, during the free-rolling state of the tire,  $V_p$  is equal to the vehicle speed; thus,  $S$  is zero. For a locked or fully braked wheel,  $V_p$  is zero, so the sliding speed or slip speed is equal to the vehicle speed ( $V$ ). A locked-wheel state is often referred to as a 100 percent slip ratio, and the free-rolling state is a zero percent slip ratio. The following mathematical relationships give the calculation formula for slip ratio (Meyer, 1982)[16].

$$SR = \frac{V - V_p}{V} \times 100 = \frac{S}{V} \times 100 \quad \text{—————}3$$

Where: SR = Slip ratio, percent.

$V$  = Vehicle speed, mi/hr.

$V_p$  = Average peripheral speed of the tire, mi/hr.

$S$  = Slip speed, mi/hr.

Similar to the previous explanation, during the free-rolling state of the tire,  $V_p$  is equal to the vehicle speed and  $S$  is zero, thus the slip ratio (SR) is zero percent. For a locked wheel,  $V_p$  is zero,  $S$  equals the vehicle speed ( $V$ ), and so the slip ratio (SR) is 100 percent.



Figure 2.35 shows the ground force acting on a free rolling tire. In this mode, the ground force is at the center of pressure of the tire contact area and is off center by the amount  $a$ . This offset causes a moment that must be overcome to rotate the tire. The force required to counter this moment is called the rolling resistance force (FR). The value  $a$  is a function of speed and increases with speed. Thus, FR increases with speed. In the constant-braked mode (figure 2.36), an additional force called the braking slip force[16] (FB) is required to counter the added moment (MB) created by braking. The force is proportional to the level of braking and the resulting slip ratio. The total frictional force is the sum of the free-rolling resistance force (FR) and the braking slip force (FB) [16].

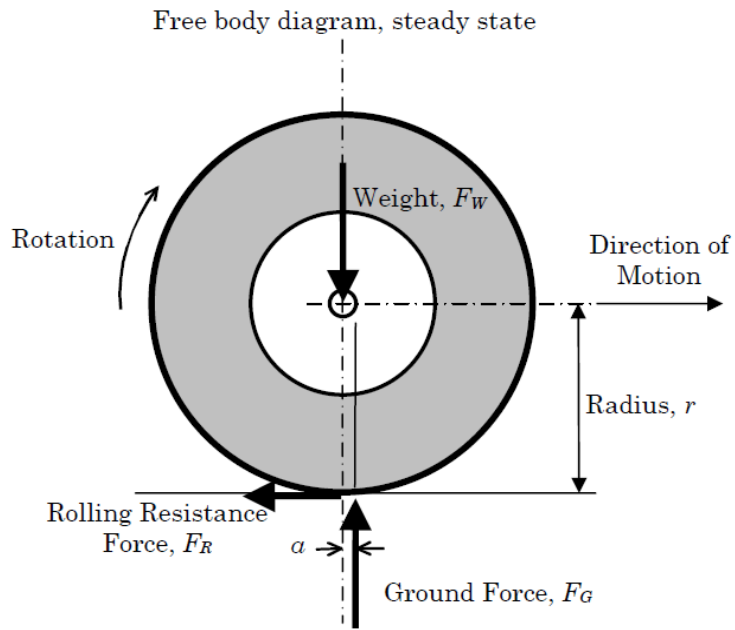


Figure 2.35 Rolling resistance force with a free-rolling tire at a constant speed on a bare, dry paved surface [16].

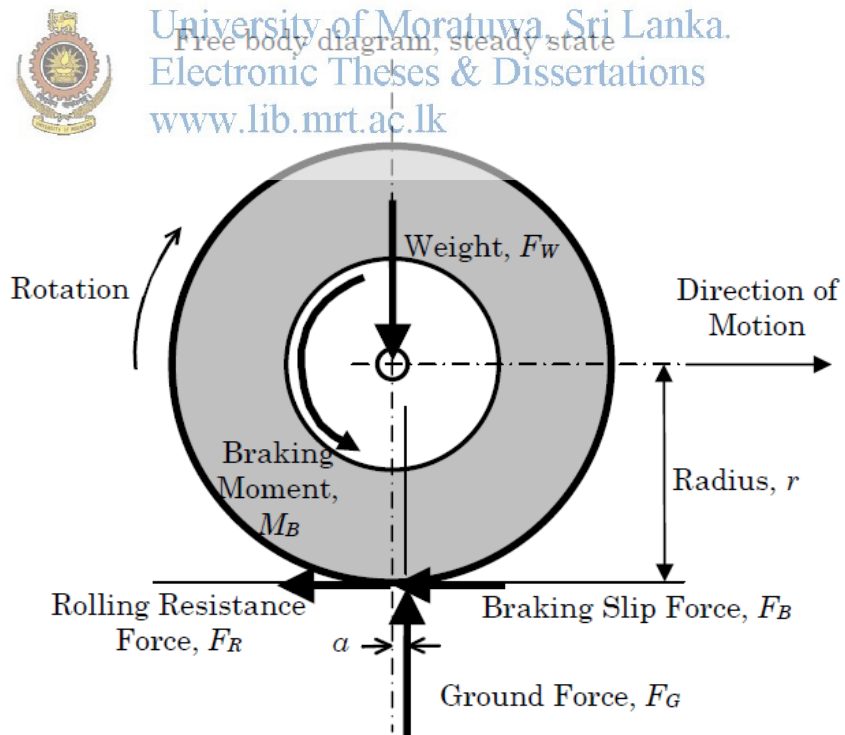


Figure 2.36 Forces and moments of a constant-braked wheel on a bare, dry paved surface [16].



The coefficient of friction between a tire and the pavement changes with varying slip, as shown in figure 2.37 [17]. The coefficient of friction increases rapidly with increasing slip to a peak value that usually occurs between 10 and 20 percent slip (critical slip). The friction then decreases to a value known as the coefficient of sliding friction, which occurs at 100 percent slip. The difference between the peak and sliding coefficients of friction may equal up to 50 percent of the sliding value, and is much greater on wet pavements than on dry pavements [16].

The relationship shown in figure 2.37 is the basis for the anti-locking brake system (ABS), which takes advantage of the front side of peak friction and minimizes the loss of side/steering friction due to sliding action. Vehicles with ABS are designed to apply the brakes on and off (i.e., pump the brakes) repeatedly, such that the slip is held near the peak. The braking is turned off before the peak is reached and turned on at a set time or percent slip below the peak. The actual timing is a proprietary design of the manufacturer [16].

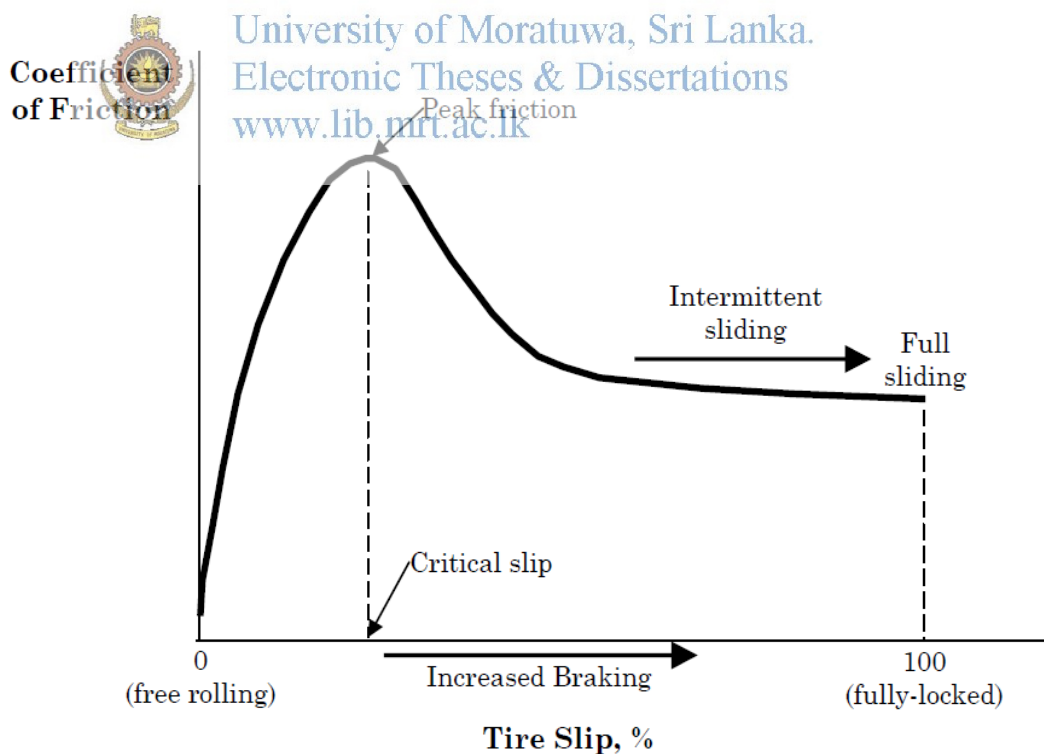


Figure 2.37 Pavement friction versus tire slip [16].

### 2.3.2 Lateral frictional forces

Another important aspect of friction relates to the lateral or side-force friction that occurs as a vehicle changes direction or compensates for pavement cross-slope and/or cross wind effects. The relationship between the forces acting on the vehicle tire and the pavement surface as the vehicle steers around a curve, changes lanes, or compensates for lateral forces is as follows[16].

$$F_s = \frac{V^2}{15R} - e \quad \text{-----} \quad 4$$

Where: FS = Side friction.

V = Vehicle speed, mi/hr.

R = Radius of the path of the vehicle's center of gravity (also, the radius of curvature in a curve), ft.

e = Pavement super-elevation, ft/ft.

This equation is based on the pavement-tire steering/cornering force diagram in figure 12. It shows how the side-force friction factor acts as a counterbalance to the centripetal force developed as a vehicle perform a lateral movement.

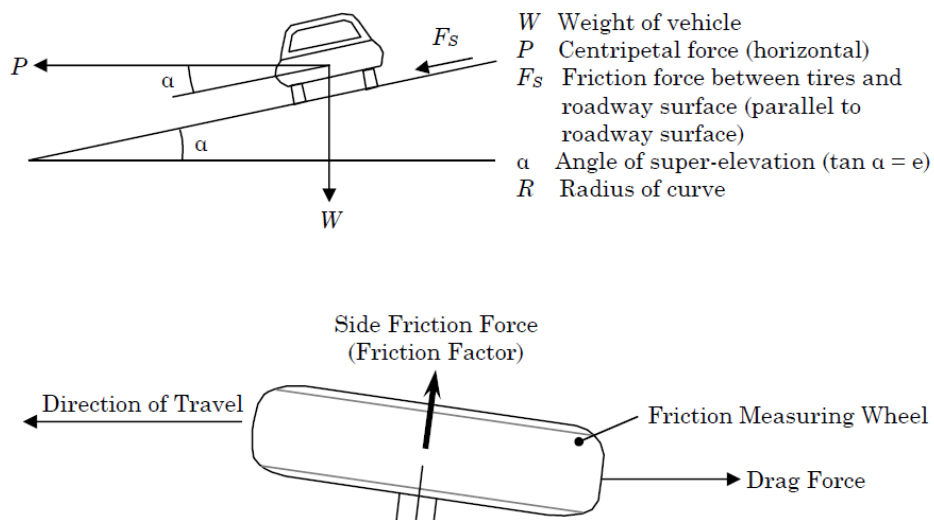


Figure 2.38 Dynamics of a vehicle traveling around a constant radius curve at a constant speed, and the forces acting on the rotating wheel [16].



### 2.3.3 Combined braking and cornering

With combined braking and cornering, a driver either risks not stopping as rapidly or losing control due to reduced lateral/side forces. When operating at the limits of tire grip, the interaction of the longitudinal and lateral forces is such that as one force increases, the other must decrease by a proportional amount. The application of longitudinal braking reduces the lateral force significantly. Similarly, the application of high lateral force reduces the longitudinal braking. Figure 2.39 shows these effects [16].

Commonly referred to as the friction circle or friction ellipse, the vector sum of the two combined forces remains constant (circle) or near constant (ellipse) (see figure 2.310). When operating within the limits of tire grip, the amount of braking and turning friction components can vary independently as long as the vector sum of these components does not exceed the limits of tire grip as defined by the friction circle or friction ellipse. The degree of ellipse depends on the tire and pavement properties [16].

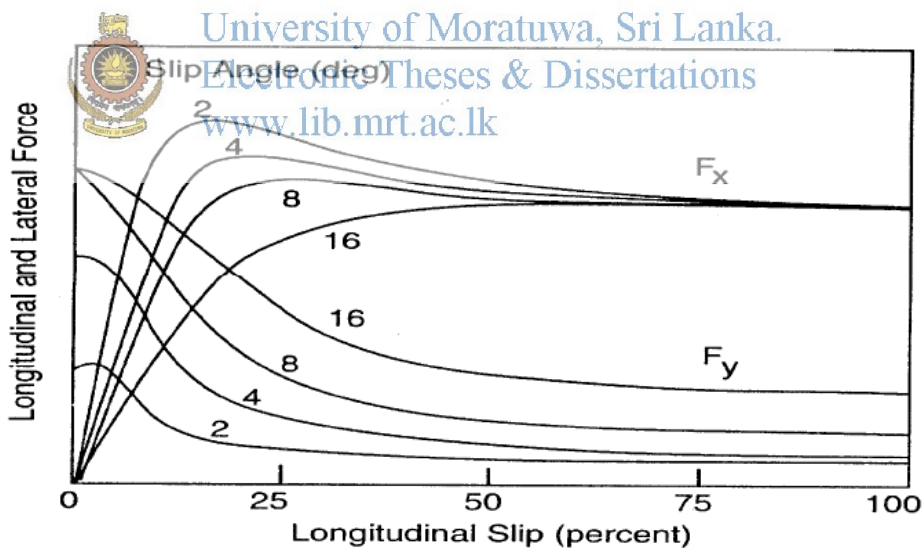


Figure 2.39 Brake ( $F_x$ ) and lateral ( $F_y$ ) forces as a function of longitudinal slip [16].

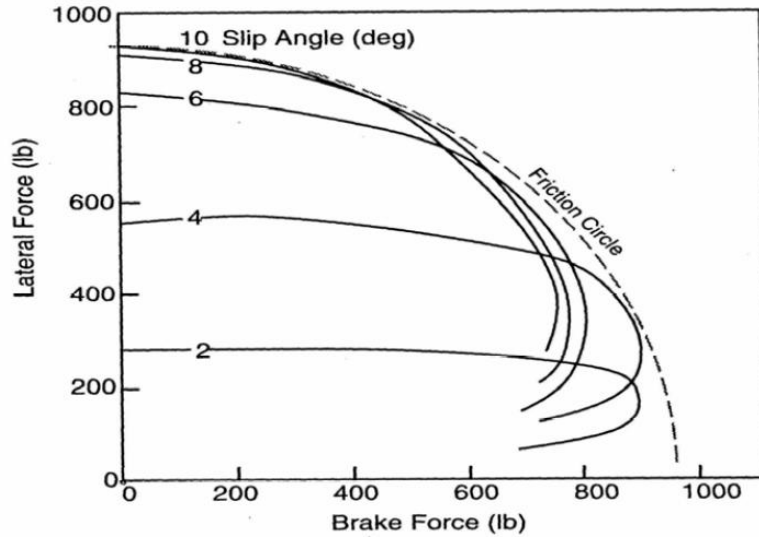


Figure 2.310 Lateral force versus longitudinal force at constant slip angles [16].

### 2.3.4 Friction mechanisms

Pavement friction is the result of a complex interplay between two principal frictional force components—adhesion and hysteresis (figure 2.311). Adhesion is the friction that results from the small-scale bonding/interlocking of the vehicle tire rubber and the pavement surface as they come into contact with each other. It is a function of the interface shear strength and contact area. The hysteresis component of frictional forces results from the energy loss due to bulk deformation of the vehicle tire.

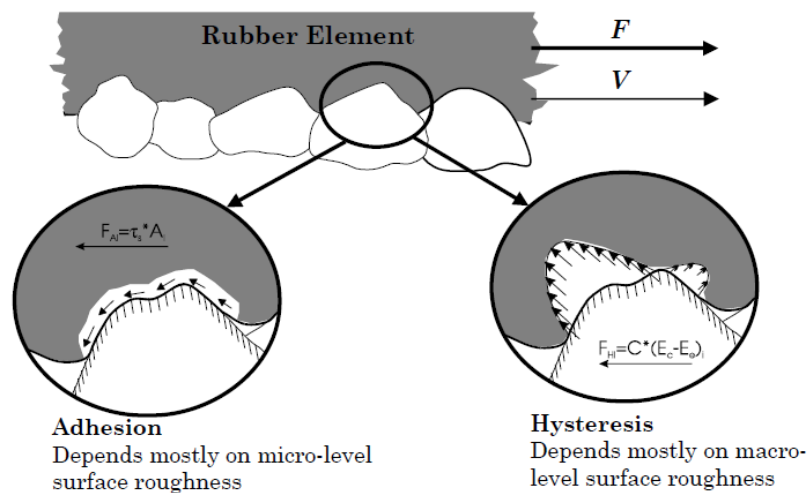


Figure 2.311 Key mechanisms of pavement–tire friction [16].

The deformation is commonly referred to as enveloping of the tire around the texture. When a tire compresses against the pavement surface, the stress distribution causes the deformation energy to be stored within the rubber. As the tire relaxes, part of the stored energy is recovered, while the other part is lost in the form of heat (hysteresis), which is irreversible. That loss leaves a net frictional force to help stop the forward motion.

Although there are other components of pavement friction (e.g., tire rubber shear), they are insignificant when compared to the adhesion and hysteresis force components. Thus, friction can be viewed as the sum of the adhesion and hysteresis frictional forces [16].

$$F = F_A + F_H \text{ —————} 5$$

Both components depend largely on pavement surface characteristics, the contact between tire and pavement, and the properties of the tire. Also, because tire rubber is a visco-elastic material, temperature and sliding speed affect both components. Because adhesion force is developed at the pavement–tire interface, it is most responsive to the micro-level asperities (micro-texture) of the aggregate particles contained in the pavement surface. In contrast, the hysteresis force developed within the tire is most responsive to the macro-level asperities (macro-texture) formed in the surface via mix design and/or construction techniques. As a result of this phenomenon, adhesion governs the overall friction on smooth-textured and dry pavements, while hysteresis is the dominant component on wet and rough-textured pavements[16].

### **2.3.5 Factors affecting available pavement friction**

The factors that influence pavement friction forces can be grouped into four categories pavement surface characteristics, vehicle operational parameters, tire properties, and environmental factors. Table 2.32 lists the various factors comprising each category. Because each factor in this table plays a role in defining pavement friction, friction must be viewed as a process instead of an inherent property of the pavement. It is only when all these factors are fully specified that friction takes on a

definite value. The more critical factors are shown in bold in Table 2.32 and are briefly discussed below [16]. Among these factors, the ones considered to be within a highway agency's control are micro-texture and macro-texture, pavement materials properties, and slip speed.

Table 2.32: Factors affecting available pavement friction (modified from Wallman and Astrom, 2001) [16].

<b>Pavement surface characteristic</b>	<b>Vehicle operating parameters</b>	<b>Tyre properties</b>	<b>Environment</b>
Micro- texture	Slip speed	Foot print	Climate
Macro- texture	-Vehicle speed	Tread design and condition	-Wind
Mega- texture/ unevenness	-Braking action	Rubber composition and hardness	-Temperature
Material properties	Driving maneuver	Inflation pressure	-Water (rainfall, condensation)
Temperature	-Turning	Load	-Snow and ice
	-Overtaking	Temperature	contaminants
			-Anti skid material (salt, sand)
			- Dirt, mud, debris

Note: there is no relation between rows.



University of Moratuwa, Sri Lanka.  
Electronic Theses & Dissertations  
[www.lib.mrt.ac.lk](http://www.lib.mrt.ac.lk)

### 2.3.6 Pavement surface characteristics

- **Surface Texture:** Pavement surface texture is characterized by the asperities present in a pavement surface. Such asperities may range from the micro-level roughness contained in individual aggregate particles to a span of unevenness stretching several feet in length. The two levels of texture that predominantly affect friction are micro-texture and macro-texture [14].

As figure 2.312 shows, micro-texture is the degree of roughness imparted by individual aggregate particles, whereas macro-texture is the degree of roughness imparted by the deviations among particles. Micro-texture is mainly responsible for pavement friction at low speeds, whereas macro-texture is mainly responsible for reducing the potential for separation of tire and pavement surface due to

hydroplaning and for inducing friction caused by hysteresis for vehicles traveling at high speeds. Further discussions on micro texture and macro-texture are provided later in this chapter under the heading “Pavement Surface Texture” [16].

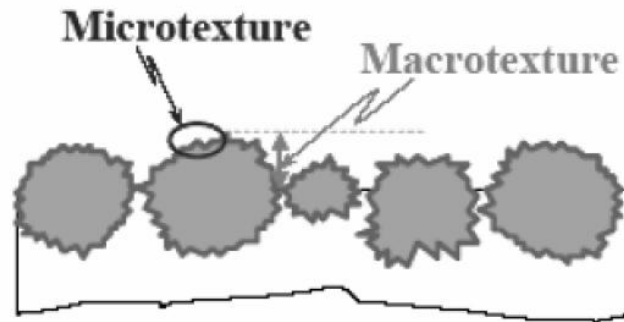


Figure 2.312 Micro-texture versus macro-texture [16].

- **Surface Material Properties:** Pavement surface material properties (i.e., aggregate and mix characteristics, texturing patterns) help to define surface texture. These properties also affect the long-term durability of texture through their capacities to resist aggregate polishing and abrasion/wear of both aggregate and mix under accumulated traffic and environmental loadings.

### Vehicle Operating Parameters

- **Slip Speed:** The coefficient of friction between a tire and the pavement changes with varying slip. It increases rapidly with increasing slip to a peak value that usually occurs between 10 and 20 percent slip. The friction then decreases to a value known as the coefficient of sliding friction, which occurs at 100 percent slip [16].

### Tire Properties

- **Tire Tread Design and Condition:** Tire tread design (i.e., type, pattern, and depth) and condition have a significant influence on draining water that accumulates at the pavement surface. Water trapped between the pavement and the tire can be expelled through the channels provided by the pavement surface texture and by

the tire tread. The depth of tread is particularly important for vehicles driving over thick films of water at high speeds. Some studies [16] have reported a decrease in wet friction of 45 to 70 percent for fully worn tires, compared to new ones [16].

- **Tire Inflation Pressure:** Tire under-inflation can significantly reduce friction at high speeds. Under-inflated tires allow the center of the tire tread to collapse and become very concave, resulting in the constriction of drainage channels within the tire tread and a reduction of contact pressure. The effect is for the tire to trap water at the pavement surface rather than allow it to flow through the treads. As a consequence, hydroplaning speed is decreased. Tire over-inflation, on the other hand, causes only a small loss of pavement friction [16]. Over-inflated tires reduce the trapping effect and yield higher pressure for forcing water from below the vehicle's tire. The increased tire pressure and smaller tire contact area result in a higher hydroplaning speed.

#### **Environment**

- **Thermal Properties:** Automotive tires are visco-elastic materials, and their properties can be significantly affected by changes in temperature and other thermal properties, such as thermal conductivity and specific heat. Research indicates that pavement-tire friction generally decreases with increasing tire temperature, though this is difficult to quantify.
- **Water:** Water, in the form of rainfall or condensation, can act as a lubricant, significantly reducing the friction between tire and pavement. The effect of water film thickness (WFT) on friction is minimal at low speeds (<20 mi/hr (32 km/hr)) and quite pronounced at higher speeds (>40 mi/hr (64 km/hr)). As shown in figure 17, the coefficient of friction of a vehicle tire sliding over wet pavement surface decreases exponentially as WFT increases. The rate at which the coefficient of friction decreases generally becomes smaller as WFT increases. In addition, the effect of WFT is influenced by tire design and condition, with worn tires being most sensitive to WFT [16].

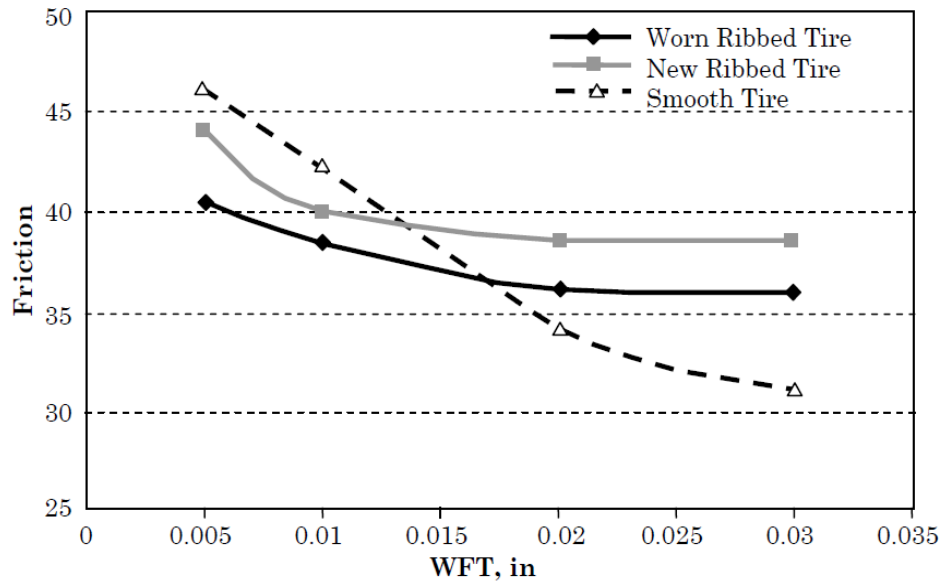


Figure 2.313 Effect of water film thickness on pavement friction [16].

Hydroplaning can occur when relatively thick water layers or films are present and vehicles are traveling at higher speeds. Hydroplaning occurs when a vehicle tire is separated from the pavement surface by the water pressure that builds up at the pavement-tire interface [16], causing friction to drop to a near-zero level. It is a complex phenomenon, affected by several parameters, including water depth, vehicle speed, pavement macro-texture, tire tread depth, tire inflation pressure, and tire contact area. Relatively thick water films form on a pavement surface when drainage is inadequate during heavy rainfalls or when pavement rutting or wearing creates puddles. Loss of direct pavement-tire contact can occur at speeds as low as 40 to 45 mi/hr (64 to 72 km/hr) on puddles about 1 in (25 mm) deep and 30 ft (9 m) long [16].

### Contaminants

Contaminants commonly found on highways include dirt, sand, oil, water, snow, and ice. Any kind of contamination at the pavement tire interface will have an adverse effect on pavement tire friction. Foreign materials act like the balls in a ball bearing, or as lubricant between a piston and cylinder in an engine, reducing friction between the two surfaces. The thicker or more viscous is the contaminant, the greater the



reduction in pavement tire friction. The grinding effect of hard contaminants, such as sand, accelerates the rate of wearing at the pavement surface [16].

### 2.3.7 Pavement surface texture

Pavement surface texture is defined as the deviations of the pavement surface from a true planar surface. These deviations occur at three distinct levels of scale, each defined by the wavelength ( $\lambda$ ) and peak-to-peak amplitude (A) of its components. The three levels of texture, as established in 1987 by the Permanent International Association of Road Congresses (PIARC), are as follows [16].

- Micro-texture ( $\lambda < 0.02$  in [0.5 mm], A = 0.04 to 20 mils [1 to 500  $\mu\text{m}$ ]) Surface roughness quality at the sub-visible or microscopic level. It is a function of the surface properties of the aggregate particles contained in the asphalt or concrete paving material.
- Macro-texture ( $\lambda = 0.02$  to 2 in [0.5 to 50 mm], A = 0.005 to 0.8 in [0.1 to 20 mm]) Surface roughness quality defined by the mixture properties (shape, size, and gradation of aggregate) of asphalt paving mixtures and the method of finishing/texturing (dragging, tinning, grooving; depth, width, spacing and orientation of channels/grooves) used on a concrete paved surfaces.
- Mega-texture ( $\lambda = 2$  to 20 in [50 to 500 mm], A = 0.005 to 2 in [0.1 to 50 mm]) Texture with wavelengths in the same order of size as the pavement–tire interface. It is largely defined by the distress, defects, or “waviness” on the pavement surface.

Wavelengths longer than the upper limit (20 in [500 mm]) of mega-texture are defined as roughness or unevenness. Figure 2.314 illustrates the three texture ranges, as well as a fourth level roughness/unevenness representing wavelengths longer than the upper limit (20 in [500 mm]) of mega-texture [16].

It is widely recognized that pavement surface texture influences many different pavement tire interactions. Figure 2.315 shows the ranges of texture wavelengths affecting various vehicle road interactions, including friction, interior and exterior



noise, splash and spray, rolling resistance, and tire wear. As can be seen, friction is primarily affected by micro texture and macro-texture, which correspond to the adhesion and hysteresis friction components, respectively.

Figure 2.316 shows the relative influences of micro-texture, macro-texture, and speed on pavement friction. As can be seen, micro-texture influences the magnitude of tire friction, while macro-texture impacts the friction–speed gradient. At low speeds, micro-texture dominates the wet and dry friction level. At higher speeds, the presence of high macro texture facilitates the drainage of water so that the adhesive component of friction afforded by micro-texture is re-established by being above the water. Hysteresis increases with speed exponentially, and at speeds above 65 mi/hr (105 km/hr) accounts for over 95 percent of the friction [16].

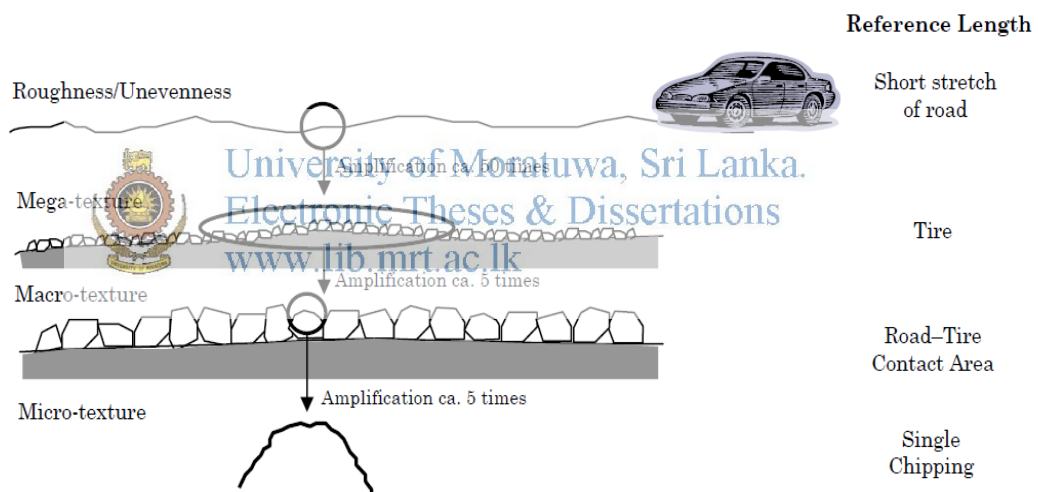


Figure 2.314 Simplified illustrations of the various texture ranges that exist for a given pavement surface [16].

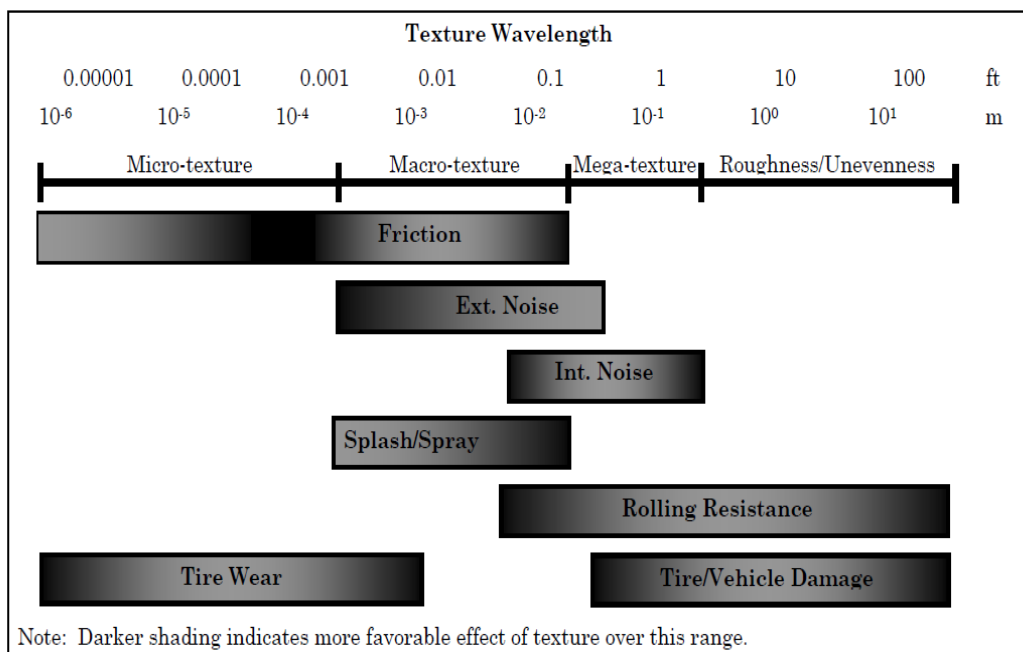


Figure 2.315 Texture wavelength influence on pavement–tire interactions [16].

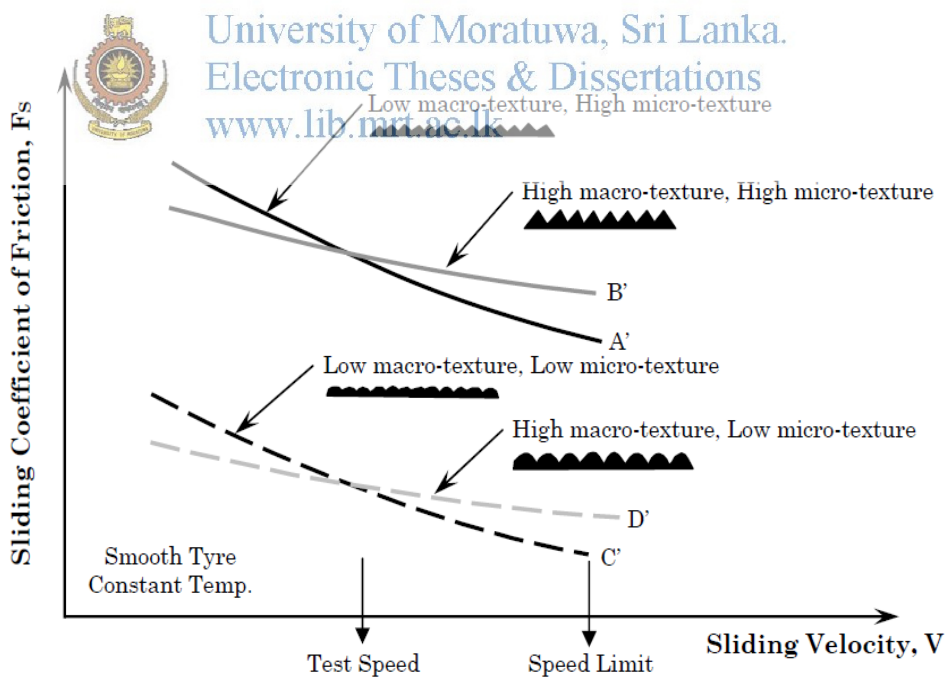


Figure 2.316 Effect of micro-texture and macro-texture on pavement–tire friction at different sliding speeds [16].

## Factors Affecting Texture

The factors that affect pavement surface texture, which relate to the aggregate, binder, and mix properties of the surface material and any texturing done to the material after placement, are as follows [16]:

- **Maximum Aggregate Dimensions**—The size of the largest aggregates in an asphalt concrete (AC) or exposed aggregate PCC pavement will provide the dominant macro texture wavelength, if closely and evenly spaced.
- **Coarse Aggregate Type**—The selection of coarse aggregate type will control the stone material, its angularity, its shape factor, and its durability. This is particularly critical for AC and exposed aggregate PCC pavements.
- **Fine Aggregate Type**—The angularity and durability of the selected fine aggregate type will be controlled by the material selected and whether it is crushed.
- **Binder Viscosity and Content**—Binders with low viscosities tend to cause bleeding more easily than the harder grades. Also, excessive amounts of binder (all types) can result in bleeding. Bleeding results in a reduction or total loss of pavement surface micro-texture and macro-texture. Because binder also holds the aggregate particles in position, a binder with good resistance to weathering is very important.
- **Mix Gradation**—Gradation of the mix, particularly for porous pavements, will affect the stability and air voids of the pavement.
- **Mix Air Voids**—Increased air content provides increased water drainage to improve friction and increased air drainage to reduce noise.
- **Layer Thickness**—Increased layer thickness for porous pavements provides a larger volume for water dispersal. On the other hand, increased thickness reduces the frequency of the peak sound absorption.
- **Texture Dimensions**—The dimensions of PCC tinning, grooving, grinding, and turf dragging affect the macro-texture, and therefore the friction and noise.
- **Texture Spacing**—Spacing of transverse PCC tinning and grooving not only increases the amplitude of certain macro-texture wavelengths, but can affect the noise frequency spectrum.



- Texture Orientation—PCC surface texturing can be oriented transverse, longitudinal, and diagonally to the direction of traffic. The orientation affects tire vibrations and, hence, noise.
- Isotropic or Anisotropic—Consistency in the surface texture in all directions (isotropic) will minimize longer wavelengths, thereby reducing noise.
- Texture skew—Positive skew results from the majority of peaks in the macro texture profile, while negative skew results from a majority of valleys in the profile.

### 2.3.8 Friction and texture measurement methods

Many different types of equipment have been developed and used to measure these properties, and their differences (in terms of measurement principles and procedures and the way measurement data are processed and reported) can be significant.

In general, the measurement devices requiring lane closure are simpler and relatively inexpensive, whereas the highway-speed devices are more complex, more expensive, and require more training to maintain and operate. With the recent development of technology in data acquisition, sensor technology, and data processing power of computers, the once true superiority of data quality for the stationary and low-speed devices is diminishing [14]. The resolution and accuracy of the data acquired from low-speed or stationary devices can still supersede that of the high-speed devices, but with smaller and smaller margins.

#### Friction

The two devices commonly used to measure pavement friction characteristics in the laboratory or at low speeds in the field are the British Pendulum Tester (BPT) (AASHTO T 278 or ASTM E 303) and the Dynamic Friction Tester (DFT) (ASTM E 1911). Both these devices measure frictional properties by determining the loss in kinetic energy of a sliding pendulum or rotating disc when in contact with the pavement surface. The loss of kinetic energy is converted to a frictional force and thus pavement friction. These two methods are highly portable and easy to handle. The DFT has the added advantage of being able to measure the speed dependency of the pavement friction by measuring friction at various speeds [16].

High-speed friction measurements utilize one or two full-scale test tires to measure pavement friction properties in one of four modes: locked-wheel, side-force, fixed-slip, or variable slip [16]. And confirmed by the state survey conducted in this study, the most common method for measuring pavement friction in the U.S. is the locked wheel method (ASTM E 274). This method is meant to test the frictional properties of the surface under emergency braking conditions for a vehicle without anti-lock brakes. Unlike the side-force and fixed-slip methods, the locked-wheel approach tests at a slip speed equal to the vehicle speed, this means that the wheel is locked and unable to rotate [16].

The results of the locked-wheel test are reported as a friction number (FN, or skid number [SN]), which is computed using the following equation: [16]

$$FN(V) = 100\mu = 100 \times (F/W) \text{-----}6$$

Where:  $V$  = Velocity of the test tire, mi/hr.  
 $\mu$  = Coefficient of friction

$F$  = Tractive horizontal force applied to the tire, lb.

$W$  = Vertical load applied to the tire, lb.

Locked-wheel friction testers usually operate at speeds between 40 and 60 mi/hr (64 and 96 km/hr). Testing can be done using a smooth (ASTM E 524) or ribbed tire (ASTM E 501). The ribbed tire is insensitive to the pavement surface water film thickness; thus it is insensitive to the pavement macro-texture. The smooth tire, on the other hand, is sensitive to macro-texture.

The side-force method (ASTM E 670) measures the ability of vehicles to maintain control in curves and involves maintaining a constant angle, the yaw angle, between the tire and the direction of motion. The side-force coefficient (SFC) is calculated as follows:

$$\text{SFC}(V, \alpha) = 100 \times (\text{FS}/W) \text{-----}7$$

Where: V = Velocity of the test tire, mi/hr.

$\alpha$  = Yaw angle.

FS = Force perpendicular to plane of rotation, lb.

W = Vertical load applied to the tire, lb.

Since the yaw angle is typically small, between 7.5 and 20°, the slip speed is also quite low; this means that side-force testers are particularly sensitive to the pavement micro-texture but are generally insensitive to changes in the pavement macro-texture.

The two most common side-force measuring devices are the Mu-Meter and the Side-Force Coefficient Road Inventory Machine (SCRIM). The primary advantage offered by side-force measuring devices is the ability for continuous friction measurement throughout a test section [16]. This ensures that areas of low friction are not skipped due to a sampling procedure.

 University of Moratuwa, Sri Lanka.  
Electronic Theses & Dissertations  
[www.lib.mrt.ac.lk](http://www.lib.mrt.ac.lk)

#### Texture

Texture measuring equipment requiring lane closures include the sand patch method (SPM) (ASTM E 965), the outflow meter (OFM) (ASTM E 2380), and the circular texture meter (CTM) (ASTM E 2157).

The SPM is a volumetric-based spot test method that assesses pavement surface macro texture through the spreading of a known volume of glass beads in a circle onto a cleaned surface and the measurement of the diameter of the resulting circle. The volume divided by the area of the circle is reported as the mean texture depth (MTD) [14].

The OFM is a volumetric test method that measures the water drainage rate through surface texture and interior voids. It indicates the hydroplaning potential of a surface by relating to the escape time of water beneath a moving tire. The equipment consists of a cylinder with a rubber ring on the bottom and an open top. Sensors measure the time required for a known volume of water to pass under the seal or into the

pavement. The measurement parameter, outflow time (OFT), defines the macro-texture; high OFTs indicating smooth macro-texture and low OFTs rough macro-texture. The CTM is a non-contact laser device that measures the surface profile along an 11.25-in (286-mm) diameter circular path of the pavement surface at intervals of 0.034 in (0.868 mm). The texture meter device rotates at 20 ft/min (6 m/min) and generates profile traces of the pavement surface, which are transmitted and stored on a portable computer. Two different macro-texture indices can be computed from these profiles—mean profile depth (MPD) and root mean square (RMS). The MPD, which is a two-dimensional estimate of the three-dimensional MTD (Flintsch et al., 2003), [16] represents the average of the highest profile peaks occurring within eight individual segments comprising the circle of measurement. The RMS is a statistical value, which offers a measure of how much the actual data (measured profile) deviates from a best-fit (modeled profile) of the data [16].

### **Friction Number**

The Friction Number (FN) (or Skid Number [SN]) produced by the ASTM E 274 locked wheel testing device represents the average coefficient of friction measured across a test interval. It is computed using equation 6, given previously. The reporting values range from 0 to 100, with 0 representing no friction and 100 representing complete friction. FN values are generally designated by the speed at which the test is conducted and by the type of tire used in the test. For example, FN40R = 36 indicates a friction value of 36, as measured at a test speed of 40 mi/hr (64 km/hr) and with a ribbed (R) tire. Similarly, FN50S = 29 indicates a friction value of 29, as measured at a test speed of 50 mi/hr (81 km/hr) and with a smooth (S) tire [16].


## **2.4 Tyre abuses**

It was received huge amount of claim regarding rapid wearing of tyre from different places of world the lack of available correct testing method was one of major reason for receive that claim details bellow listed.

Table 2.41 Tyre claim against tyre sizes

Tyre size	Manufacturing year				Total
	2008	2010	2011	Year unidentified	
15x41/2-8		2	12	2	16
16x6x101/2				4	4
18X7-8		3	8	1	12
200/50-10			5		5
21x7-15				4	4
21x8-15				2	2
21X8-9		2			2
23X9-10	1	2		7	10
27X10-12			6		6
28X9-15			6	1	7
300-15				2	2
5.00-8			19		19
6.00-9		5	17	3	25
6.50-10			14	2	16
7.00-12	3		9	1	13
8.25-15			3		3
Total	4	14	99	29	146

Table 2.42 Tyre claim against country basis



University of Moratuwa, Sri Lanka.  
Electronic Theses & Dissertations  
www.lib.mrt.ac.lk

Country	Manufacturing year				Total
	2008	2010	2011	Year unidentified	
Netherlands			2		2
Italy	3		4	1	8
France	1	1			2
Germany		1	8	10	19
UK		3	71	16	90
South Africa			1	1	2
Saudi Arabia		5	2		7
Origin was not available			2		2
New Zealand		2	2		4
USA		2	7	1	10
Grand Total	4	14	99	29	146

Actual situation in the market is much more critical than the figures listed in above as immediate action company hold suspected tyre stock then analyze one by one each factor bellow listed,



1. Tyre design: this was old and market well recognize then can be seen this had dramatic increase in 2011 therefore this should be not a main reason for increase claim
2. Customer fault: this can be possible although same customer was not claim in each year they were more than five years old,
3. Tyre production process fault: that is if tyre was not unloaded at correct time after curing was completed then there was possibility to drop compound abrasion property although process was not changed that's very old process used in this company therefore probability of occurrence was comparatively low,
4. Finally suspect about compound formulation this was not easy to change or study because this available company unique secretes although from this identify material changes during this period fairly parallel to suspected defect then gather abrasion results from different field testing and lab testing for complete study pass more than six month then identify used of reclaim rubber into tyre tread was effect to drop abrasion property while running with load and speed that's mean due to load and speed tyre temperature increase during this period effect to sudden failure of tyres. Bellow listed each suspect material and there consumption with month

Table 2.43 Claim tyre production date and raw material

Claim Tyre Production Date-year 2011	Reclaim supplier and quantity (Kg)
19-Feb	DSI-2017 & Balagi-1992
25-Feb	DSI-2310 & Alum -1660
10-Mar	Alum-1410 & Sun -1250
16-Mar	Alum-980 & Sun 920
16-Mar	Alum -980 & Sun-920
16-Mar	Alum-1310 & DSI 125
18-Mar	DSI-6806 & Sun -1100
20-Mar	Alum- 1476 & Sun -1750
21-Mar	Alum -1178 & Sun -720
23-Mar	Alum- 1706 & Sun -1100
3-Apr	Alum-1360 & DSI- 1200
6-Apr	Alum -980 & DSI- 953
21-Apr	Alum-2250 & DSI -2380

Until receive this claim company should not aware about this situation analyzing and finding of problem cannot stop loosing of valuable customers after this scenario company loss most of their loyal customers and work hard to survive in the market after that company over design its compound formulation into very high abrasion resistance one question is why company used reclaim rubber (reclaim rubber is a substitution for rubber to certain degree, this produced from tyre recycling that called de-vulcanizing of rubbers) in to tyre compound the reason is make cheap more price competitive tyre in the market then what will be the reason for failure that is lack of testing whether this should be properly fitted to selected application and can be identify real working back ground before release to commercial production this project is base on this that is most of tyre raw material price increase day by day alternative or substitute material can be used if testing facility is available in current system required more than six month to get results sometimes accuracy also cannot be assured.



University of Moratuwa, Sri Lanka.  
Electronic Theses & Dissertations  
[www.lib.mrt.ac.lk](http://www.lib.mrt.ac.lk)

## CHAPTER 3

### 3. SPECIFIC SOLID TYRES

#### 3.1. Solid resilience tyres

Solid Tyres are best for tough applications on slow vehicles or trailers with a high risk of impact and cut damage. They are extremely stable, puncture resistant and maintenance free. Solid tyres have a high load capacity and are extremely economical, ideal for all types of forklift trucks.

This had some special features that is

- can be fitted on pneumatic-tyre rims
- clean tyres designed for minimum floor marking in dust sensitive applications that is tyre color is white
- robust sidewall
- easy to fit with SIT-retaining bead (only for SIT-Tyres this is kind of rim design special used for solid tyres)

This can be further categorised in to below groups,



University of Moratuwa, Sri Lanka.  
Electronic Theses & Dissertations  
[www.lib.mrt.ac.lk](http://www.lib.mrt.ac.lk)

#### **Antistatic tyres**

Tyre is produced with a special compound. This could be used in high risk operating environments such as

Explosives or ammunition stores, where the constant risk of fire or explosion is high.

Eg. Paint and varnishing industries, Pyrotechnical industries, Chemical industry etc.

#### **Non-marking tyres**

These tyres are also produced with the popular special compounds. Non-Marking Tyres are often used in the food, chemical, pharmaceutical and paint industries due to hygiene factors. Non-Marker tyre avoids marking floor surfaces. It also eliminates the problem of worn black tread crumb being attracted to the static charge created by shrink wrapping machine.

The white side wall and the tread compounds of this tyre eliminate black driving and braking marks and residue caused by tyre wearing, which contributes to a cleaner

working environment. Performance is equivalent to black tyre in terms of good traction, low rolling resistance, low heat build –up and optimum tread life.

### 3.1.1. Tyre construction

This is generally a split between three and two stage construction. Tyre consists of three stages is the most sophisticated and technically advanced tyre targeted towards high speed (hard) applications covering long distances for sustained periods.

Most of customers are designed with fully tested advanced three layers and with creel beads which ensures secure wheel and rim fitment for all forklifts, trailers and other related applications. Base, center and tread layers are carefully developed to be well suited to each other and the tyre architecture assures excellent comfort, low rolling resistance, reduced heat buildup and a long lasting life time.

#### Tread area and sidewall protection

The tread area is exceptionally tough and wear resistant, giving the tyre a long service life (see picture 3.1.1).

#### Cushion compound

The whole structural and material content of the tyre guarantees not only good impact and vibration-damping properties but also allows rolling resistance

#### Tyre base

The tyre base is made of a hard tough compound in which the wire cores are embedded, ensuring the tyre sits firmly on the rim.

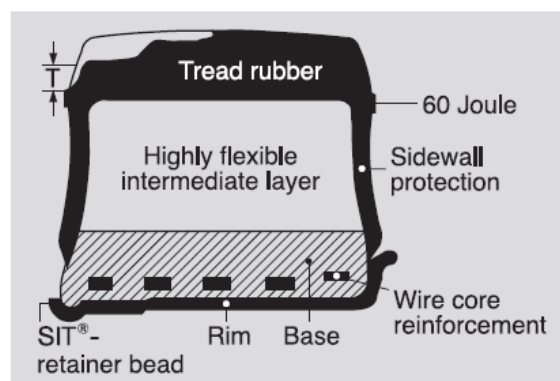


Figure 3.1.1 [11]

**Technical specification for solid resilience tyres**

Table 3.1.1[11] Solid tyre technical specification



University of Moratuwa, Sri Lanka.  
Electronic Theses & Dissertations  
[www.lib.mrt.ac.lk](http://www.lib.mrt.ac.lk)

### 3.2. Press on band tyres

Press on band tyres are produced with large footprint area, low heat buildup and low rolling resistance. Press on band tyre is also available in special compounds namely non-marking white. Puncture proof, high load capacity and square tread profile ensuring good stability are the features and benefits that manufactures offers to Press on Band users.

Table 3.2.1 [11] Press on band technical specification

Tyre Size		Kg/ Tyre	Kg/ Tyre	Kg/ Tyre
		Ultimate with steel band	SM with Steel band	Lug with Steel band
Inch	mm			
10x4x6 1/2	254/102-165		5.7	
10x5x6 1/2	254/127-165		7.4	
13 1/2x4 1/2x8	343/114-203		10.1	
13 1/2x5 1/2x8	343/140-203		13.3	
13 1/2x6 1/2x8	343/165-203		16.5	
14x4 1/2x8	356/114-203		11.4	10.9
14x5x10	356x127-254		11.5	
15x5x11 1/4	381/127-286		12.4	
15x6x11 1/4	381/152-286		14.8	
16x5x10 1/2	406/127-267		14.7	14.4
16x6x10 1/2	406/152-267		17.9	17.9
16x7x10 1/2			21.4	
16 1/4x5x11 1/4	413/127-286		14.1	
16 1/4x6x11 1/4	413/152-286		17.5	17.0
16 1/4x7x11 1/4	413/178-286		21.0	
18x5x12 1/8	457/127-308		17.3	
18x6x12 1/8	457/152-308	21.4	20.8	20.0
18x7x12 1/8	457/178-308	24.5	24.2	23.8
18x8x12 1/8	457/203-308		27.7	27.2
18x9x12 1/8	457/229-308			31.1
21x6x15	533/152-381			25.0
21x7x15	533/178-381	30.1	30.7	29.5
21x8x15	533/203-381	34.3	35.0	34.1
22x8x16	559/203-406		40.1	38.7
22x9x16	559/229-406	45.1	44.9	44.1
22x12x16	559/305-406		60.5	
22x16x16	559/406-406			
28x10x22	711/254-559		67.0	
28x12x22	711/305-559		81.1	
40x16x30	1016/406-762		225.5	230
40x16x30	1016/406-762		225.5	230

Load Capacity (Kg) at max. speed				Tire load capacity on forklifts at Max. Speed			
				10 Miles/h (Lbs)		16 Km/h (Kg)	
6 km/h	10 km/h	16 km/h	20 km/h	Load wheel	Steer wheel	Load wheel	Steer wheel
850	640	510	420	1530	1290	695	585
995	795	500	500	1995	1675	905	760
				2205	1850	1000	840
1350	1075	810	680	2965	2490	1345	1130
				3240	2710	1470	1230
1150	920	690	580	2300	1930	1045	875
				2648	2207	1200	1000
				2735	2305	1240	1045
				3385	2845	1535	1290
1350	1075	810	680	2965	2490	1345	1130
1575	1250	950	790	3770	3165	1710	1435
1800	1450	1075	900	4563	3836	2070	1740
1375	1100	825	690	3000	2525	1360	1145
1600	1275	960	800	3780	3175	1715	1440
1825	1450	1100	910	4555	3825	2065	1735
1500	1200	900	750	3230	2710	1465	1230
1750	1400	1050	880	4120	3470	1870	1575
2000	1600	1200	1000	5925	4220	2280	1915
2280	1825	1370	1140	5920	4970	2685	2255
2560	2050	1535	1280	6810	5720	3090	2595
2100	1675	1250	1050	4640	3890	2105	1765
2400	1925	1450	1200	5645	4740	2560	2150
2700	2150	1625	1350	6660	5590	3020	2535
				6900	5790	3130	2625
				7950	6670	3605	3025
4275	3300	2475	2075	11090	9315	5030	4225
8315	6095	5540	4155	13850	11640	6925	5820
				10285	8290	4665	3760
				12135	10230	5505	4640
12905	9195	8065	6450	21610	17740	10805	8870

## CHAPTER 4

### 4. TESTING METHODS

#### 4.1 Abrasion testing of rubber compound

DIN Abrasion Tester:

The method conforming to DIN 53516 / DIN ISO 4649 has proven to be the best way of simulating long term wear. This method enables comparative tests for the control of the uniformity of a specific material. The achieved test results provide important parameters in respect to the wear of elastomers in practical use.

General Machine specification is listed below

Table 4.1.1 DIN abrasion tester specification [18].

Weight	2.5±0.1 N; 5±0.1 N; 10.0±0.2 N
Rubbing length	40 ± 0.2 m
Lateral displacement of damp	4.20±0.04 mm (Drum rotates 1 cycle)
Sandpaper	60# Grain, Average thickness 1 ± 0.2 mm
Abrasion Path	40m / 20m correspond to rotations of the drum
Cylinder revolution	40 ± 1 rev/min
Test Method	Rotation and non-rotation
Dimension (W×D×H)	75 × 42× 40 cm
Weight	60 kg
Power	1φ,AC220 V, 50 Hz (Specified by user)

Machine picture is listed bellow part A is hold test specimen this size is standard that should be cut from standard die before operation start weight of specimen was measured, part B is sand paper after operation start test specimen press to sand paper that is rotating when that reach from left end to right end test should be over after that weight loss will be calculated,

Abrasion value should be calculated according to standard given formula,

Volume loss = weight loss of sample (mg) x 200/ (specific gravity x weight loss of reference sample)



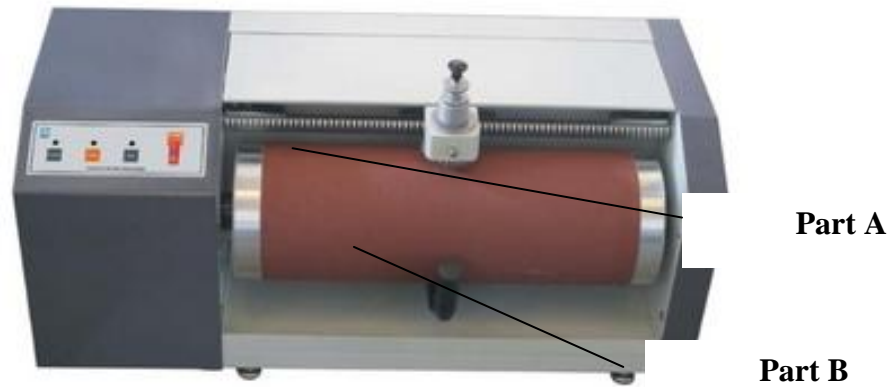


Figure 4.1.1 DIN abrasion tester [18].

#### 4.2 Tyre field testing

This is kind of test should be conducted in condition of actual load and speed here required tyres should be mounted in to forklift (there are different kind of vehicle available although in Sri Lanka it is available this type of testing vehicle only.) where selected test location after that initial meter reading was recorded testing speed and testing load should be recorded until test will be completed this should be observed and monitored in chapter 5 test results are further elaborated.



University of Moratuwa, Sri Lanka.  
Electronic Theses & Dissertations  
[www.lib.mrt.ac.lk](http://www.lib.mrt.ac.lk)

#### 4.3 Drum testing

From this testing it should be not possible to analyze about abrasion of tyre this is basically used to analyze rolling resistance heat build-up run time and deflection of tyres.



Figure 4.3.1 Drum testing machine [19].

Design Standard: SAE J1987--Force and Moment Test Method SAE J1106--  
Laboratory Testing Machines for Measuring the Steady State Force and Moment  
Properties of Tires. Test machine consists of main machine, motor driving system,  
hydraulic load system and control system. The drum surface is coated with high anti-  
wearing material such as SiO<sub>2</sub>, which is driven by DC motor and controlled by  
Siemens SIMOREG DC Master. Loading and positioning system is driven by  
hydraulic servo system in closed-loop control. Positioning system consists of two  
transmission systems. Measuring system is of high technology, which can be  
controlled by PLC and IPC, and which completes with transducers and electronic  
chipset [19].

This machine completes with measuring and recording functions, which can measure  
the normal force ( $F_z$ ), lateral force ( $F_y$ ), aligning moment ( $M_z$ ), slip angle ( $\alpha$ ),  
loaded radius ( $R$ ), Longitudinal force ( $F_x$ ), overturning force ( $M_x$ ), and rolling  
moment ( $M_y$ ).

Some standard specific information listed below,  
Driving method: Drum driving

Brake method: tire braking

Multi-moment force sensor: Mount on the non-center tire plane

Drum outside diameter:  $\Phi$  3000

Drum width: 500 mm

Tire Diameter: 8"~24"

Drum surface: coating in 80 mesh grinding material,

Drum circumferential speed and accuracy: 0~120 km/h,  $\pm 1$  km/h

Tire max outside diameter:  $\Phi$  1000

Tire max unloaded radius: 500 mm, accuracy  $\pm 1.0$  mm

Tire min unloaded radius: 250 mm, accuracy  $\pm 1.0$  mm

Rim min nominal diameter: 13"

Tire max width: 400 mm

Tire max test air pressure: 1000 kPa

Tire max test load & accuracy: 50 kN  $\pm 500$  N

Tire camber range:  $\pm 15^\circ$ , accuracy  $\pm 0.05^\circ$

Camber angle changing speed: 2°/sec

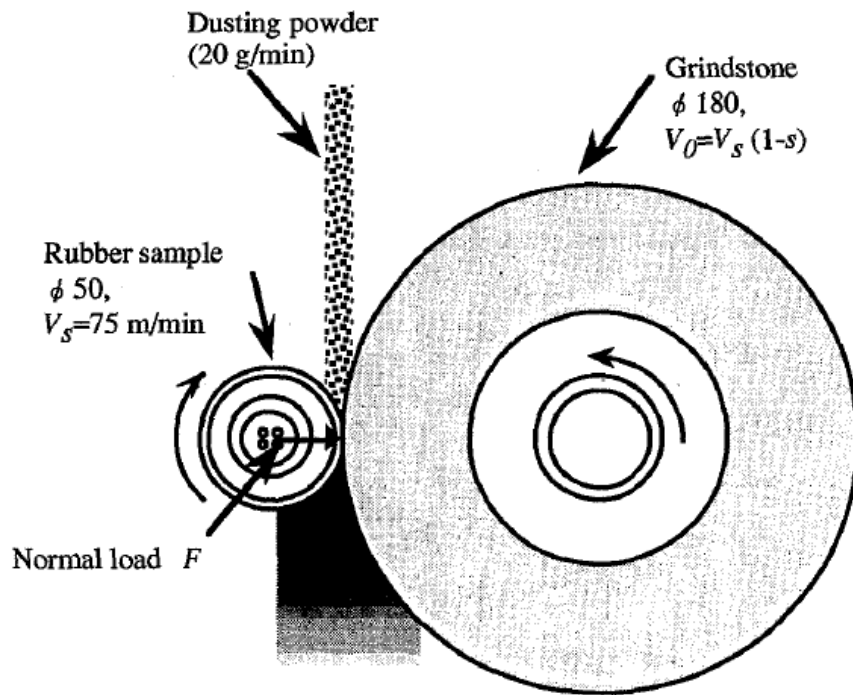
Camber angle changing style: changing in step

Machine Total Weight: Approx. 62 t [19]



#### 4.4 Tyre wear life tester

The authors analyzed the causes that the tyres were lives estimated by the current test method are not always correct, and found that the correct lives are given only under the premise that the wear rate ratio of tested tyre is always constant under any condition. With regards to the tyre tread rubber compounds, the Lambourn type wear test were carried out. These tests have made it clear that the normal load or the surface roughness of the grindstone changes, namely the above mentioned assumption does not always come into existence. In these cases, were test must be carried out under the equivalent condition to the real world. The test conditions of lambourn-type wear test were investigated in order to reproduce the wear mode of the tyres collected from the field. The grindstone of # 240 or more smooth and the slip ratio of 2% or so are predicted to be desirable, but further investigations are needed to find the optimum conditions.



University of Moratuwa, Sri Lanka.  
Electronic Theses & Dissertations

www.lib.mrt.ac.lk

Figure 4.4 Tyre wear life tester [8]  
Table 4.4.1 Test results s-slip ratio % and F- normal load N [8]

Rubber	Item abrader	Wear rate $M$ ( $10^{-3}$ cc / min)								Surface roughness $Ra$ ( $\mu\text{m}$ )							
		#80				#220				#80				#220			
		$F$	$s$	6	12	24	50	6	12	24	50	6	12	24	50	6	12
H	15	----	1.68	12.2	34.9	----	3.25	9.12	14.0	----	4.95	6.24	5.79	----	2.16	2.39	2.51
	30	----	2.61	30.1	61.6	0.87	5.63	18.7	38.1	----	5.06	8.80	6.64	3.63	2.49	3.29	3.06
L	15	0.26	1.89	11.8	32.2	----	2.80	7.84	13.4	2.52	4.89	5.85	5.30	----	2.14	2.00	1.86
	30	0.40	3.52	27.4	53.4	1.01	5.71	17.8	32.4	3.07	6.39	6.73	7.16	2.24	2.17	2.74	2.46

Table 4.4.2 surface roughness  $Ra$  for aggregate [8]

Aggregate	$Ra$ ( $\mu\text{m}$ )
Basalt	12.5
Diabase	8.1
Diarite	10.9
Sandstone	9.9
Pea Gravel	3

#### 4.5 Advances in indoor tire tread wear simulation

There are many reasons for conducting tire wear testing on test machines in the laboratory as opposed to vehicle testing on proving grounds or public road courses. Indoor testing offers consistency and well-defined tire force sequences, consistency of the abrasive surface, a controlled environment, and opportunities for test acceleration. Factors such as vehicle and suspension differences, driver characteristics, weather, differences in pavements, etc. can make it difficult to evaluate changes in tire constructions or materials using outdoor vehicle wear testing. Indoor tests can often be run in a week as opposed to one or more months for fleet tests or a year or more for commercial tests

It is highly desirable to characterize the tire force component of a wear route or course independently of a specific vehicle. If the course signature is independent of the vehicle, then it is necessary to only characterize it once. Commercial and fleet wear tests not only have very prescribed details for the route but also for the vehicle velocity on each and every part of the route. This requirement prevents a test driver, for example, of a sports car from driving any differently than the test driver of a light truck. When both route and vehicle velocity are fixed and controlled, then the accelerations are relatively free of the influence of a specific driver or vehicle. By recording the signals based on distance traveled as opposed to time, the post processing required to create the drive files for the test machine becomes more straightforward. For example, data will not be recorded when the test vehicle is at a stop light. Tire wear is a primarily a function of distance traveled, not time.

The course characterization method consists of the measurement of four signals at the center of gravity (CG) of the vehicle; accelerations in the fore/aft ( $A_x$ ), lateral ( $A_y$ ), and normal ( $A_z$ ) direction, and the vehicle forward velocity ( $V_x$ ) as illustrated in Fig.4.5 1. One of the wear courses that have been characterized with this method is the National Highway and Traffic Administration's UTQG route in the San Angelo, TX area . Even though the real-time sequential file is used for input to the simulation process, the "signature" of the 640 km course is best viewed as

histograms of  $A_y$  and  $A_x$  accelerations as in Fig. 4.5.1. The acceleration data is plotted with respect to the log of the percent occurrence. This allows the less frequent occurring events, but yet very important for tire wear, to be clearly viewed as part of the course “signature”. Even more descriptive, however, is the 2-D histogram shown in Fig. 4.5.2 where the two accelerations are plotted together using contours to represent the log frequency of occurrence. Positive lateral accelerations represent cornering right, negative represent cornering left, positive fore/aft accelerations represent vehicle accelerations, and negative represents vehicle braking.

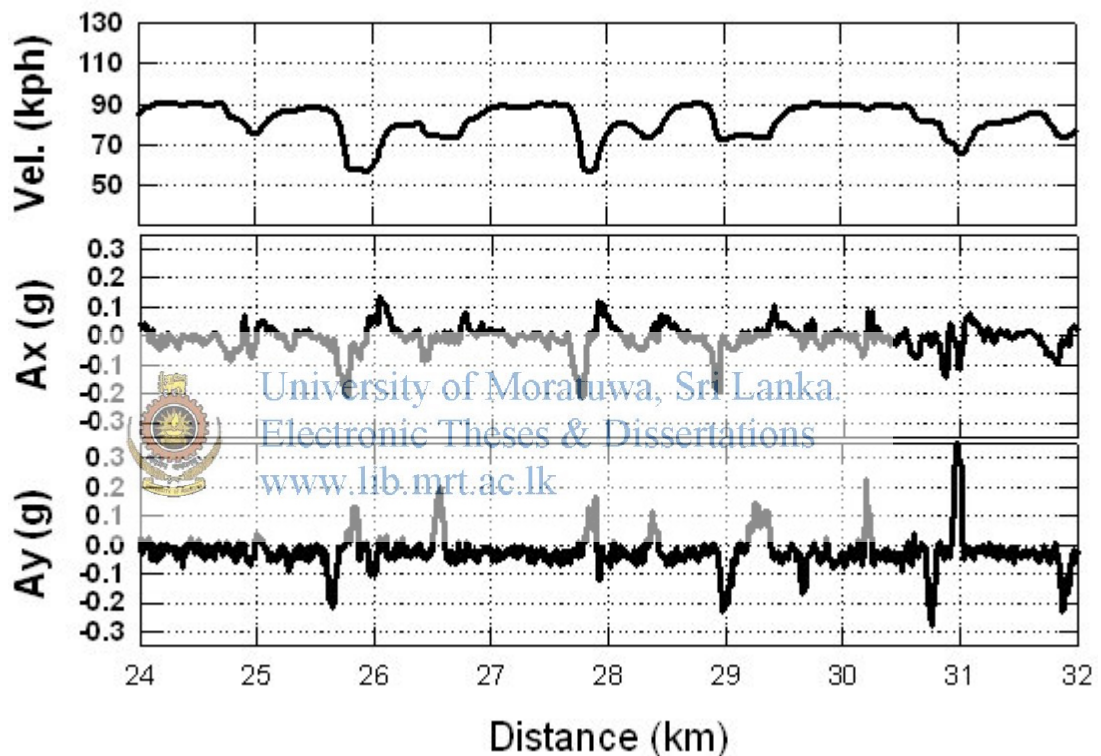


Figure 4.5.1 Advance tyre wear simulation graph [5].



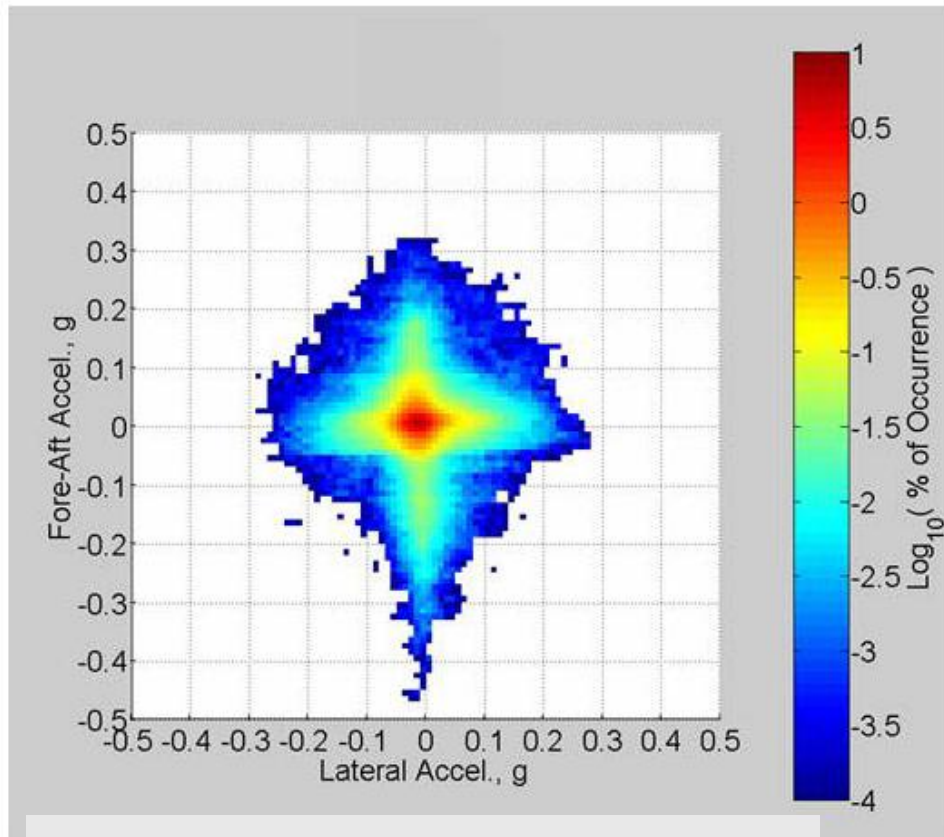


Figure 4.5.2: Advanced hydro wear simulation results [5].

Electronic Theses & Dissertations  
[www.lib.mrt.ac.lk](http://www.lib.mrt.ac.lk)

A second wear route will also be used to illustrate the capability of the TS/Sim model to capture differences in tire wear as a result of the wear route. This wear route is a proving ground route consisting of low speed city cornering and track driving. Fig. 4 shows the signature of this route to be predominately lateral accelerations and steady-state track driving which is almost totally void of fore-aft accelerations. The vehicle velocity and normal accelerations are also important for tire wear and following sections will discuss how they are used in the TS/Sim model, however, the lateral and fore/aft accelerations are key variables for visualizing the wear route.

The basic approach to vehicle characterization for application to indoor wear testing involves the development of equations for wheel force and inclination angle (IA) prediction. It is necessary that the predictive equations provide the desired drive file variables for programming the indoor wear machine. It is also desirable that the

predictive equations utilize easily measured parameters from an outdoor wear course characterization. The use of vehicle mechanics concepts together with experimental and numerical investigations resulted in a set of suitable equations for achieving the desired goal. The example set of equations are shown in Fig. 4.5.3 for the right front (RF) and right rear (RR) positions on a compact pick-up truck.

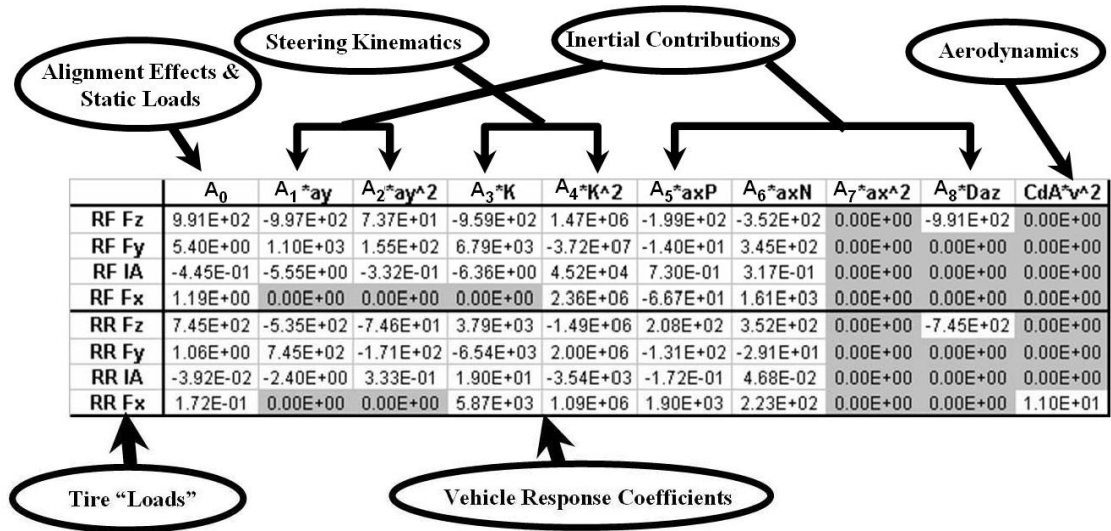


Figure 4.5.3 Vehicle mechanics programmed equation [5]



University of Moratuwa, Sri Lanka.  
Electronic Theses & Dissertations  
www.lib.mrt.ac.lk

The computed variables are those needed for driving the indoor wear machine, i.e. the three forces  $F_x$ ,  $F_y$ ,  $F_z$ , and  $IA$ . The road speed  $V_x$  is directly measured on the wear course and not computed. The model equations are expressible as algebraic polynomials in terms of five “course” variables, vehicle accelerations  $A_x$ ,  $A_y$ ,  $A_z$ , forward speed  $V_x$  and path curvature  $K$ . A measure of the front position steer angle change is needed in the characterization to account for Ackerman effects that can significantly contribute to the lateral forces,  $F_y$ , even in the absence of lateral acceleration of the vehicle. Road path curvature,  $K$ , can be used to include this effect. Experience has shown that road path curvature can be adequately approximated by simple kinematics calculations using the quotient of measured lateral acceleration and the square of the forward velocity histories. This approach eliminates the need for steering angle measurements and simplifies the course characterization. Thus the five “course” variables are reducible to four independent measured variables,  $A_x$ ,  $A_y$ ,  $A_z$  and  $V_x$ .



The coefficient matrix defines the vehicle characteristics for wheel force and inclination angle dynamics. These equations are suitable for representing effects due to static loading, suspension characteristics, inertial induced load transfer, steering geometry effects and aerodynamic contributions to load transfer and inclination angle response. These equations are intended for applications involving limited acceleration levels, generally not exceeding 0.5 g. These levels are more than adequate for representing typical wear course and consumer driving conditions of the type to be replicated on a wear drum.

A separate set of matrix coefficients are needed for each wheel position. In most cases, symmetry between the left and right side wheel positions is an acceptable approximation. The empirical method developed for computing the coefficient matrix uses least squares regression to fit the modeling equations to measured or computer simulated data. A vehicle is put through a series of maneuvers covering the range of velocities, accelerations, and path curvatures of interest. By measuring the wheel forces, inclinations angles, vehicle accelerations and speeds, data for the regression analysis is produced.



University of Moratuwa, Sri Lanka.

Electronic Theses & Dissertations

[www.lib.mrt.ac.lk](http://www.lib.mrt.ac.lk)

Alternative to making experimental measurements, a vehicle computer model such as produced with ADAMS1 or CarSim2 can be used to conduct a set of basic test maneuvers to provide the required data for the regression analysis. The TS-Sim model can then be used to extend the predictive capabilities of a traditional vehicle computer model by utilizing the course mapping variables over hundreds or thousands of miles with relative ease. "Driving" a traditional vehicle dynamics computer model over a lengthy real world course is generally not feasible. The TS-Sim model is far more computationally robust than a multi-body dynamics model and better suited for use with load frame control over lengthy test time intervals, e.g. hours or days. An efficient laboratory method has been developed for experimental vehicle characterization. The laboratory features two in-ground force and moment measurement platforms for conducting "drive by" experiments. The force platforms are used to record the left and right position tri-axial tire/ground interactive forces in each pass-by test. Straight path acceleration and deceleration tests as well as cornering on different path radii can be conducted with this facility. Typically,

foreaft and lateral accelerations over a range of  $\pm 0.5$  g are produced in the laboratory test maneuvers. Test path radii ranging from 10 m to 50 m are adequate for vehicle characterization. Typical wear courses produce conditions well within these test limits.

Laser based inclinometers are used to measure wheel inclination angles during the laboratory experiments. Accelerometers are placed near the vehicle CG and the force platforms provide a measure of vehicle speed as well as tire forces for each pass-by experiment. A total of 50 to 75 passes are normally sufficient to fully determine the force and IA response function coefficients for all four wheel positions. A vehicle can be fully characterized by this method in about a day of laboratory testing.

A method of indoor wear testing that can accurately capture tire-vehicle-course interaction is described. The method is suitable for investigating tire wear phenomena in the absence of an actual vehicle. The method has high potential for early diagnostics, optimization of the tire-vehicle system for wear performance, and for reducing test costs (i.e. no prototype vehicle or outdoor wear test is needed).



Figure 4.5.4 feature of indoor test wear equipment [5].

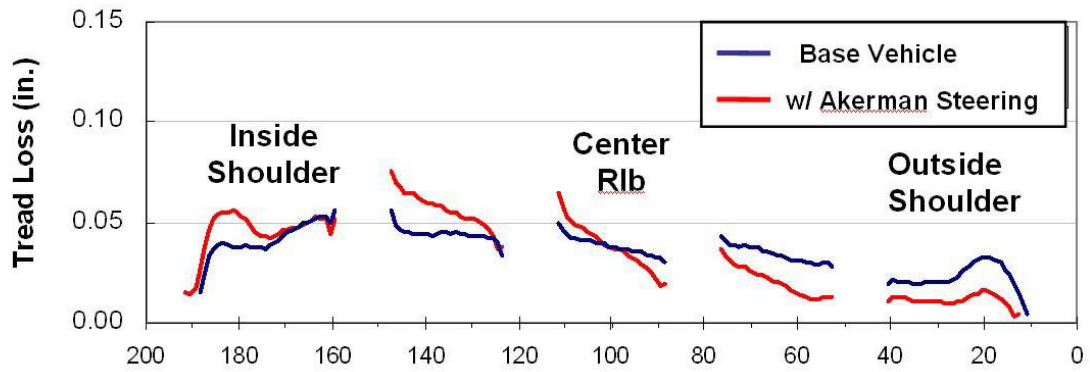


Figure 4.5.5 the effect of altering the steering curves produces higher wear rates on the inside shoulder and immediate rib with each rib wearing faster on the inner side but reduced outside shoulder wear [5].

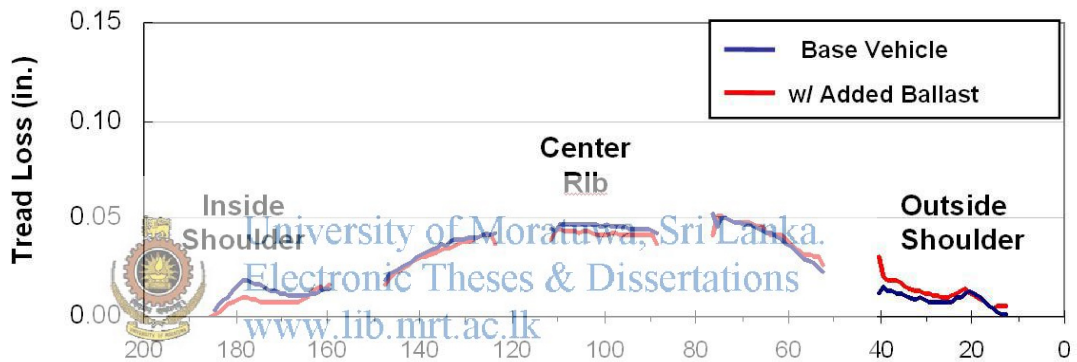


Figure 4.5.6 the tread loss profiles for the base load and ballasted load case show essentially the same wear [5].

#### 4.6 Measurement and modelling of tyre forces on a low coefficient surface

The model was used on the National Advanced Driving Simulator (NADS) for a study to investigate the safety benefits of Electronic Stability and Control (ESC) systems. The research was not to develop ESC systems, but rather to use an existing ESC system to study drivers' performances from a human factors perspective. The low coefficient of friction tire model was needed to increase the incidences of ESC activation as test subjects drove through the various NADS scenarios. The vehicle modeled was a 2002 Oldsmobile Intrigue with Goodyear Eagle RSA P225/60R16

tires. To make the NADS study realistic and useful, the vehicle dynamics model must be of high fidelity; that is, the physics predicted through the simulation should be very close to real-world experiences.

NADS vehicle dynamics have been validated with various vehicles (1994 Ford Taurus, 1998 Chevrolet Malibu, 1997 Jeep Cherokee, and 1991 GM-Volvo heavy truck with 1992 Fruehauf trailer), but not with cases involving low coefficients of friction, like driving on wet roads and ice. In order to properly model the low coefficient surface, tire tests were performed under low friction conditions. Modeling tire mechanics for vehicle dynamics relies heavily on tire testing, and most models are dominated by empirical formulations. Transportation Research Center, Inc. Using formulations and parameters obtained on dry roads, and then simply scaling the friction level and associated forces and moments to that of a lower coefficient road, is not sufficient to accurately replicate tire forces, particularly when the vehicle is operating at highway speeds. Therefore, this research involved measuring tire forces at different speeds on a low friction, wet test surface, and to developing a tire model with speed dependency. The tire model based on these measurements provides realistic forces in the linear and nonlinear range, and the peak friction is at a level where ESC engages during driving tasks specified by the NADS ESC study testing protocol.

The tyre model developed in this research was used with the existing Oldsmobile Intrigue model for the NADS ESC study. The low friction model simulation predictions were compared and validated with vehicle field experiments on the wet Jennite surface with ASTM-measured peak and sliding friction values of 40-45 and 15-20 respectively, at the Transportation Research Center, Inc. (TRC). Likewise, simulation predictions using the normal tire model were validated using vehicle field tests on the dry asphalt surfaces at TRC. For the case of the wet Jennite, slight adjustments of the peak coefficient of friction were made to narrow the differences between simulation predictions and field measurements. The validation procedures and results will be documented separately.

Figure 4.6.1 was generated from data compiled by Blythe and Day from wet tire testing that was performed at the CALSPAN Tire Research Facility (TIRF). We used the graph in Figure 4.6.1 to select the tread depth (4/32"). Figure 4.6.2 shows peak longitudinal coefficient of friction data from the 4/32" tread depth tire. The curves in Figure 4.6.2 bound our target peak friction value of about 0.5 at 50 mph. We selected a water depth of 0.05" for our tests, with the expectation that we would get similar peak longitudinal force values from our tests, suiting the needs of our driving simulator research. A tread depth of 4/32" represents a moderately well worn tire. NHTSA studies have indicated that the average tread depth for in-service tires, based on measurements made on 11,530 vehicles, to be 7/32". Shaving a tire does not produce the same effects that would come about by allowing a tire to wear down to 4/32 inches through normal use. However, for this study, only the coefficient of friction needed to be reduced.

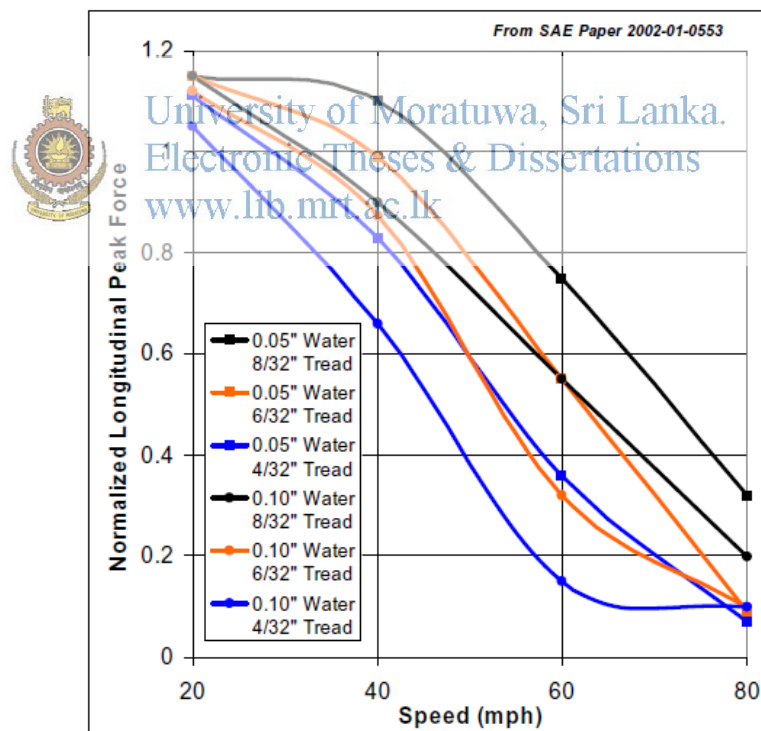


Figure 4.6.1 Peak Longitudinal Coefficient of Friction [20].

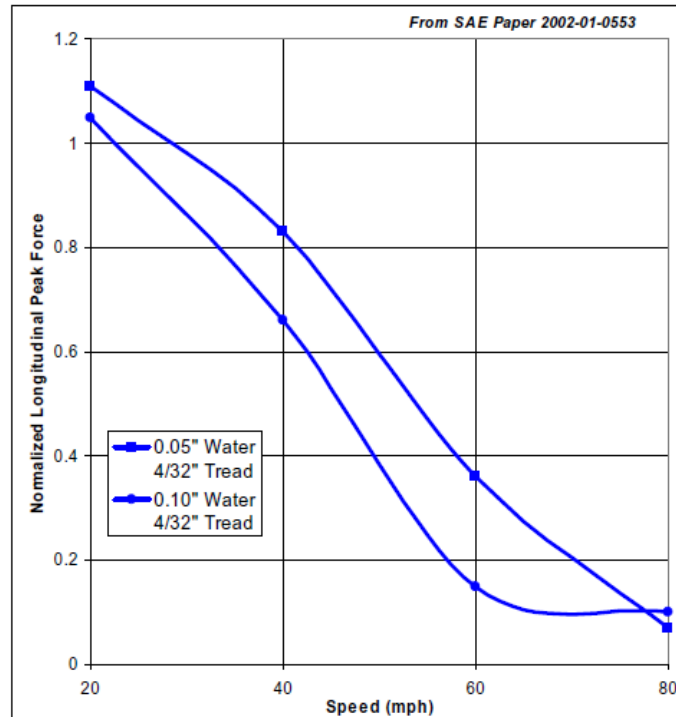


Figure 4.6.2 Peak Longitudinal Coefficient of Friction [20].

The testing included wet and dry cambering, cornering, and braking/driving test procedures. The wet and dry test programs included four test procedures: two free rolling test procedures (one cambering and one steering) and two braking/driving test procedures (one straight-line and one combined with steering). The tires used were all shaved to a tread depth of 4/32", and all had the same DOT number as indicated on Table 4.6.1. A constant water depth of 0.050" and regulated test inflation pressure of 34 psi were used throughout the test program. Each wet test was performed at four velocity conditions of 30, 45, 60 and 75 mph. All of the dry tests were performed at a single velocity of 30 mph. A reference load of 1150 lbs was used for the entire test program. The maximum test load was 200% of the reference, or 2300 lbs. Figure 3 shows a test in progress.



Table 4.6.1 Tires For CALSPAN Testing [20].

Goodyear Eagle SA P225/60R16 All Tyres Shaved to 4/32" Tread Depth All tyre Pressure at 34 psi		
Tyre No	Reference	Description
1	GY1381-DOT4304	Testing
2	GY1382-DOT4304	
3	GY1383-DOT4304	
4	GY1384-DOT4304	
5	GY1385-DOT4304	Reserve



Figure 4.6.3 Tire Test at CALSPAN [20]

Figures 4.6.4-4.6.8 show the measured and modeled lateral forces versus slip angle for the dry test (30 mph) and four wet tests done at different speeds (30, 45, 60, and 75 mph). (The 200% rated load data was not used for the 60 mph wet test.) Overall, the model does a good job of predicting the peak forces and linear range stiffnesses for all conditions, and a decent job of modeling the forces when the tires reach high slip angles.

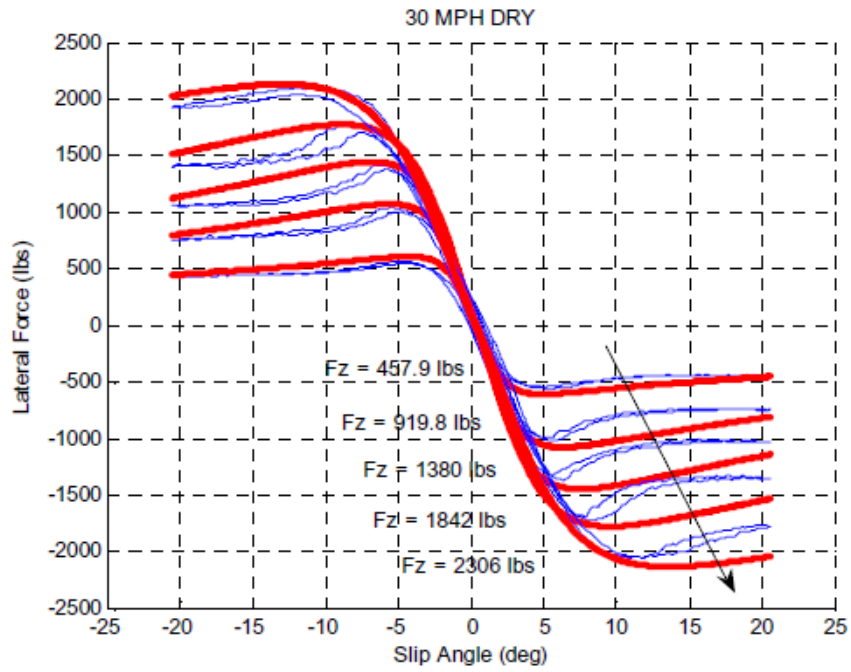


Figure 4.6.4 Lateral Forces at 30 mph Dry [20].

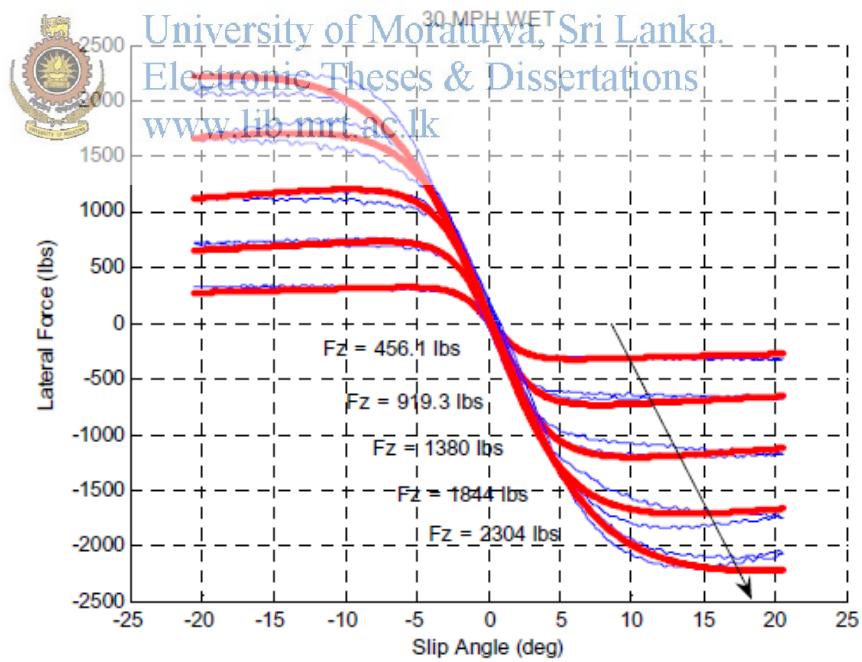


Figure 4.6.5 Lateral Forces at 30 mph Wet [20].



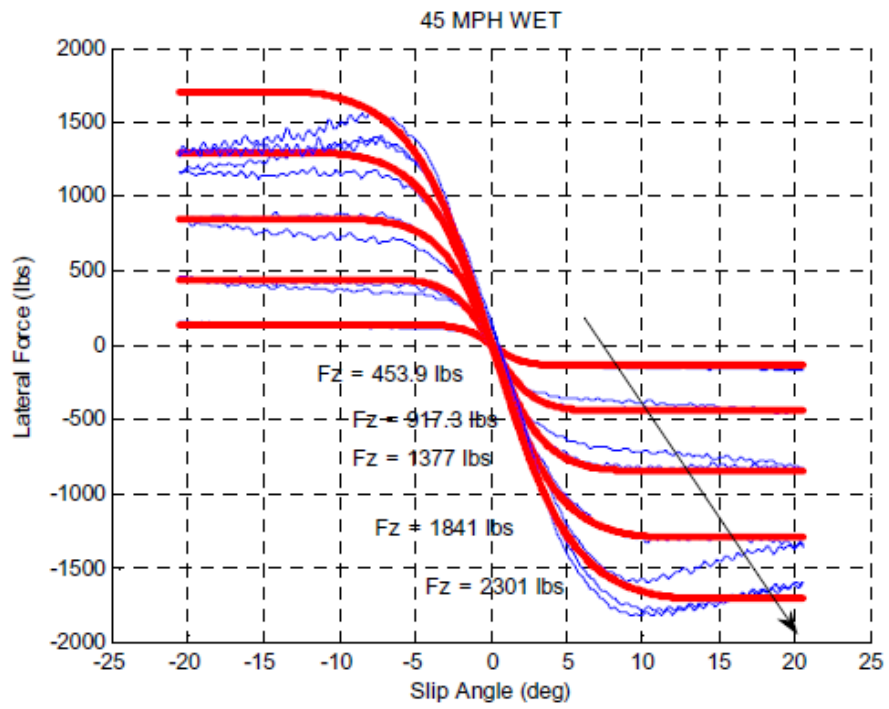


Figure 4.6.6 Lateral Forces at 45 mph Wet [20].

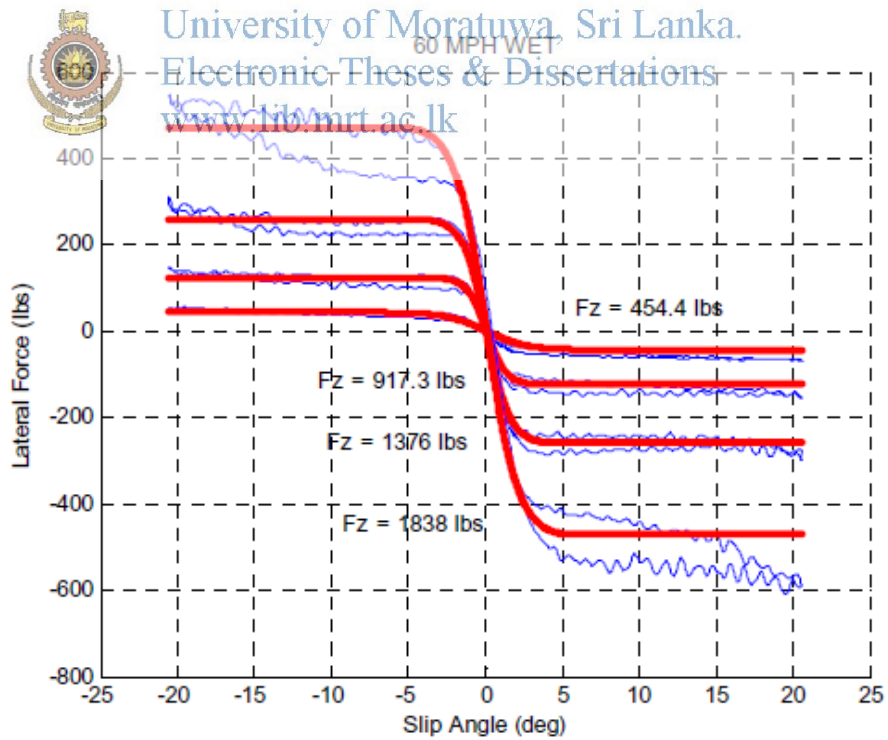


Figure 4.6.7 Lateral Forces at 60 mph Wet [20].

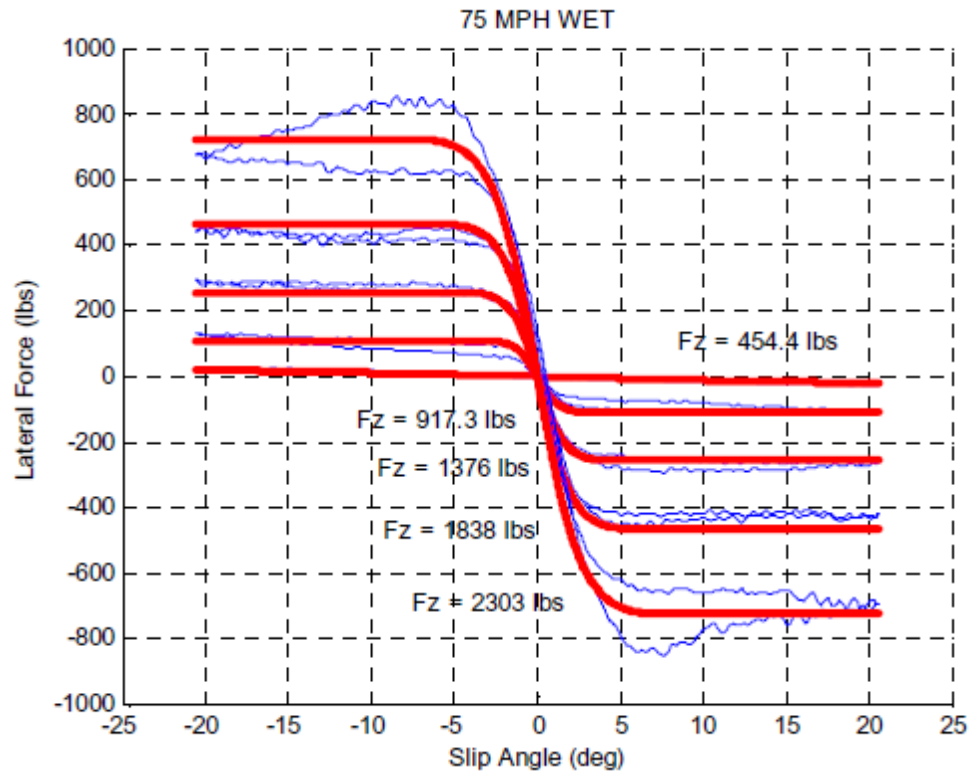


Figure 4.6.8 Lateral Forces at 75 mph Wet [20].



University of Moratuwa, Sri Lanka.

Electronic Theses & Dissertations

www.lib.mrt.ac.lk

This paper presented the results from testing shaved passenger car tires on a low-coefficient test surface. Straight-line and cornering tests were performed, yielding data for both longitudinal and lateral forces and cornering moments. Five loading conditions were used, yielding a good fit in the lateral direction and a reasonable fit in the longitudinal direction (despite some difficulties with the test procedure in this mode). One of the goals for the testing program was to find the combination of tread depth and water depth which would yield a high coefficient of friction at low speeds and a low coefficient at high speeds. This goal was accomplished. It should be noted that shaving a tire does not produce the same effects that would come about by allowing a tire to wear down to 4/32 inches through normal use. The aging effects of rubber were ignored. The tire forces and moments were then used to generate the tire parameters required by the STI tire model used by the NADS vehicle simulation dynamics. Some of these parameters include coefficients for equations describing the lateral and longitudinal peak coefficient of friction for varying loads at different speeds, effective lateral stiffness, effective aligning moment stiffness, several other

stiffnesses, and the tire saturation function. The STI model was then exercised with the generated coefficients. Overall, the model did a good job of predicting peak forces and linear range stiffnesses for all conditions, and a decent job of modeling the forces when the tires reach high slip angles.

#### **4.7 A versatile flat track tire testing machine**

A flat track tire testing machine developed by the IMMa group is described. It permits the simulation and study of the dynamic behavior of a great variety of tires under controllable and repetitive highly dynamic realistic working conditions in the laboratory for a diversity of vehicles, from motorcycles to light trucks. The machine incorporates a hydraulically operated tire support and loading system with wide operating ranges a computer controlled brake system to simulate braking maneuvers with ABS systems a complete sensorial system a data acquisition and control system continually monitoring and acting on the experimental variables, i.e., tire and belt speed, longitudinal slip, slip and camber angles, tire pressure, tire normal force, etc.

Basically, the tire testing machine (Figure 4.7.1) consists of a high stiffness tire loading and positioning assembly, a flexible closed-loop flat track system, and a specifically design data acquisition and control system. The bench is able to test solid rubber or pneumatic tires with radii within 10 to 60 cm at maximum road speeds of up to 100 km/h. It has the capacity to monitor and control a diversity of operative parameters, each varying within a wide range of values as shown in Tables 1 and 2. This is accomplished by means of a set of appropriately placed sensors and actuators, sending and receiving control signals through a specifically designed data acquisition and control system. The software required for these tasks has been developed by the research group.



University of Moratuwa, Sri Lanka.

Electronic Theses & Dissertations

www.lib.mrt.ac.lk

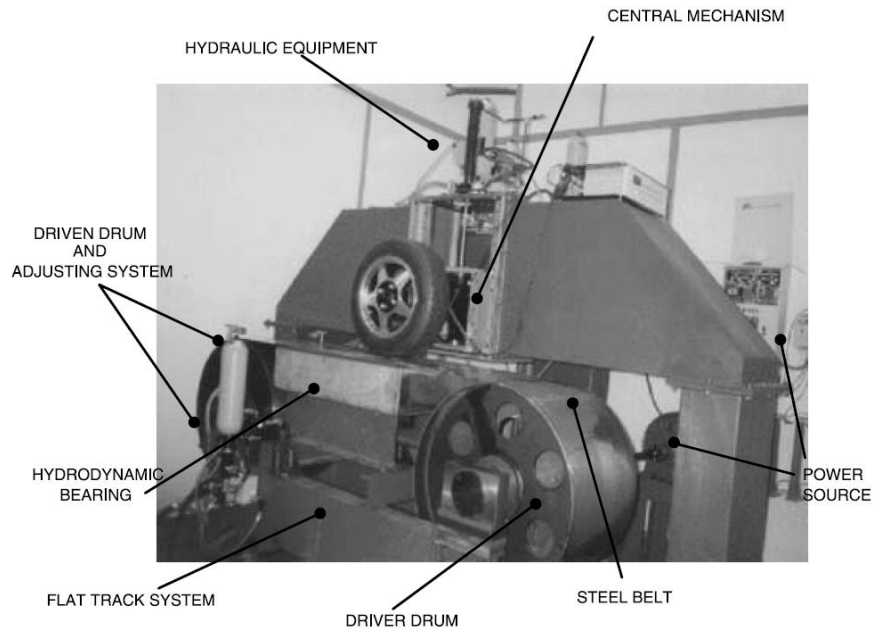


Figure 4.7.1 Dynamic tire testing machine [21].

Table 4.7.1 Output variables [21].

Output variable	Range	Kind of sensor
$Z_{ini}$ (vertical position)	0 to 350 mm.	Linear position sensor
$Y_{ini}$ (lateral position)	0 to 200 mm.	Linear position sensor
$\alpha$ (slip angle)	$-20^\circ$ to $20^\circ$	Linear position sensor
$\gamma$ (camber angle)	$-50^\circ$ to $50^\circ$	Linear position sensor
$F_{ez}$ (vertical force)	0 to 1500 kg	Pressure sensor
$F_{ey}$ (lateral force)	0 to 1500 kg	Pressure sensor
$F_x$ (tire longitudinal force)	$-1730$ kg to $1730$ kg	Force sensor
$F_y$ (tire lateral force)	$-3530$ kg to $3530$ kg	Force sensor
$F_z$ (tire vertical force)	$-1730$ kg to $1730$ kg	Force sensor
$M_x$ (tire overturning torque)	$-125$ kg m to $125$ kg m	Torque sensor
$M_y$ (tire rolling torque)	$-125$ kg m to $125$ kg m	Torque sensor
$M_z$ (tire autoaligning torque)	$-125$ kg m to $125$ kg m	Torque sensor
$a_x$ (tire acceleration X-axis)	$-5$ g to $5$ g	Acceleration sensor
$a_y$ (tire acceleration Y-axis)	$-5$ g to $5$ g	Acceleration sensor
$a_z$ (tire acceleration Z-axis)	$-5$ g to $5$ g	Acceleration sensor
$\omega$ (tire angular speed)	0 to 10000 rpm	Hall sensor
$V$ (steel belt speed)	0 to 40 m/s	Tachometer
$T_b$ (brake torque)	0 to 150 kg m	Pressure sensor
$t_n$ (tire temperature)	0 to $538^\circ\text{C}$	Infrared sensor

Table 4.7.2 Input variables [21].

Input variables	Control range	Functions
Vertical force ( $F_{ez}$ )	0 to 1500 kg	Sine-Random-Linear-Constant value
Lateral force ( $F_{ey}$ )	0 to 1500 kg	Sine-Random-Linear-Constant value
Vertical posición ( $Z_{ini}$ )	0 to 350 mm.	Sine-Random-Linear-Constant value
Lateral position ( $Y_{ini}$ )	0 to 200 mm.	Sine-Random-Linear-Constant value
Slip angle ( $\alpha$ )	$-20^\circ$ to $+20^\circ$	Sine-Random-Linear-Constant value
Camber angle ( $\gamma$ )	$-50^\circ$ to $+50^\circ$	Sine-Random-Linear-Constant value
Motor angular speed ( $\omega_m$ )	0 to 2000 rpm	Linear-Constant value
Brake Torque ( $T_b$ )	0 to 125 kg m.	Sine-Random-Linear-Constant value

All movements and forces in the machine are imposed by different components of a hydraulic system. In the described assembly, the tire displacement and rotations, vertical displacement, orientation angle and slip angle, are conducted by three independent hydraulic actuators, respectively actuators no. 1, no. 2 and no. 3 as shown in Figure 4.7.2, controlled by servo valves. The vertical displacement imposed through actuator no 1 can alternatively be used to apply vertical load to the tire in a range of 0 to 1500 kg. In this case, a control system is used for the close loop control of the relation between vertical deflection of a tire and pressure given by the actuator, with an error of 1 kg.



University of Moratuwa, Sri Lanka.  
Electronic Theses & Dissertations  
[www.lib.mrt.ac.lk](http://www.lib.mrt.ac.lk)

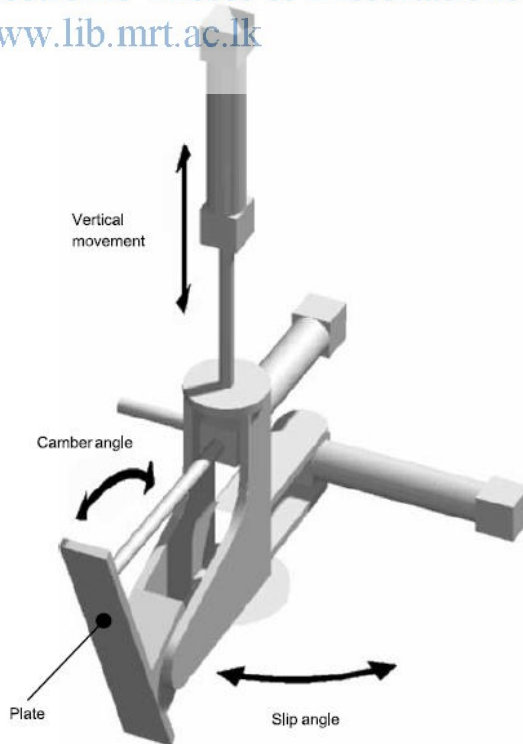


Figure 4.7.2 Central mechanism [21].

The hydraulic equipment also provides the necessary pressure to the caliper of the braking system to act on the disc, as can be observed in Figure 4.7.3. The braking pressure is controlled by a proportional pressure control valve.



Figure 4.7.3 Three dimensional sensor and braking system [21].

This system consists of a 0.8 mm thick close-loop steel belt placed over two drums, one of which is powered by an A/C motor, and supported by a hydrodynamic flat water bearing located between the drums, all mounted on a high stiffness steel frame which can displace laterally along two lineal guides to permit the simulation of lateral loads acting on the tire. The guides are fixed to a solid foundation that isolates the vibrations (see Figure. 4.7.4).



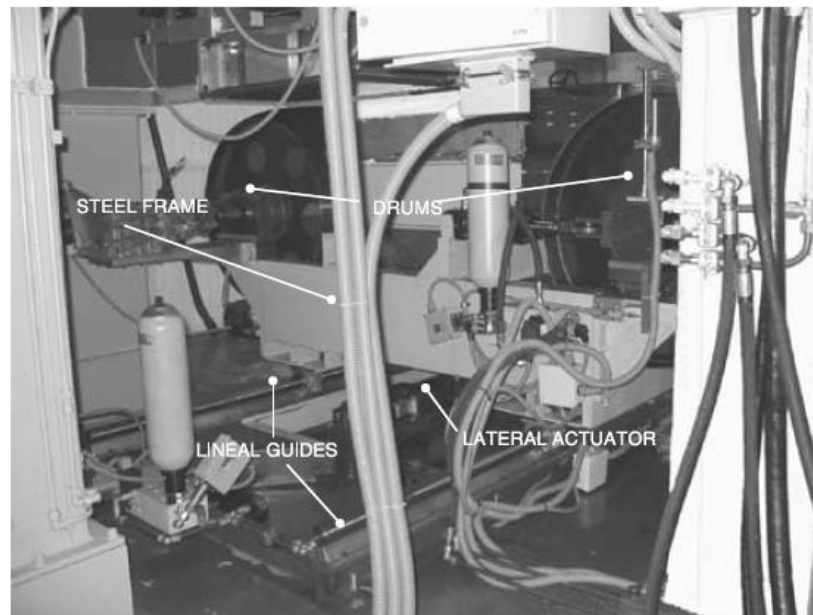


Figure 4.7.4 Lateral movement system [21].

A 30 kW A/C electric motor coupled to a gearbox, powers the driver drum supported by ball bearings. The other drum turns free. The friction between the belt and drum surfaces is responsible for the movement of the rolling surface. In order to produce enough friction force for a non-slipping traction, the belt tension has to be maintained by forcing the drums apart. Furthermore, the position of the belt needs to be continually controlled and corrected, especially when lateral forces are applied.

For these purposes, a belt adjusting system has been designed: The shaft of the driven drum is supported by tapered roller bearings on two lineal guides, and a hydraulic actuator acts on each support in the longitudinal direction. While one makes a constant force, the other displaces the drum axle appropriately according to the signal sent to the control system by two photodiode-position sensor sets. The drums are slightly conical to favour the alignment of the belt centre line with the central sections of the drums. Due to the elevated forces acting on the tire, the tension of the belt is not sufficient to ensure a flat contact. A support surface is needed, but it may imply high friction between surfaces in movement. The hydrodynamic flat water bearing has been designed to accomplish this task at a low surface friction. It has a rigid steel operating table and, located on top of it, a 30mm

thick Teflon plate with a 50 x 50 mm mesh of  $\phi$  40 mm x 10 mm cavities, each with a  $\phi$  2 mm x 20 mm capillarity drilled on. The holes are connected to a hydraulic pump through a pipe line system. Water is pumped out of the drills, acting both as a lubricant and as a cooler. The fluid is swept off the belt using a brush and a scraper system, and is collected back into a recirculation tank where the pump is confined.

To characterise the realistic behaviour of tires and their influence in vehicle dynamics, simulation of riding conditions in a flat rolling surface is recognised as necessary. In this paper, a flat track tire testing machine developed by the IMMA group has been presented which is able to perform a variety of tests in a wide range of dynamic conditions and tire models. The different systems that compose the device have been described in detail, as well as its operating variables and control system. The test machine can perform tests in pure slip conditions, (pure slip angle, pure camber angle and pure slip ratio) as well as combined conditions (combined slip ratio, camber and slip angle). Furthermore, it is possible to simulate braking manoeuvres with antilock braking systems (ABS), making it possible to study the ABS efficiency. Its use also permits to adjust and validate the existing experimental tire models for steady and transient state conditions.



University of Moratuwa, Sri Lanka  
Electronic Theses & Dissertations  
[www.lib.mrt.ac.lk](http://www.lib.mrt.ac.lk)

#### **4.8 Abrasive wear amount estimate for 3D patterned tire utilising frictional dynamic rolling analysis**

In general, the wear performance of a tire that has been already manufactured has been traditionally evaluated either by outdoor tire wear testing along a specified wear test course or using indoor wear testing system making use of a MTS machine equipped with the control system that reproduces the actual outdoor force conditions. However, these experimental methods are impractical for the design of a new tire model satisfying the target wear performance, because the need of a number of trial tire productions and time-consuming wear tests cannot meet the design cycle times that are shortened in response to car maker requirements. In this context, a time- and cost-effective numerical technique for accurately predicting the tread wear amount is highly desired at the design stage. On the other hand, the tread wear is influenced by



many factors such as the material and structural compositions of tread, ground and loading/driving conditions, environmental conditions, and so on. This implies that the reliability of wear amount and wear depth predicted by a numerical technique is strongly dependent on how accurately these conditions are taken into consideration. Thus, the essential considerations for the reliable wear prediction are the elaborate 3D detailed modeling of the complex tire material composition and the tread pattern blocks, a suitable wear model to correlate the frictional energy dissipation and the tread wear rate, the acquirement of driving and loading conditions exerted on the tire during the actual outdoor wear test

Contrary to the evaluation reliability, the cost and time required for the outdoor wear test has been a troublesome subject to overcome. Furthermore, this dilemma becomes more serious at the design stage because a number of trial tire productions and field test are required to reach the final tire model satisfying the target wear performance. In this connection, the indoor wear testing systems are now widely adopted to reduce the test cost and time. Even though the structure may become different according to the test goal, typical indoor wear test equipment shown in Fig. 4.8.1 (a) is composed of an MTS machine and the control system for mimicking the outdoor driving conditions. The control system is operated by a set of drive files in which radial, lateral, fore/aft forces, inclination angle, velocity, and so are recorded. These conditions can be either measured directly from the actual outdoor test driving or extracted from the virtual simulation using

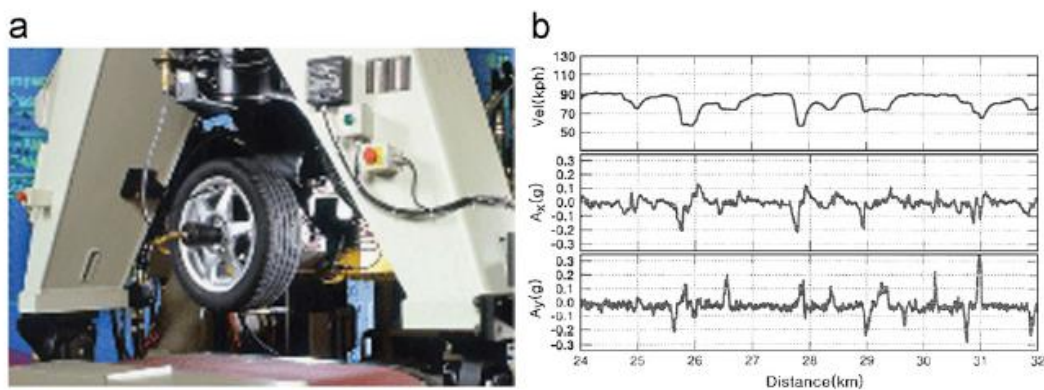


Figure 4.8.1 Illustration: (a) indoor wear test equipment and (b) acceleration history for generating drive files for the UTQG wear course [22].

Fig. 4.8.1 (b) shows an acceleration history used to generate the drive file in conjunction with the tire/vehicle model. On the other hand, another alternative technique, which is the subject of the current study, is the replacement of the actual tread abrasion by MTS machine with the wear simulation by utilizing the frictional dynamic rolling analysis. There is no doubt that this simulation-based technique would be more suitable at the design stage of a new tire model because the test time and cost can be significantly reduced. However, compared to the indoor wear test, the reliability of this technique is strongly influenced by the 3D finite element modeling of patterned tire and the correlation between the frictional dissipation and the tread wear rate.

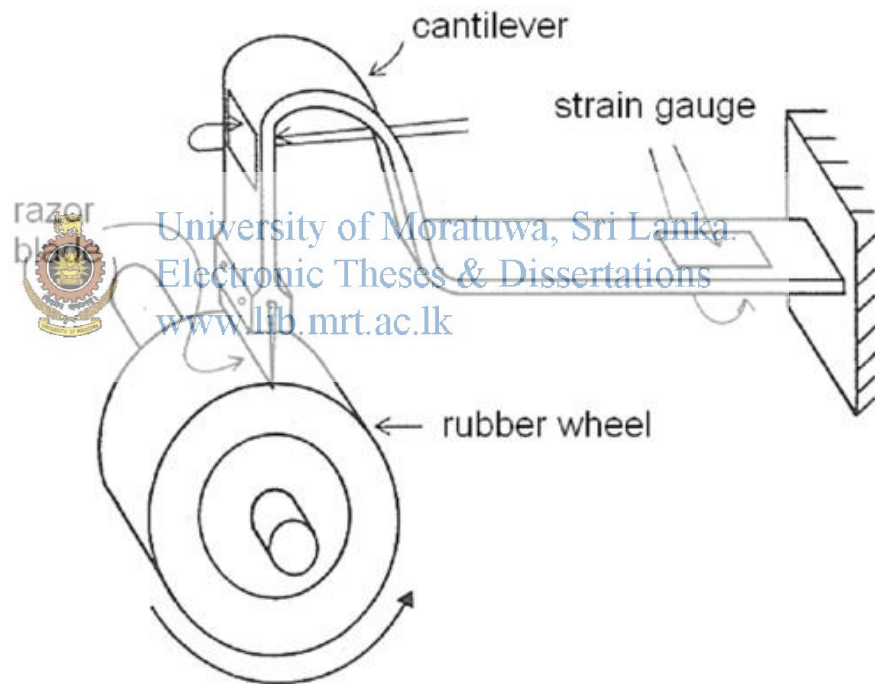


Figure 4.8.2 Schematic representation of blade abrader [22].

Figure 4.8.2 shows the apparatus used for testing the wear rate of rubber, where the width  $b$  and the outer diameter  $d$  of a rubber wheel

$$Hr \text{ (m/rev)} = C_{EA} [W_F \text{ (j/m}^2\text{)}]^m \text{-----} a$$

Where  $H_r$  is denotes the reduction in radial thickness per revolution. On the other hand,  $C_{EA}$  is called the abrasability, which is the function of rubber material and the exponent  $m$  ranges from 1.5 to 3.5 depending on the rubber material and the slip conditions [22].

### **Material modeling and mesh generation of patterned tire**

The material composition of most tires is distinguished largely into the fiber-reinforced rubber (FRR) parts and the remaining pure rubber part, as represented in Fig. 4.8.3 (a). The FRR parts of the tire model considered here are composed of a single-ply polyester carcass, two steel belt layers, and several steel bead cords. Since the FRR parts are in the highly complex structure, their material models are chosen based on the goal of the numerical simulation. In the static tire analysis, those parts are usually modeled using solid elements like rebar elements, and which does not make too much trouble in aspect of CPU time. However, in the dynamic tire analysis this full modeling requires extremely long CPU time, so the FRR parts are modeled as either composite membrane or composite shell. In the current study, two belt layers in underlying rubber matrix and a carcass layer shield with inner liner are modeled using composite shells. On the other hand, steel cords and underlying rubber matrix in the bead region are modeled as homogenized solid by utilizing the modified rule of mixtures. Fig. 4.8.3 (b) illustrates the modeling of two belt layers in the underlying rubber matrix as a single layer composed of orthotropic shells, in which individual steel wires and rubber are treated as isotropic and the equivalent composite material constants are calculated by the Halpin–Tsai formulation.

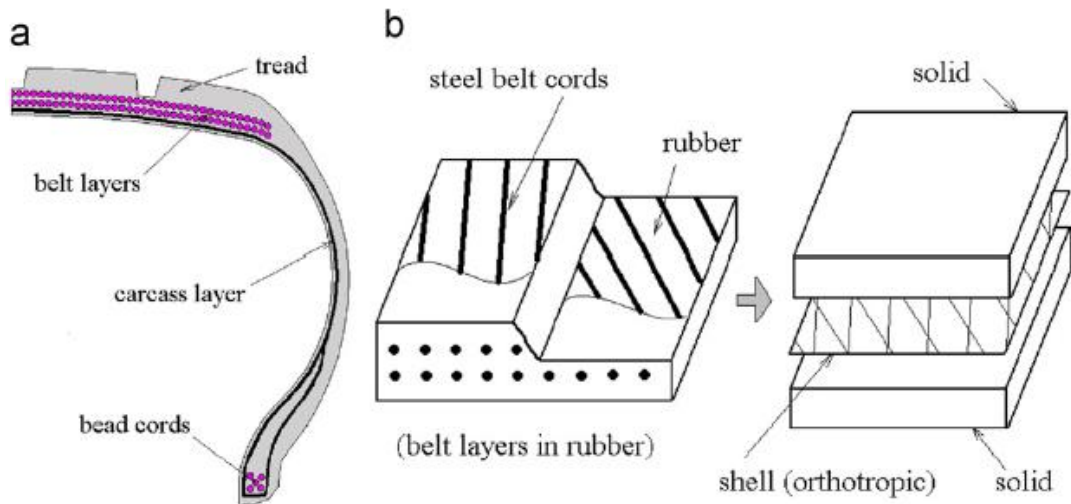


Figure 4.8.3. Material modeling of tire:(a)material composition and(b)modeling of belt layers [22].

Rubbers except for the FRR parts are modeled by the penalized first-order Mooney–Rivlin model in which the strain density function is defined by

$$W(J_1, J_2, J_3; K) = C_{10} J_1 + C_{01} J_2 + \frac{1}{2} K (J_3 - 1)^2 \quad (4.8.3)$$

Where  $J_i$  are the invariants of the Green–Lagrangian strain tensor and  $C_{10}$  and  $C_{01}$  are the rubber material constants determined from the experiment. On the other hand,  $K$  is a sort of penalty parameter controlling the rubber in compressibility. The shear modulus  $\pi$  and the bulk modulus  $k$  of rubber are related as  $2(C_{10} + C_{01}) = \pi$  and  $K = 2k$ , from which one can easily obtain the following relation for Poisson’s relation

$$V = \left[ \frac{3K}{4} (C_{10} + C_{01}) - 2 \right] / \left[ \frac{3K}{2} (C_{10} + C_{01}) + 2 \right] \quad (4.8.4)$$

It is clear that the incompressibility of rubber is asymptotically enforced as the penalty parameter approaches infinity, but the choice of  $K$  near 100 is usually recommended for the stable transient dynamic response with the reasonable time step size.

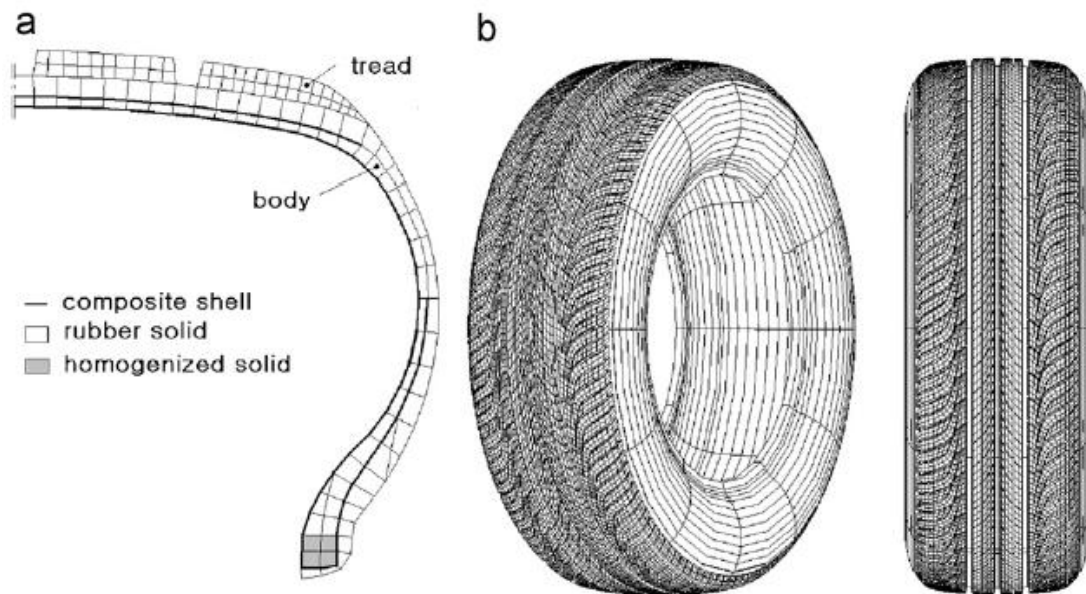


Figure 4.8.4. Tire FEM meshes:(a)2Dsectionmeshand(b)3Dpatternedmesh [22].

Fig.4.8.4(a) shows a 2D section mesh constructed according to the above-mentioned material modeling such that pure rubber solid, composite shell, and homogenized solid elements are mixed. Meanwhile, the tire body and tread meshes have different mesh densities so that both are incompatible along the common interface, and their corresponding 3D meshes are represented in Fig. 4.8.4 (b). The tread and body meshes are separately generated at the beginning and then both are to be assembled by the incompatible surface-to-surface tying algorithm supported by

ABAQUS. The 3D body mesh can be easily generated by a simple revolution of its 2D section mesh, but the generation of the 3D tread mesh is not so simple owing to the complexity of tread blocks and grooves. The 3D tread mesh shown in Fig. 4.8.4 (b) is constructed by our in-house program, which utilizes a series of basic meshing operations. The reader may refer to our previous papers for more details on the tread mesh generation and the incompatible tying algorithm.

### Estimation of tread wear amount

While driving a vehicle, tires are subjected to various dynamic forces and moments from the vehicle body and the ground, and most of them are transferred to the tire axes. Meanwhile, the loading condition of a tire depends largely on the driving



condition of a vehicle, even though other factors such as the road and environmental conditions that are characterized by the steering (or slip) angle, cruising, acceleration, and braking are also involved Fig. 4.8.5(a) shows a schematic representation of tire driving modes and the maneuvering parameters that are concerned in this study. From the tire mechanics point of view, both the lateral force and the camber angle are strongly affected by the slip angle while the wheel torque displays the remarkable change to cruising, accelerating, and braking. In this context, we classify the tire driving conditions into nine major modes: cruising, accelerating, and braking modes in the left, center, and right directions, respectively. On the other hand, the loading conditions and the occurrence frequencies of individual driving modes in an actual wear test can be either measured directly from the outdoor test driving with the special instruments or extracted from the virtual simulation by ADAMS utilizing the vehicle acceleration histogram, as illustrated in Fig. 4.8.5(b). This subject is out of the scope of the current study owing to its complexity, but the reader may refer to Kohmura et al, Stalnaker and Turner, and Zheng for the detailed explanation.

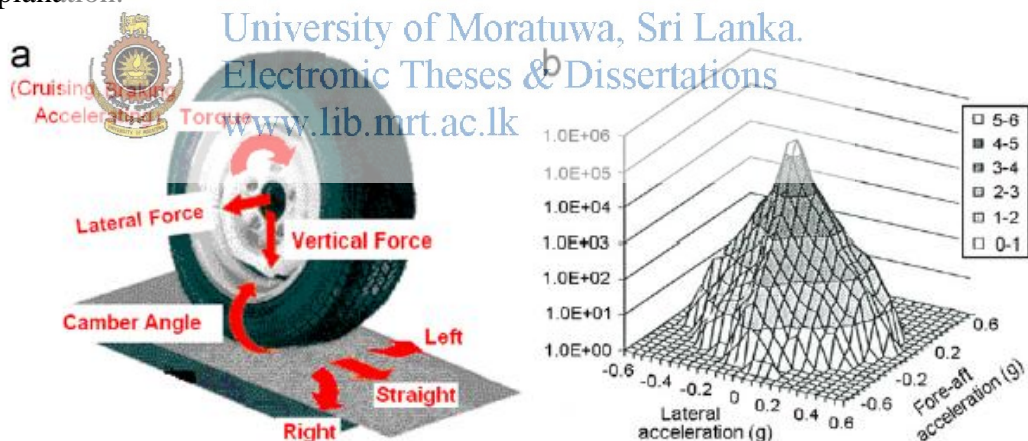


Figure 4.8.5. Representation: (a) driving modes and(b) vehicle acceleration histogram. J.R. Choetal./TribologyInternational44(2011)850–858 854 [22].

Occurrence frequencies that are available from the reference are used for the current study. For the numerical simulation to compute the frictional energy densities in above Eq. the required conditions except for usual simulation parameters are vehicle velocity, lateral and vertical forces, wheel torque, camber and slip angle, and the occurrence weight corresponding to each driving mode.

## Numerical experiments

A non-symmetric patterned tire P205/60R15 is considered for the numerical implementation of the proposed wear amount estimate, and its FEM mesh shown in Fig. 4.8.6(a) was generated with 35,363 tri-linear elements. Tread rubber blocks are manufactured with carbon-black-filled poly butadiene (PB) and the outer radius  $R$  and the width  $b$  are 313.5 and 205 mm, respectively,

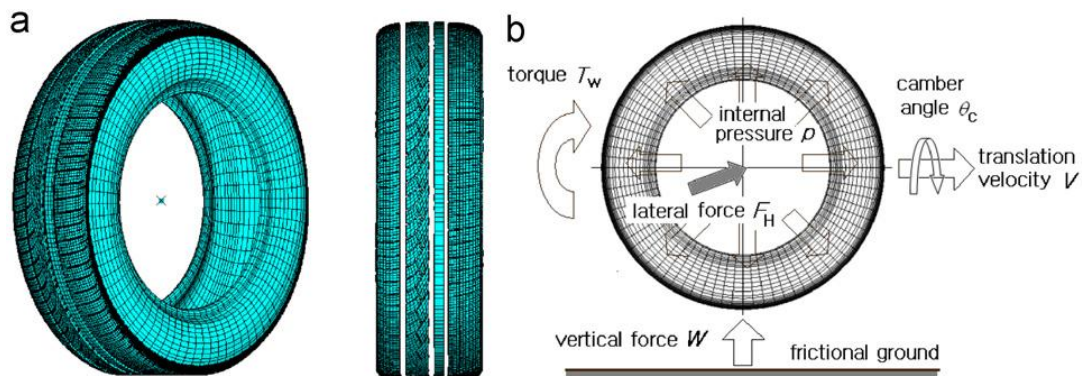


Figure 4.8.6. A simulation tire model: (a) FEM mesh and (b) specification of loading and driving conditions [22].

Detailed material properties of the model tire. The frictional dynamic rolling analyses were performed by ABAQUS/Explicit code, and individual driving modes are implemented after the tire reaches the steady-state dynamic rolling. Here, the steady-state rolling of a tire with the preset vehicle speed  $V$  is reached by a series of three sequential simulations: inflation up to the preset inflation pressure  $p$ , contact with the ground by the action of vertical force  $F_v$  and linear acceleration from rest to the desired uniform speed  $V$ .

Table 4.8.1 Loading condition and driving mode [22].

Driving mode	Vertical force, $FV$ (N)	Lateral force, $FH$ (N)	Torque, $TW$ (N m)	Camber angle, $\theta_c$ (deg.)
Left accelerating	4225.94	731.43	233.65	-0.2533
Left cruising	4474.24	671.91	32.82	-0.2506
Left braking	4576.59	842.05	-125.87	-0.4437
Center accelerating	4800.82	-205.10	275.56	0.4228
Center cruising	4942.08	-140.11	81.88	0.3380
Center braking	5232.27	-88.78	-209.03	0.1911
Right accelerating	5491.41	-1355.71	238.59	1.1481
Right cruising	5492.57	-1042.61	26.99	0.9103
Right braking	5725.42	-1178.19	-129.76	0.9358

A numerical method for predicting the tire wear amount has been introduced in this paper to reduce the troublesome time and cost that are required for outdoor and indoor wear tests of a model tire at the design stage. The frictional energy dissipation through the tire footprint contacting with the abrasive ground was computed by the frictional dynamic simulation of the 3D patterned tire model. The driving conditions in the actual outdoor wear test were classified into nine modes for which corresponding occurrence frequency weights and load conditions were specified. The frictional energy rate was correlated with the tread wear rate by a power function wear rate model that was derived on an experimental basis. As illustrated through numerical experiments, the tread wear amount can be estimated by the proposed method in extremely short period of time once the outdoor driving and load conditions are specified. Furthermore, this numerical method can be a useful tool to determine the rubber compound, the tread pattern, and the material and structural compositions in the design of a tire model, which satisfies the preset wear performance.



#### 4.9 Tread wear and footprint geometrical characters of truck bus radial tires

By virtue of the importance of the tire-ground contact issue, a lot of experiments have been performed. Applying to various techniques, equipments and methodologies, engineers and researchers have published an extensive literature and obtained some useful results. SAKAI[SAKAI E. Measurement and visualization of the contact pressure distribution of rubber disks and tires. *Tire Science and Technology*, 1995, 23(4): 238–255.] employed an optical measurement system to characterize the stress distribution between a tire and the contact surface. IVANOV, et al[IVANOV V, AUGSBURG K, SHIROKOV B. Evaluation of tire contact properties using nondestructive testing. Part 2: Experimental determination and fuzzy model of the contact patch in the static state *Journal of Friction and Wear*, 2008, 29(6): 448–454.], investigated the contact patch area of various automobile tires using visual processing in response to normal loading on the wheel and tire inflation pressure. These studies are useful to obtain the 3D tire-ground footprint area by visual processing, but accuracy pressure distribution in the contact area between tire and road cannot be acquired for instruments limited. KOEHNE, et al[KOEHNE S H, MATUTE B, MUNDL R. Evaluation of tire tread and body interactions in the contact patch. *Tire Science and Technology*, 2003, 31(3): 159–172. provided a solution to measure the contact stresses of the investigated tread blocks through precise stepwise change of tire position over the course of an experiment. By finite element analysis (FEA) method [23].

WALTERS[WALTERS M H. Uneven wear of vehicle tires. *Tire Science and Technology*, 1993, 21(4): 202–219] observed that the shear energy developed as the tire rolls through the footprint may lead to a rise in temperature and uneven wear. Adopted several parameters to describe the footprint shape, but hardly any of these conclusions have figured out the correlations between the parameters and the performance of the tires. However, these conclusions are mostly only experimental results. And few of them have considered the relationship between the results and the performance or mileage wear of the tires. This paper is concerned with the

geometrical character of the footprint, and took into consideration the relationship between the geometrical characters of the footprint shape and tire performance. The parameters used for describing the footprint shape in this paper have provided a simple method for predicting tire performance in the point of footprint [23].

In order to compare the tire-ground contact performance, three truck bus radial (TBR) tires were selected. These tires were produced by different companies yet were of similar types. These three types of tires have totally different performance during usage. The details of the three tires are shown in Table 4.9.1.

Table 4.9.1 Details of the three tires [23].

No	Type	Pressure P/kPa	Rating load m/kg
T1	385/55R22.5	830	4250
T2	385/55R22.5	830	4250
T3	385/55R22.5	830	4250

According to consumer survey and factory feedback information, among these three types of tires, T1 is the worst. For T1 tire, both sides of the shoulders always wear seriously and cracks easily appear on the bottom of the groove nearby the shoulder. While T2 tire has a better performance with little wear in the shoulder and cracks in the groove very rarely appear. And with the most praise, T3 tire shows a good performance and normal tread wear. Examples of T1 tire with cracks and shoulder wear are shown in Figure. 4.9.1. The statistics from the consumer survey and factory feedback are shown in Table 4.9.2. And the statistical results stand for the percentage of tires with cracks that appear in the bottom of the groove, tires with serious shoulder wear, and tires with both the former two problems of the three types of tires. Numbers in column “Total” are the amount of each type of tires surveyed. The main experimental instruments are the tire endurance tester, tire static load tester and Tekscan (tire pressure measurement system). The sample tire, static load tester and Tekscan are shown in Figure. 4.9.2



(a) T1 tire with cracks



(b) T1 tire with shoulder wear seriously

Figure 4.9.1 Examples of problem tires [23].



University of Moratuwa, Sri Lanka.  
Electronic Theses & Dissertations

Table 4.9.2 Statistics of feedback information [23].

No	Groove crack A%	Shoulders wear B%	Groove cracks & shoulder wear C%	Total
T1	61.9	47.6	38	21
T2	5.8	17.6	5.8	17
T3	0	5.8	0	17



Figure 4.9.2 Sample tire, tire static loaded test machine and Tekscan [23].

## Test condition and experimental procedure

To conduct this experiment, the environment in the laboratory and experimental procedure were set according to GB/T 22038-2008. During the test, the temperature in the laboratory is  $28 \pm 1$  °C and the relative humidity is 58%. The experimental steps are as follows. Step 1. Fix the sample tire on the rim and make sure the air pressure meets the standard of GB/T22038-2008. This means the air pressure is acceptable from 820 kPa to 840 kPa. Keep the tire in the lab for about 24 h and check whether the air pressure is maintained. If not, the air pressure needs to be adjusted for the test. Step 2. Remove the flashing and the rubber hair to make sure the tire surface clean, and then install the tire on the tire endurance tester. Run the tester for 10 h with the speed at 55 km/h, 80% of the maximum speed, and with the load at 1 700 kg, and 40% of the rating load, to relax the tire inner stress. Step 3. Take off the tire from the endurance tester and install the tire on the tire static load tester. Then debug the Tekscan system and carry on the test when the temperature of the tire and the temperature of the surroundings are approximate. Step 4. Record the data of the test.



University of Moratuwa, Sri Lanka.

Electronic Theses & Dissertations

[www.lib.mrt.ac.lk](http://www.lib.mrt.ac.lk)

Figure 4.9.3 indicates that the contact area coefficients of the three tires increase a little with the higher loads. When the load approaches the rating load, the contact area coefficient of T1 and T2 tires tend to be equal (both are 0.85) while the T3 tire, with the larger contact area coefficient, is greater (0.9). In the loading process, the contact area coefficients of the three tires first increase at a high speed then remain almost unchanged until the end [23].

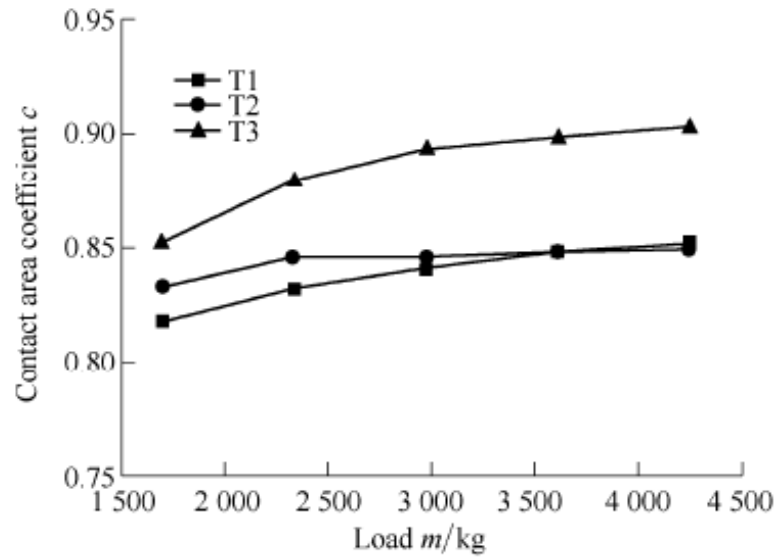


Figure 4.9.3 Load vs. contact area coefficient [23].

The illustration of Figure 4.9.4 points out that the tread contact length of the three tires increase with the load almost linearly and the T3 tire has the smallest increasing speed among the three tires

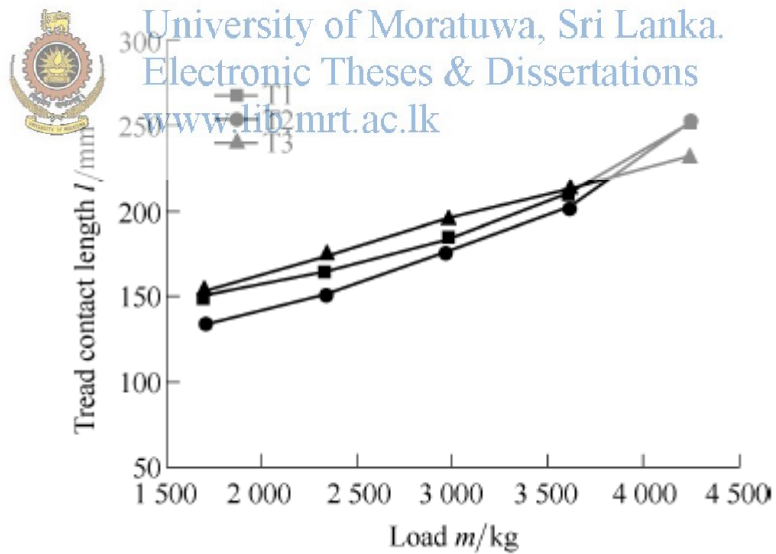


Figure 4.9.4 Load vs. tread contact length [23].

The conclusion of this research listed bellow,

- (1) The results indicate that the size of the contact area or footprint area has little correlations with the tread wear. But the ratio between contact area and footprint

area, which is the contact area coefficient, shows that a greater contact area coefficient means a more average wear of the tire.

(2) The tread contact length obviously changes with the load while the tread contact width changes very little. An analysis of the coefficient of contact illustrates that a greater and steady coefficient of contact results in a better wear performance of the tread.

(3) The footprint-shape coefficient changing laws have a very good coincidence with the tread wear of the three types of tires. The T1 tire has the largest footprint-shape coefficient and the worst tread wear performance. The tread always wears seriously and cracks often appear on the bottom of the groove. The T3 tire has the smallest footprint-shape coefficient and the best tread wear performance.

(4) This experimental study on the correlations between the tread fatigue failure and the footprint geometrical characters of TBR tires has provided several useful conclusions and a simple way of predicting the tire performance at the point of footprint. This can be useful for the tire factories to improve their tire structure designs. This paper is mainly concerning the relationship between the tread wear and the footprint of TBR tires, more work is needed to determine whether these conclusions can be applied to other types of tires. Also, taking into account of the tire working conditions as well as the road texture, is also needed in future work. [23]



## CHAPTER 5

### 5. TYRE FIELD TESTIG RESULTS

#### 5.1 Tyre test in-house under observation

- This test was conducted under 100% supervision which was travelling on tar road and 8 hours per day this forklift was manufactured in Taiwan under brand name of Tai Lift capacity of this was 2.5 tone, test speed was 10 km/h. Bellow listed collected data

Table 5.1 In-house field test analyze data

NO	Serial No	Tyre size	Brand	Weight	Tread Weight/Kg	Tread batch no	Density of Tread	Maximum Center T°C
1	A111100858	7.00-12	GS-STD	44.95	18.95	426	1.172	92
2	A111100863	7.00-12	GS-STD	44.95	18.95	427	1.172	106.5
5	A111103191	6.00-9	GS-STD	25.85	10.75	725	1.163	70.8
6	A111103193	6.00-9	GS-STD	25.04	10.37	725	1.163	74

Serial No	Abrasion loss	OD/mm	Width/mm	Tread depth up to 60J at start	Tread depth up to 60J at Finished	Final tyre weight/Kg
A111100858	171	644.4	156.7	46.05	43.1	44
A111100863	196.9	644.2	152	46.45	40.9	44
A111103191	191.81	518.9	131.3	38.4	32.6	25.25
A111103193	210.02	518.5	130.4	40.75	35.5	24.9

Serial No	Loss per/mm <sup>3</sup>	Predicted Life in 1500Kg/hr	Predicted Life in 2500Kg/hr
A111100858	2.95	1561.0	936.6
A111100863	5.55	836.9	502.2
A111103191	5.8	662.1	397.2
A111103193	5.25	776.2	465.7



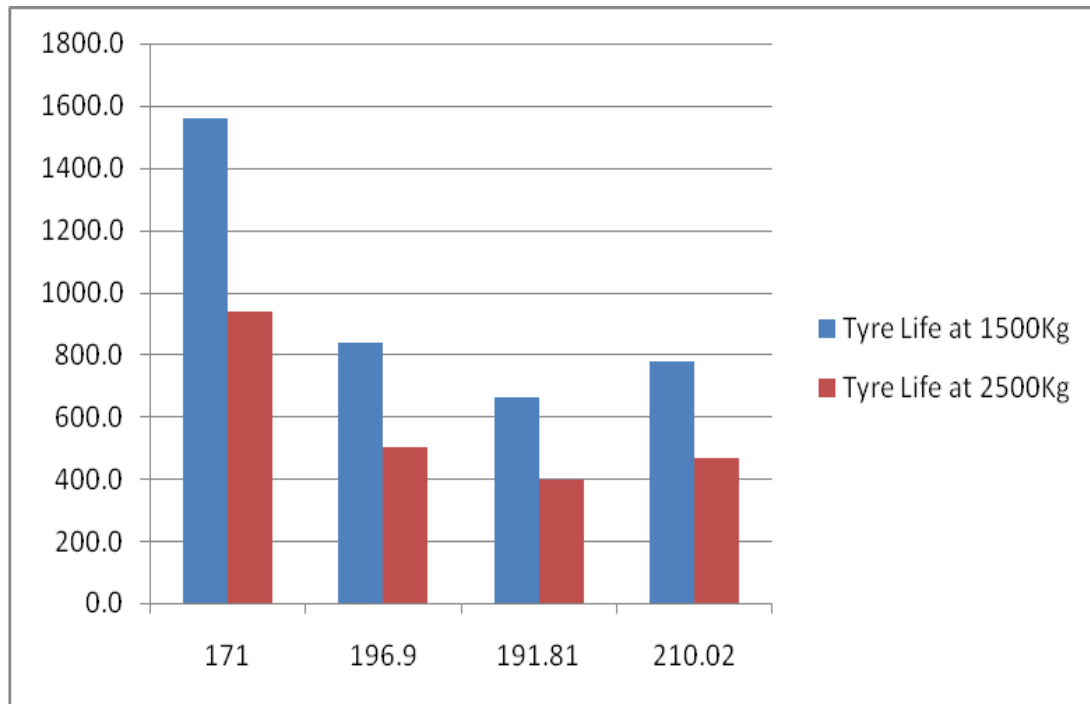


Figure 5.1 Tyre abrasion life base on volume loss

From this test it was identify when abrasion loss value increase tyre life time was decrease, this test conducted under Standard of BS-903 DIN53516 ISO-4649 GB/T 9867 SATRA-TM174 JIS-K6264 from graph 5.1 it can be identify when abrasion loss is 171 mm<sup>2</sup> (Abrasion loss = weight loss of sample (mg) x 200 / (specific gravity x weight loss of reference sample) the life time of tyre 1561 hours when same forklift if increase load up to 2500 kg then same abrasion value decrease its life time up to 936 hours.

## 5.2 Tyre test at outside under random observation

Few places were selected and sample tyres were send for testing in each location summary discussed bellow.

- Ace cargo: flow type is tar, average running speed is 15-20 km/h, and basically used Nissan and Komatsu forklifts
- Ashok Steel: flow is concrete with steel particle, average running speed is 10km/h forklift brand is TCL and Toyota,



- GRI: this is Global rubber industry flow type is concrete, average running speed is 15 km/h forklift brand is TaiLift
- Rhino: Flow type is tar, average running speed is 30-40 km/h, and forklift brand is Mitsubishi.

Altogether 158 tyres were tested in different location, the Rhino factory used for test front wheel tyres only because they suspect their suspension goes down when used all four tyres, other test area used all four tyres for testing,

- Ace cargo 8 tyres,
- Ashok steel 22 tyres
- Global rubber industry 70 tyres,
- Rhino 58 tyres

Each size working hours with brands listed bellow,

Table 5.2 test results against tyre brand and running hours

Tyre Brand and running hours	Tyre size					Grand Total	
	16x6-8	200x50-10	6.00-9	6.50-10	7.00-12		8.15-15
Ecomega PM 2071.2			4				4
Running			2				2
Excalibure					4	6	10
1845.6					2		2
1918						1	1
1968.2						2	2
Running					2	3	5
Globe Star	2		18	12	18	32	82
820						2	2
1191.3				1			1
1330						1	1
1417						1	1
1659						2	2
1754.8			1				1
1791.3				1		1	2
1807.9			1				1
1840						1	1
1864						1	1
1891.3						1	1

Tyre Brand and running hours	Tyre size						Grand Total
	16x6-8	200x50-10	6.00-9	6.50-10	7.00-12	8.15-15	
Ecomega PM			4				4
1987.7				2			2
1992.3						1	1
2040			1				1
2106						1	1
2117						1	1
2707.9			1		2		3
NA			2		4		6
Running	2		11	8	12	18	51
Magnum-Solideal			1			2	3
1473.2						1	1
NA			1				1
Running						1	1
Peakmaster			5		8	16	29
1714.1					1		1
1911.8						2	2
1914.1			1				1
1948.6					1		1
1958			1				1
1987.7						1	1
2014.1					1		1
2043						1	1
2048.6					1		1
2087						2	2
NA			1				1
Running			2		4	10	16
The Performer		2	2		4	2	10
1892.3						1	1
Running		2	2		4	1	9
Ultimate PM				4		16	20
1987.7						1	1
3059.4						2	2
3473.2						1	1
3874						1	1
3876						1	1
Running				4		10	14
Grand Total	2	2	30	16	34	74	158

From table 5.2 it can be identify same tyre brand had different running hours when tyre sizes are changed maximum running hour reported in Ultimate tyre that value is 3473.2 hours, minimum is Globe Star reported that as 820 hours this was more related to used of tyre construction and its tread compound. Addition to that from the location it can be identify different location had different running hours maximum running hour reported in Rhino factory the tyre size is 8.15-15 and running hours is 3876, minimum also reported in same factory for same tyre size that as 820 hours the main reason for that was two tread compounds even though same tyre size if used same compound also give different results as 6.00-9 at GRI and Ashok steel that is maximum reports at GRI was 2707.9 hours and Ashok steel as 1942.7 hours because very aggressive surface was available at Ashok steel but in GRI it was old concrete road.

### 5.3 Tyre drum testing results

Table 5.5 Drum testing tyre results for 18x7-8

NO:	TYRE SIZE	TYRE construction	TYRE Brads	Rolling Resistance (N)	Rolling Resistance Coefficient (x1000)	RUN TIME (min)	RADIAL DEFLECTION PERCENTAGE @ 100% LOAD	ABRASION LOSS OF TYRE (mm <sup>3</sup> )
01	18X7-8 CLIP	3-stage	SOFTY - GUMASOL (EU-RETEC)	203	126.17	121	18.1	103.21
02	18X7-8 CLIP	3-stage	CONTINENTAL - SC 20 (GERMANY)	165	102.55	134	18.5	106.87
03	18X7-8 CLIP	3-stage	BERGOUIGNAN ELITE XP	234	145.43	156	17.3	104.87
04	18X7-8 CLIP	3-stage	MAGNUM SOLIDEAL	208	129.27	102	16.4	91.71
05	18X7-8 CLIP	3-stage	PEAKMASTER	210	125.00	119	19.5	125
06	18X7-8 CLIP	3-stage	ULTIMATE PM	135	83.90	167	17	102.4
07	18X7-8 CLIP	3-stage	ECOMEGA PM	215	130.00	105	19	140
08	18X7-8 CLIP	3-stage	EXCALIBURE	220	155.00	105	22	145

NO:	TYRE SIZE	Tyre construction	TYRE Brads	Rolling Resistance (N)	Rolling Resistance Coefficient (x1000)	RUN TIME (min)	RADIAL DEFLECTION PERCENTAGE @ 100% LOAD	ABRASION LOSS OF TYRE (mm <sup>3</sup> )
09	18X7-8 CLIP	3-stage	GLOBE STAR	225	162.00	107	20	145
10	18X7-8 CLIP	2-stage	THE PERFORMER	290	180.00	85	20	145

One tyre size that is 18x7-8 was tested for rolling resistance and run time for different brands under same load 1609 kg and speed is 16 km/h that is when internal temperature of tyre increase more than 100 °C the run time was completed because after that tyre cannot run and it possible to blast. This is important understand because even though tyre should not completely wear which can not be used further if run time was low.



University of Moratuwa, Sri Lanka.  
 Electronic Theses & Dissertations  
[www.lib.mrt.ac.lk](http://www.lib.mrt.ac.lk)

## CHAPTER 6

### 6. DESIGN

#### 6.1 Design Tree

Principle problem-PP

PP1: Wrong prediction of tyre life time from abrasion standard DIN53516

PP2: Actual tyre testing takes more time and more money during different territory

Dependant problem- DP

DP1: Not availability of suitable tyre abrasion testing equipment according to correct load, speed and surface

DP2: Existing equipment cannot change type of abrasion.

DP3: During field testing it's difficult to maintain speed and environment as constant.

Secondary problem- SP

SP1: Equipments are expensive

SP2: Solid tyre testing machine are rare to find



University of Moratuwa, Sri Lanka.  
Electronic Theses & Dissertations  
[www.lib.mrt.ac.lk](http://www.lib.mrt.ac.lk)

Alternative solution set,

S1PP1: Buy new machine that suitable for test abrasion

S2PP1: Develop exiting machine to get required testing

S3PP1: Design new machine to get required testing.

S1PP2: Develop field testing process,

S1DP1: Design new machine which including speed load and surface,

S1DP2: Develop exiting machine with possible changes of type of abrasion

S2DP2: Develop new machine with required change of type of abrasion

S1DP3: Develop field testing facility with possibility of changing parameters

S1SP1: Develop economical machine available in market to required facility

S2SP1: Develop new machine economically for required facility,

S1SP2: Developed exiting machine

S2SP2: Developed new machine.

There are 24 solution set available from design tree if it is considered algorithm for this case,

S1PP1 → S1PP2 → S1DP1 → S1DP2 → S1DP3 → S1SP1 → S1SP2

S1PP1 → S1PP2 → S1DP1 → S1DP2 → S1DP3 → S1SP1 → S2SP2

S1PP1 → S1PP2 → S1DP1 → S1DP2 → S1DP3 → S2SP1 → S1SP2

S1PP1 → S1PP2 → S1DP1 → S1DP2 → S1DP3 → S2SP1 → S2SP2

S3PP1 → S1PP2 → S1DP1 → S2DP2 → S1DP3 → S2SP1 → S1SP2

S3PP1 → S1PP2 → S1DP1 → S2DP2 → S1DP3 → S2SP1 → S2SP2



University of Moratuwa, Sri Lanka.

Electronic Theses & Dissertations

www.lib.mrt.ac.lk

Now let's see the compatibility of these solutions as set,

1. S1PP1, S2PP1, S3PP1 and S1PP2 are independent solutions therefore combination of each are obviously unsuitable,
2. S1PP1 and S2PP1 are not compatible with S1DP1 and S2DP2
3. S1PP1 and S3PP1 are not compatible with S2DP2
4. S1PP1, S2PP1, S3PP1 obviously unsuitable with S1DP3
5. S3PP1 is not compatible with S1SP1 and S1SP2
6. S1PP1 and S2PP1 are not compatible with S2SP1 and S2SP2

Then admissible solution sets are listed below

1. S1PP1 → S2PP1 → S1DP2 → S1SP1 → S1SP2

Existing machine are capable of measure rolling resistance, heat build-up and run time of tyre although abrasion of tyres are unable to measure from that but some research papers were founded they have developed by using abrasive paper [5], [7] and abrasion mix falling between tyre and rotary drum

[8], [9] approximate capital cost for basic test machine is start from LKR 10 million

2. S3PP1 → S1DP1 → S2DP2 → S2SP1 → S2SP2

From this research is focus on the development of abrasion surface as required with maintaining other testing facility as heat build –up and run time as economical as possible,

3. S1PP2 → S1DP3

This is the test that most factories currently practicing in Sri Lanka that is if required to test tyre against concrete flow make required arrangement in forklift and run more than 3 or 4 month to get results, the results obtain from this test is accurate although its related with time and preparation of deferent territory, initial investment is only for buying forklift but per tyre test cost is high compare with in-house testing due to land preparation, load balancing, etc. From this it is limited to test range of tyre due to forklift capacity if need to increase testing range need to buy another forklift, this is out door test therefore sudden environment changes are effected to test results.

## 6.2 Design requirements

S3PP1 → S1DP1 → S2DP2 → S2SP1 → S2SP2

Base on this selected design variables are defined;

There are different methods available to incorporate the conveyor speed factor into the apparatus, for example, chain drives [24], [25], belt drives [26], rollers [27] and drums [5]. Out of these, a chain drive was selected to enable controlling of slipping, bear high loads and carry abrasion material with easy maintenance. In order to simulate the load, a hydraulic system [19] or a pneumatic system [28] could be selected. A hydraulic system was selected to enable the maintenance of a high load safely. Literature suggests to use relative velocity between the surfaces [18] to



include abrasion as a feature in the apparatus. However, keeping one surface (i.e either the tyre or the rubbing surface against tyre) stationary [5] would induce material loss from tyres while also increasing the surface temperature. Both open [3] and closed [5] environments are used for tyre testing. A closed type environment where the environment can be artificially controlled is suggested for the apparatus. Rotational speed can be changed using a DC motor as in tyre endurance testing machines (e.g. RC-TE-M1 model) [19] or an AC motor [30]. Since DC motor speed controlling can be performed more accurately, this method was used to create rotational speed. In order to apply the load, hydraulic piston type [19] or pneumatic piston type [27] actuators can be used. Out of these, hydraulic piston type was selected to enable high loads and accuracy. Sand paper [5], abrasion mixture [8], mixture filled boxes [25] are the common methods used to induce abrasion. Method of mixture filled boxes was selected to enable incorporation of different surface roughness values. In order to accommodate varying temperature, an air conditioner [19] and to encompass humidity variation, a water spray with a heater [20] were selected.



### 6.3 Design features

The main envisaged advantage of the suggested system is the flexibility it has to change the working surface according to required specifications, and to have it with minimal loss of worn off particles of testing surface for the tyres to obtain an accurate estimation of material loss. Thus, the apparatus is capable of withstanding a 3.2 tone load with maximum tyre outer diameter of 750 mm and maximum tyre width of 250 mm preferable for testing. Tyre circumferential speed and accuracy are respectively 0~40 km/h and  $\pm 1$  km/h. In order to obtain the necessary conditions for the tyre testing apparatus, the following options were selected. For speed control, a DC motor coupled to a chain drive; for load adjustment, used hydraulic system; to induce abrasion mixture filled boxes used and abrasion of running tyre take place due to relative velocity difference; and to change the environmental conditions used an air conditioner with water spray in a closed environment were the methods selected based on review of alternatives.



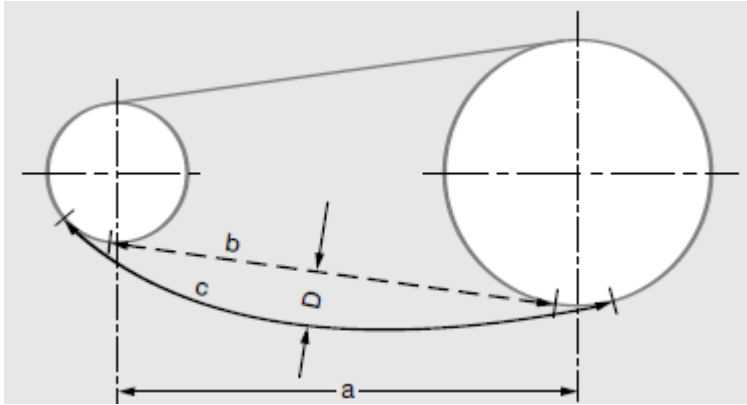


Figure 6.1 Chain and sprocket [33].

Chain sagging

$$D = \frac{\sqrt{3c^2 - 3a^2}}{4} \quad [34]$$

If 2% wear elongation is allowed, then

$$\begin{aligned} \text{Chain length} &= \text{pitch} \times \text{number of link} \quad [34] \\ &= 17.7 \times 421 \\ &= 7451.7 \text{ mm} \end{aligned}$$

$$\begin{aligned} \text{Chain length with 2\% elongation} &= 7451.7 \times 2\% \\ &= 149.03 \text{ mm} \end{aligned}$$

$$\begin{aligned} C &= a + \text{chain length with 2\% elongation} \quad [34] \\ &= 2507.02 + 149.03 \\ &= 2656.05 \text{ mm} \end{aligned}$$

$$\text{Sag} \quad D = \frac{\sqrt{3 \times 2659.05^2 - 3 \times 2507.02^2}}{4}$$

$$= 383.75 \text{ mm}$$

### Determining the tractive force, [33]

$$\begin{aligned}\text{Tractive force } F &= \text{Friction coefficient} \times \text{Vertical load} \times 9.81 \\ &= 0.12 \times 4880 \times 9.81 \\ &= 5745 \text{ N}\end{aligned}$$

16 B – 1 with 5,900 N admissible tractive to be adequate.

### Determining the vertical roller loading [35]

Considering a total 40 kg/abrasion box weight and there are 42 sets used then total weight is 1680 kg and width of box is 181 mm

$$\begin{aligned}\text{Number of rollers } n &= I (\text{contact length}) / p (\text{pitch}) \\ &= 181/25.4 \\ &= 7.12\end{aligned}$$

Although it contact two rollers and there used four chains then this should be 8 one roller 16B-1 can bear 70 kg therefore selection is within range.

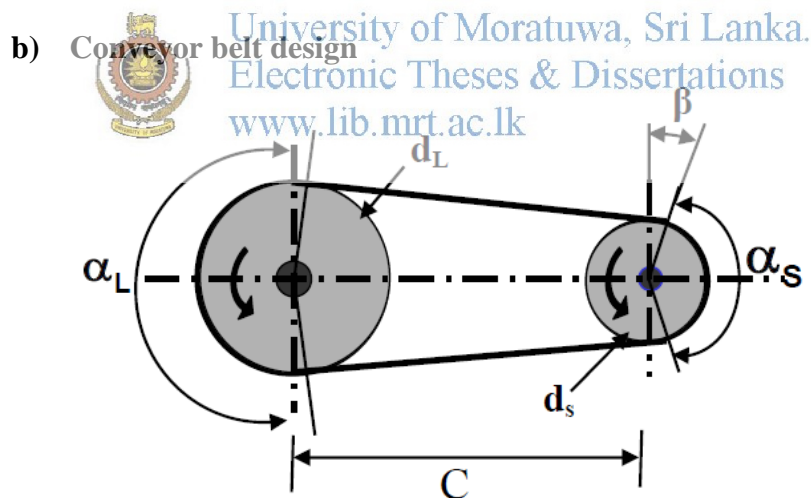


Figure 6.2 conveyor belt [36]

$$\begin{aligned}\text{Required approximate power } p &= (T_1 - T_2) \times V \\ &= 18,000 \times 2 = 36 \text{ kW}\end{aligned}$$

Power from Electric Motor is 40 kW

Selected large diameter of pulley is 500 mm DIN 2211 [37]

And small pulley diameter is 250 mm DIN 2211 [37]

Large pulley RPM =  $8 * 60 / 2\pi = 80$  rpm

Small pulley RPM =  $16 * 60 / 2\pi = 160$  rpm

Loading Factor  $c_2 = 1.4$

Design Power  $P_B = 40 \times 1.4 = 56$  kW

Therefore selected belt profile is SPC DIN 2215 [37]

Drive center distance a,

$a > 0.7$  (diameter of large pulley + diameter of small pulley)

$a < 2$  (diameter of large pulley + diameter of small pulley)

$525 < a < 1400$  therefore 1200mm is preferable,

Datum length of V-belt  $L_{dth}$

$$\begin{aligned} L_{dth} &= 2a + 1.57 (d_{dg} + d_{bk}) + (d_{dg} - d_{dk})^2 / 4a \quad [37] \\ &= 2 \times 1200 + 1.57 (750) + 250^2 / (4 \times 1200) \\ &= 3590.50 \text{ mm} \end{aligned}$$

Therefore SPC 3550mm was selected.

Center distance  $a_{nm} = a - (L_{th} - L_{dst}) / 2$  [37]

$$= 1200 - (3550 - 3451.33) / 2$$

University of Moratuwa, Sri Lanka.

$$= 1179.75 \text{ mm}$$

Electronic Theses & Dissertations

Minimum allowance for adjusting center distance  $X \leq 45, Y \leq 30$  [37]

www.lib.mrt.ac.lk

Arc of contact and correction factor

$\cos \beta / 2 = (d_{dg} - d_{dk}) / 2 a_{nm}$  [37]

$$= 250 / 2 \times 1179.75$$

$$= 0.1059$$

$\beta - 171^\circ, c_1 - 1, c_3 - 0.93$  [37]

Nominal power per belt  $P_N$ , (profile SPC,  $d_{dk} - 250, i - 2, n_k - 160$  rpm)

$P_N = 25.73$  [37]

Number of belts  $z = (p \times c_2) / (P_N \times c_1 \times c_3)$

$$= 40 \times 1.4 / (25.73 \times 1 \times 0.93)$$

$$= 2.33$$

**Therefore three belts are selected.**

$$\begin{aligned} \text{Minimum static tension per belt } T &= 500 (2.04 - c_1) P_B / (c_1 \times z \times v) + k v^2 \quad [37] \\ &= 500 (2.04 - 1) \times 140 / (1 \times 6 \times 20) + 0.37 \times 400 \\ &= 754.67 \text{ N} \end{aligned}$$

$$\text{Initial installation } (754.67 \times 1.3) = 981.1 \text{ N}$$

$$\begin{aligned} \text{Minimum static shaft load} &= 2T \sin \beta / 2 \quad [37] \\ &= 754.67 \times 0.997 \times 6 \\ &= 9028.12 \text{ N} \end{aligned}$$

$$\text{Belt deflection } E_a = E L / 100 \quad [37]$$

$$\begin{aligned} L &= a_{nm} \sin \beta / 2 \\ &= 1179.75 \times 0.997 \\ &= 1176.21 \end{aligned}$$

$$\begin{aligned} E_a &= 3.2 \times 1176.21 / 100 \\ &= 37.6 \text{ mm} \end{aligned}$$

### c) Study vibration of model

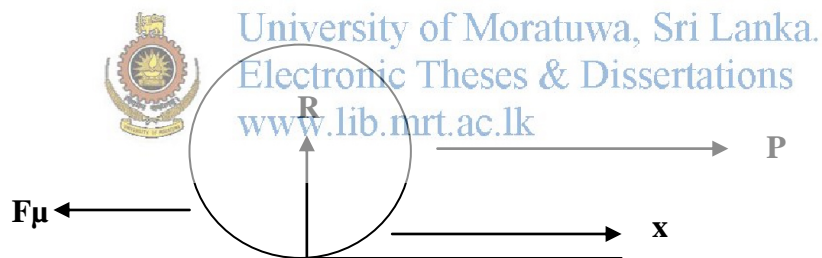


Figure 6.3 vibration model

This is categorized under force un-damped vibration that is damping coefficient identically zero and force is apply during sample frequency of time, [38], [39]

Then,

$$m\ddot{x} + kx = Ft \quad \longrightarrow \quad 6.1$$

$$Ft = F_0 \sin(\omega f t) \quad \longrightarrow \quad 6.2$$

$$\tau f = 2\pi \div \omega f \quad \text{and} \quad \omega = \sqrt{k/m}$$

From equation 1 and 5, [39]

$$X_h = x \sin \omega t + \phi \longrightarrow 6.3$$

$\omega = \sqrt{k/m}$  is natural frequency and  $x$  and  $\phi$  are constants for steady state response,

$$X_p = A_1 \sin(\omega f t) + A_2 \cos \omega f t \longrightarrow 6.4$$

$$\therefore \ddot{x}_p = -\omega f^2 (A_1 \sin(\omega f t) + A_2 \cos \omega f t) \longrightarrow 6.5$$

Complementary function  $X_h$  of this undamped system is given by,  
From equation 6.1 and 6.5,

$$(k - m\omega f^2)A_1 \sin(\omega f t) + (k - m\omega f^2)A_2 \cos \omega f t = F_0 \sin \omega f t \longrightarrow 6.6$$

$$A_1 = \frac{F_0}{k - m\omega f^2}, A_2 = 0$$

$$X_p = \frac{F_0}{k - m\omega f^2} \sin(\omega f t)$$

$$X_p = \frac{X_0}{1 - r^2} \sin(\omega f t)$$

Where,

$$X_0 = \frac{F_0}{k} \text{ and } r = \frac{\omega f}{\omega}$$

Then,



University of Moratuwa, Sri Lanka.  
Electronic Theses & Dissertations  
[www.lib.mrt.ac.lk](http://www.lib.mrt.ac.lk)

$$X_p = X_0 \beta \sin \omega f t \text{ where } \beta \text{ is magnification factor } \beta = \frac{1}{1 - r^2}$$

Complete response of the un damped single degree of freedom system under harmonic excitation, [39]



$$X_t = X_h - X_p$$

$$X_t = X \sin(\omega t + \phi) + X_o \beta \sin \omega f t \longrightarrow 6.7$$

$$\dot{X}_t = \omega X \cos(\omega t + \phi) + \omega f X_o \beta \cos \omega f t \longrightarrow 6.8$$

From equation 7 and 8,

$$X_o = X \sin \phi$$

$$\ddot{X}_o = \omega X \cos \phi + \omega f X_o \beta$$

$$\therefore X_t = A_1 \cos \omega t + A_2 \sin \omega t + X_o \beta \sin \omega f t$$

A1 and A2 are constant which can be defined by initial condition

$$A_1 = X_o$$

$$A_2 = \frac{\dot{X}_o}{\omega} - r X_o \beta$$

$$\therefore X_t = X_o \cos \omega t + \left( \frac{\dot{X}_o}{\omega} - r X_o \beta \right) \sin \omega t + X_o \beta \sin \omega f t$$

**Solution for model [39]**

$$R = 32 \text{ kN,}$$

When system running  $\mu$  is approximately equal to 0.4 then,

$$\text{Friction force } F\mu = 0.4 \times 32 \text{ kN} = 12.8 \text{ kN}$$

Power of motor 40 kW and running velocity is  $2 \text{ ms}^{-2}$

Therefore force acting P,

$$P \times 2 = 40 \times 10^3$$

$$P = 20 \text{ kN}$$

$$\text{Net force } F_o = 20 - 12.8 \text{ kN} = 7.2 \text{ kN}$$

Stiffness coefficient  $k = EA/l$  (this is effected in running change according to material used  $E = 19.17 \times 10^{10} \text{ Nm}^{-2}$  area of box along that cross section is  $39.78 \text{ mm}^2$  and length is 50 mm)

$$k = \frac{19.17 \times 10^{10} \times 39.78 \times 10^{-6}}{50 \times 10^{-3}}$$

Therefore  $k = 15 \times 10^7$  N/m

Loop length of each box running 7458 mm,

Time for one box running at each cycle =  $7458/2 = 3729$  s

Therefore frequency  $\omega f = 2\pi/3729 = 0.001685$  rads<sup>-1</sup>

Weight of box is 38 kg, then

$$\omega = \sqrt{k/m}$$

$$\omega = \sqrt{15 \times 10^7 / 38}$$

Therefore  $\omega$  is 1986.8 rads<sup>-1</sup>

Frequency ratio  $r = \omega f / \omega = 0.001685 / 1986.8 = 8.48 \times 10^{-7}$

Steady state solution is

$$Xp = Xo\beta \sin \omega ft$$

$$Xo = Fo/k = 7.2 \times 10^3 / 15 \times 10^7 = 0.48 \times 10^{-4} \text{ m}$$

$$\beta = 1 / \sqrt{1 - r^2} = 1 / \sqrt{1 - 8.47 \times 10^{-7}}$$

$$= 1.01$$

Initial condition  $Xo$  approximately equal to 2 mm  $\dot{x} = 2$  and

$$0.002 = X \sin \emptyset \longrightarrow 6.9$$

$$\dot{X}o = \omega X \cos \emptyset + \omega f Xo \beta$$

$$2 = 1986.8 X \cos \emptyset + 0.001685 \times 10^{-3} \times 2.48 \times 10^{-4} \times 1.01$$

$$X \cos \emptyset = 0.001002 \longrightarrow 6.10$$

From equation 6.9/6.10

$$\tan \phi = 1.997$$

$$\phi = 63.40^\circ$$

$$X = 0.00224$$

$$Xt = X \sin(\omega t + \phi) + Xo\beta \sin \omega t$$

$$Xt = 0.00224 \sin(1986.8t + 63.4) + 2.48 \times 10^{-4} \times 1.01 \sin 1986.8t$$

When  $t=1s$ ,

$$X(t - 1) = 0.00224 \sin(1986.8 + 63.4) + 2.48 \times 10^{-4} \times 1.01 \sin 1986.8$$

$$X(t - 1) = -21.396 \times 10^{-4}m$$

Therefore  $x$  equal to 2.14 mm

### 6.5 Detailed design

Figure 6.4 schematically shows how the forces are applied on a tyre being tested. In order to facilitate these forces, the apparatus was designed. The outward appearance of the test apparatus is shown in Figure 6.5. This offers the advantage of testing abrasion of tyres relative to different types of surfaces, i.e. concrete and tar, according to the requirement. Overall length of the machine is 3000 mm, width is 1150 mm and height is 3350 mm. The load capacity is 3.2 MT and maximum speed is 40 km/h, which are the present design specifications of solid tyres under 3T forklifts. Tyres with a maximum outer diameter 750 mm with rim diameter of 30 cm can be tested in the machine. The abrasion surface consists of 42 segments attached to a chain conveyor where each segment can be filled with concrete, tar or ceramic mixture.

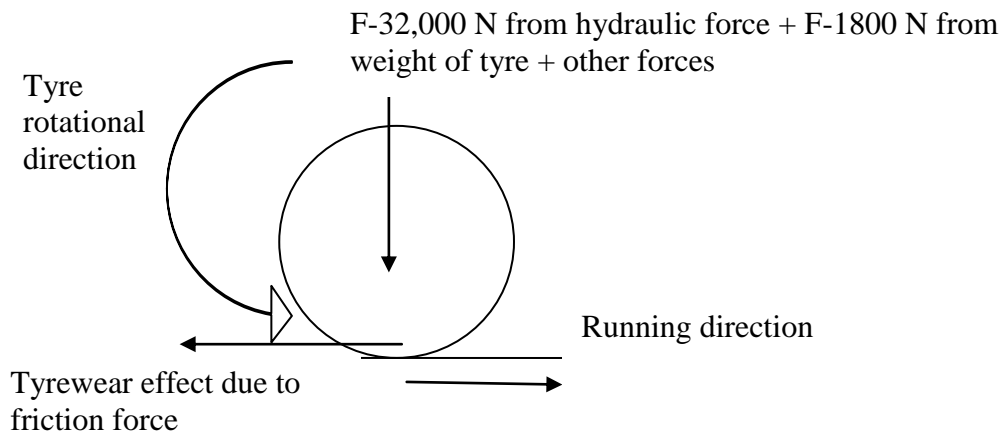


Figure 6.4: Schematic diagram of the forces acting on the tyre in the test machine



Figure 6.5 Outward appearance of the abrasion testing apparatus

The forces that are applied on the tyre during testing are in Table 6.1. The total load is applied to the surface from a hydraulic piston. Chain conveyor is driven at 1 km/h. The tyre to be tested can be rotated relative to the chain conveyor at the desired speed. The initial weight of the tyre is measured by a load cell at the installation after disconnecting the hydraulic load. Therefore, by measuring the tyre weight after testing would give the material loss due to abrasion. The apparatus is designed with

load cells and data logging capability to record the weight loss while the machine is in operation. This method provides the opportunity to measure the tyre life more accurately than by the existing methods.

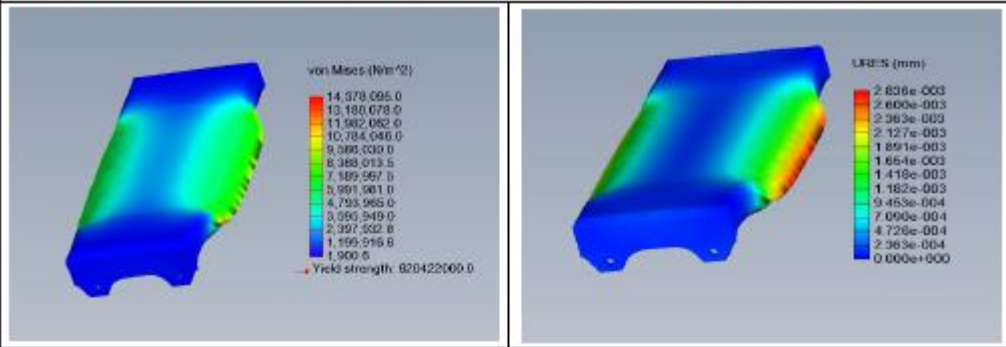
Table 6.1 Summary of parameters used for the static study

No	Parameters	Symbols	Data
1	Hydraulic load applied to running tyre	Fa	32,000 N
2	Weight applied to abrasion surfaces	Fb	1,800 N
3	Friction force	Fc	16,900 N

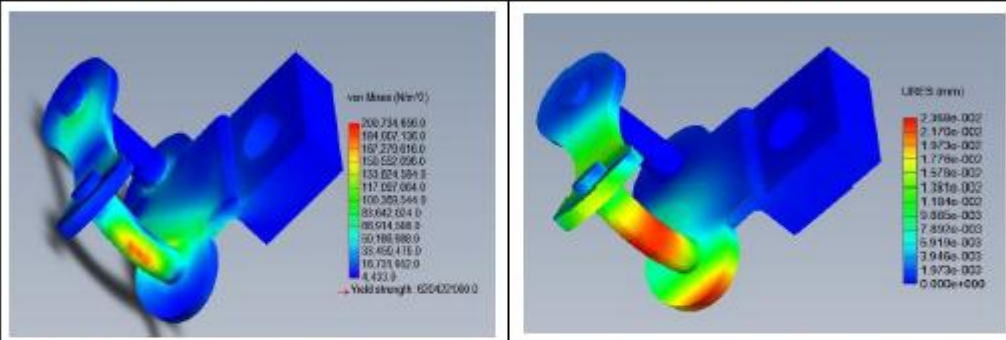
## 6.6 Design evaluation

The results of the Von Mises stress distribution and displacement obtained from the static stress analysis for each and every component in the apparatus are listed below in Figure 6.6. Colour variation indicates the magnitude of the stress and displacement in the graphical output.

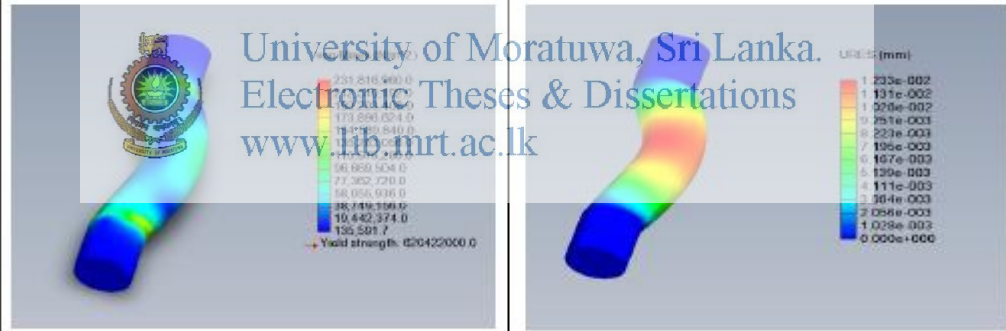
1. Part Description : Surface changing boxes, main load from tyre apply to this, Verticle load 33,800N and horizontal load 16,900N



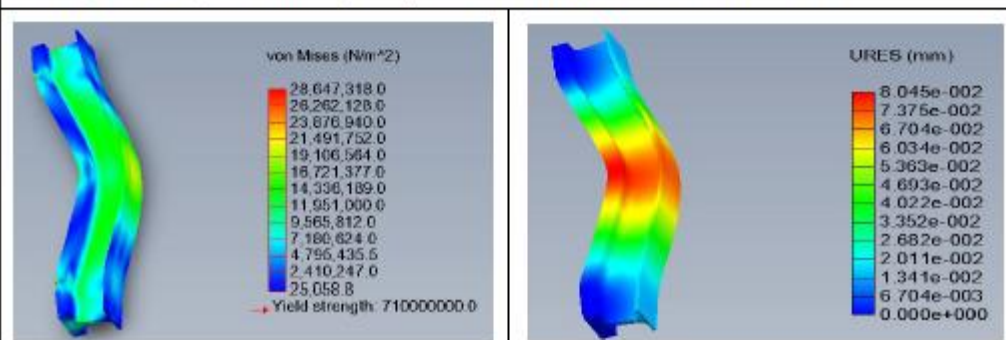
2. Part Description : Part of one chain there are four chain used for convey floor samples, Verticle load 100N and horizontal load 4,024N



3. Part Description : Connecting bar for combine two chains together with sample floor material, Verticle load 8,000N and horizontal load effect is low



4. Part Description : Main top column that hold hydraulic cylinder, Verticle load 32,000N and horizontal load effect is low



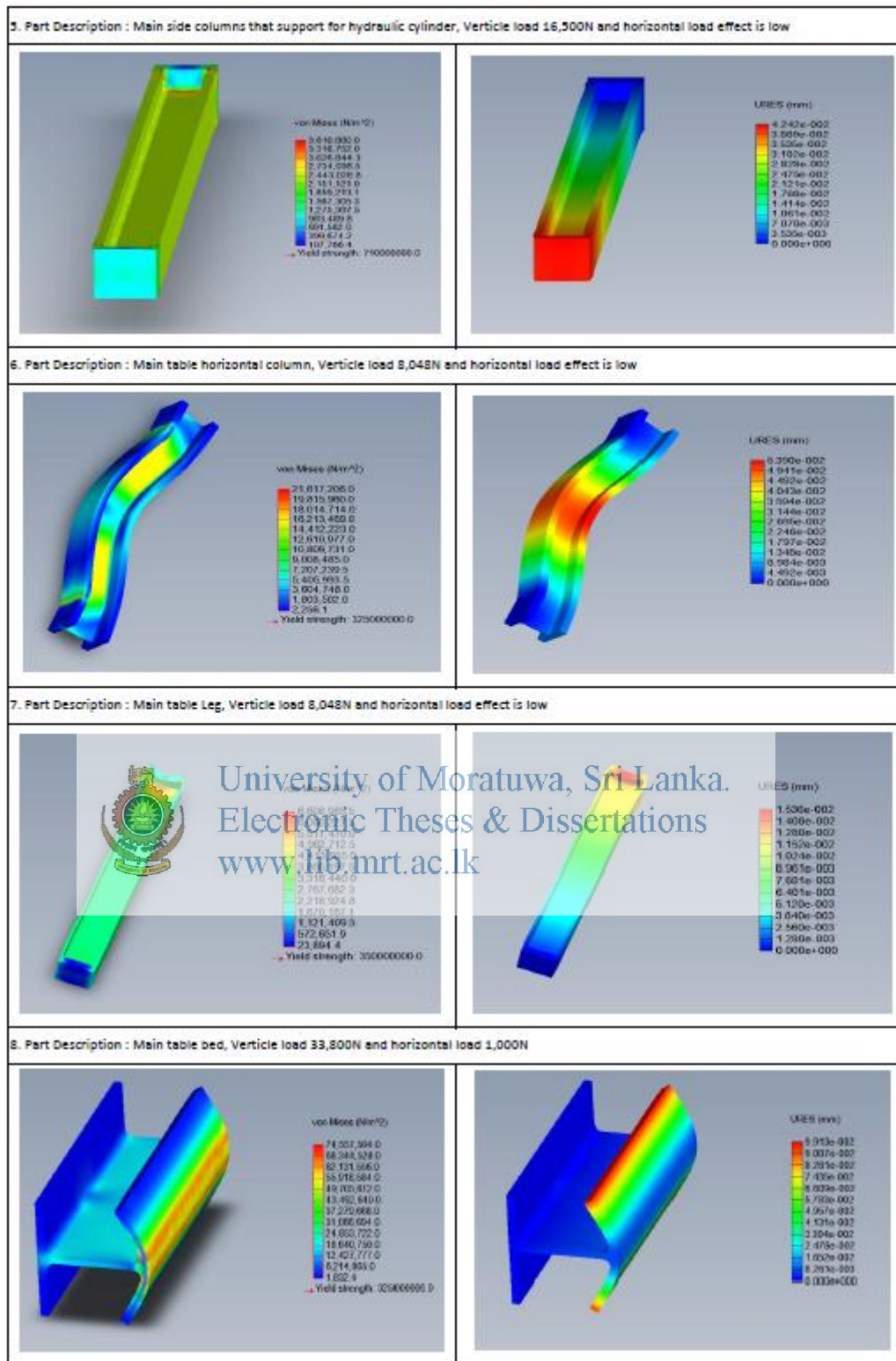


Figure 6.6 Von Misses stress and displacement distribution in machine elements



Surface changing boxes are used to carry different abrasion material to test tyre abrasion against a maximum vertical load of 33,800 N and horizontal load 16,900 N. According to the analysis in Figure 6.6, the resultant von Mises stress is 14 MN/m<sup>2</sup> and deflection is 2.53 mm. The material yield strength is 620 MN/m<sup>2</sup>.

For the driving system, four sets of chains are used. They are of grade 16B. The applied vertical load is 100 N and horizontal load is 4,024 N. Yield strength of material is 731 MN/m<sup>2</sup> resultant maximum von Mises stress is 200 MN/m<sup>2</sup> and deflection is 2.36 mm. The connecting bar is used to combine two chains together and provide support to carry abrasion material boxes. The applied vertical load is 8,000 N and horizontal load component is low. The resultant von Mises stress is 232 MN/m<sup>2</sup> and deflection is 1.23 mm while the material yield strength is 620 MN/m<sup>2</sup>.

The main top beams of the vertical structure of machine which holds the hydraulic cylinder and tyre is designed to withstand a load of 32,000 N. The horizontal load component is low. The resultant von Mises stress is 25 MN/m<sup>2</sup> and deflection is 5.22 mm. The yield strength of the selected material is 710 MN/m<sup>2</sup>.



University of Moratuwa, Sri Lanka.  
Electronic Theses & Dissertations  
[www.lib.mrt.ac.lk](http://www.lib.mrt.ac.lk)

Main side columns of the machine which hold the hydraulic cylinder and tyre will have a maximum applied vertical load of 16,500 N and horizontal load component is low. The resultant von Mises stress is 3.6 MN/m<sup>2</sup> and deflection is 4.24 mm. The yield strength of the selected material is 710 MN/m<sup>2</sup>.

The main table horizontal structural member is the element that directly needs to withstand the forces coming from abrasion boxes. The applied vertical load for each column is 8,048 N and horizontal load component is low. The resultant von Mises stress is 22 MN/m<sup>2</sup>. The deflection is 5.39 mm material when the yield strength is 325 MN/m<sup>2</sup>.

The main table vertical member this is where the main force from the tyre acts. From the abrasion boxes, there are four vertical loads of each 8,048 N acting on the structural members. The horizontal load effect is again low. The resultant von Mises

stress is  $6.61 \text{ MN/m}^2$  and deflection is  $1.53 \text{ mm}$  material yield strength is  $325 \text{ MN/m}^2$ .

Main table beds connected with roller conveyors in either side. The friction force acting on the surface is  $33,800 \text{ N}$  and its horizontal component is  $1,000 \text{ N}$ . The resultant von Mises stress is  $75 \text{ MN/m}^2$  and the deflection is  $9.91 \text{ mm}$ . The material yield strength is  $325 \text{ MN/m}^2$ .

### **6.7 Abrasion tester 2D drawing.**

Drawings were generated from SolidWork® 2011



University of Moratuwa, Sri Lanka.  
Electronic Theses & Dissertations  
[www.lib.mrt.ac.lk](http://www.lib.mrt.ac.lk)

## CHAPTER 7

### 7. PROTOTYPE TESTING

#### 7.1 Introduction of machine

Machine construction: this was low cost machine constructed by using most of waste material (as an example remove bicycle chain and hub etc, yogurt cups and wood chips) those were then assemble according to main design some critical parts were purchased, bellow illustrated two basic view of machine,



University of Moratuwa, Sri Lanka.  
Electronic Theses & Dissertations  
www.lib.mrt.ac.lk



Test piece  
Test surface  
Manual Rotation

Figure 7.2 End view of machine

## 7.2 Testing procedure

Test piece was weighted and then fixed to machine by two nuts then lower the bar according to required load that is 1 kg which was noted by test against load cell before assembly, then per minute it was rotated 15 to 20 cycle manually in here test piece was kept fixed. After 3 hrs measure temperature by IR gun after that test piece was demounted and measured its weight, after that which was repeated for next two samples. In here testing parameters were listed bellow,

- Test load approximately: 1 kg to 900 g
- Test speed approximately: 15-20 RPM this is conveyor running speed, in this case test piece is keep stationery.
- Test surface: concrete

## 7.3 Results

Three samples were tests which were manufactured in three different compounds all were conducted in same testing condition. Sample A is black tyre tread, sample B is white tyre tread, and sample C is tyre middle part (cushion) rubber, the comparison test results were listed below.



University of Moratuwa, Sri Lanka.  
Electronic Theses & Dissertations  
www.lib.mrt.ac.lk

Table 7.1 Prototype testing details

Sample	Initial weight/g	Initial Tem °C	Weight/g after 3hr	Tem °C after 3 hr
A	11.08	31	9.58	52
B	12.00	28	9.9	50
C	11.33	31	7.73	38

Table 7.2 Comparison of new test results and DIN test results.

Sample	Initial weight/g	Initial Tem °C	Weight/g after 3hr	Weight loss/Final weight	Tem °C after 3 hr	DIN 53516/DIN ISO 4649 test results
A	11.08	31	9.58	13.54	52	118
B	12	28	9.9	17.50	50	140
C	11.33	31	7.73	31.77	38	185

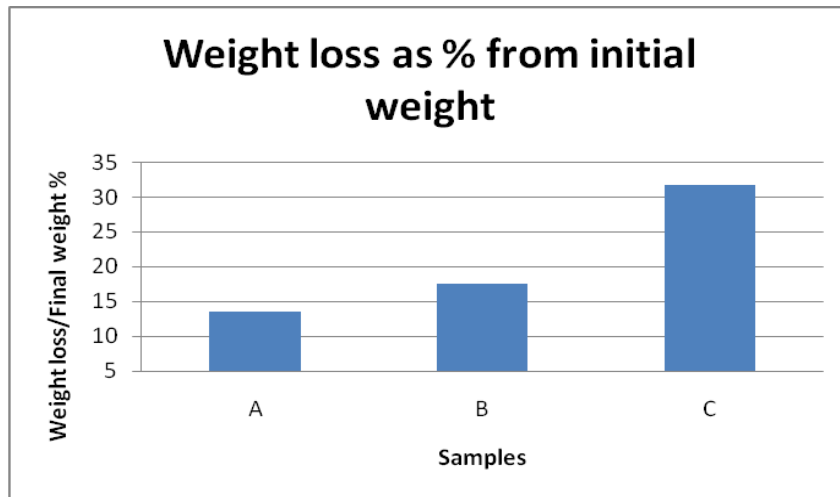


Figure 7.3 Weight loss as percentage from final weight for all samples

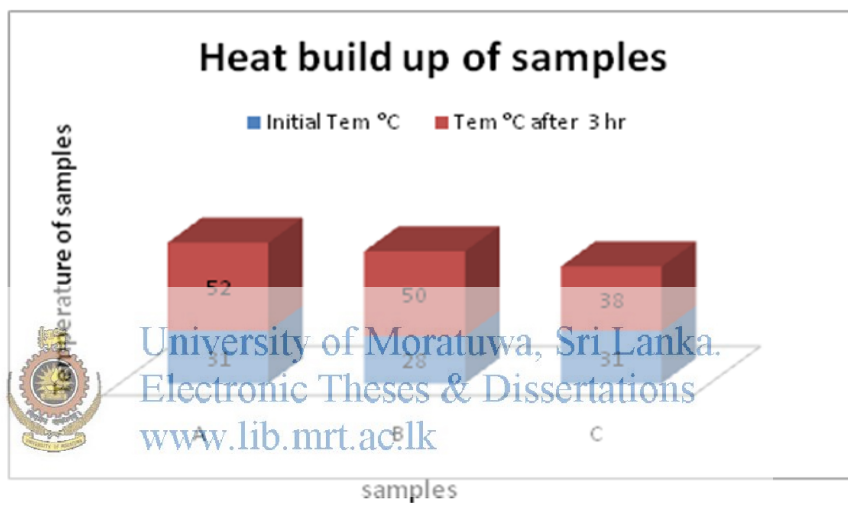


Figure 7.4 Heat build up of samples

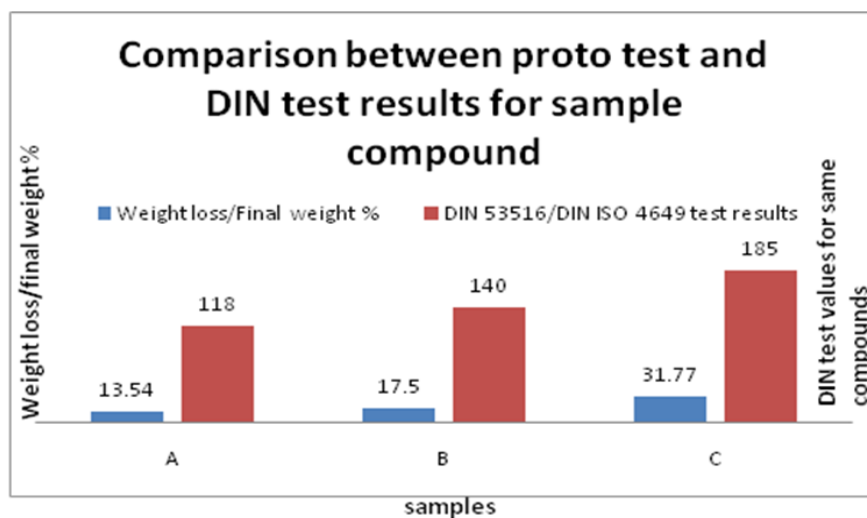


Figure 7.5 Comparison between new test and DIN test

Test surface comparison: Wear particles of rubber its mark can be seen in figure 7.5 and also wear particle of cement also visible in figure 7.7 this was very interesting because according to DIN 53516 which had high abrasion resistance cause to wear cement particle also.



Figure 7.6 Test surface of cement



Figure 7.7 Sample after test and before test





Figure 7.8 Sample A



Figure 7.9 Sample B



Figure 7.10 Sample C



#### 7.4 Analysis on abrasion of tyre compounds

Sample A was black tyre tread which has highest abrasion resistance according to DIN 53516 that was 118, the proto test abrasion surface of sample A can be compare with other two samples by figure 7.6 and its surface can be study by figure 7.7 in this sample material loss is 1.5 g after 3 hours that was lowest therefore this results is comply with DIN 53516 results,

Sample B was white tyre tread which has moderate abrasion resistance according to DIN 53516 that was 140, the proto test abrasion surface of this can be study by figure 7.8 in this sample material loss is 2.1 g after 3 hours that was also comply with DIN 53516, in graphical representation of figure 7.3 which was clearly indicate. The white tyre compounds were basically manufacture by using Titanium dioxide and black tyre tread compound consist different particle size of carbon the presence of carbon with agglomerate and particle size make completely pack that is one reason for increase abrasion resistance black tread when compare with white tread compound.

Sample C was solid tyre middle compound which used to induce cushioning effect of tyre, which had lowest abrasion resistance according to DIN 53516 that was 185, the proto test abrasion surface of this can be study by figure 7.9 in this sample material loss is 3.6 g after 3 hours this also comply with DIN 53516, the comparison between new test and DIN test is represent in figure 7.4. The important property of middle compound is low heat buildup because during running of tyre its get heated if temperature reach to 100 °C tyre will bust and get melted (observed results from drum testing machine refer table 5.5), the proto test heat buildup represent in figure 7.3.

## CHAPTER 8

### 8. DISCUSSION

To determine tyre life, a novel test apparatus was designed. The design is capable of subjecting a tyre to variable rotational speeds, loads and abrasive surfaces. The test apparatus was designed to also test the tyres in different weather conditions, such as temperature and humidity so that it could mimic the environmental conditions in which the tyres are being used.

In ductile engineering materials, von Mises found that, even though no principal stress exceeds the yield stress, it is possible for yielding to result from a combination of stresses. The von Mises criterion is a formula for combining these 3 stresses into an equivalent stress, which is then compared to the yield stress of the material. Yield stress is a known property of the isotropic material, and is usually considered to be the 1D yield stress. Design parts are evaluated according to Von Mises stress distribution and displacement each part were subjected to its maximum loads and show capability of structure, this structure is mainly design for world fast moving sizes, which are manufactured in Sri Lanka. It aligns with the tyre sizes that are in high demand, e.g. 18x7-8, 6.00-9, 6.50-10, 200/50-10, 23x9-10 and 7.00-12.



University of Moratuwa, Sri Lanka  
Electronic Theses & Dissertations  
[www.lib.mrt.ac.lk](http://www.lib.mrt.ac.lk)

Proto testing was carried out for study and evaluate design feature and design method for that prepare three test sample and carry out proto testing in equal test parameters that is conveyor speed 15-20 RPM, test load 1-0.9 kg and test piece keep stationery obtain results were comply with DIN 53516 standard which was represent in figure 7.4 abrasion resistance of sample A is higher than other two samples C is lowest that is which should give cushioning effect only because this is used in middle part of solid tyres although sample C give lowest final temperature that is mean low heat buildup basically solid tyre does not available inside air then during operation its get heated due to load, speed, running surface, environment, this test give valid results for heat build up test as well that was test by drum testing machine.

A comparison between existing testing machines with the proposed testing machine is listed below

- 1 Running speed: in propose testing machine maximum speed is 40 km/h that comply with [10],[11]. Existing machine in the market depend on supplier although on average it is around 120 km/h [19].
- 2 Working load: in propose testing maximum 3.2 MT that comply with [10],[11]. Existing machine depend on supplier although it is around 10 MT [19].
- 3 Knurling method: in propose testing variable abrasion surface can be selected that comply with [10],[11]. Existing machine limited to one surface [5],[7] or pouring a mixture rather than using a surface [8],[9] those were also some research only should not be commercialized used only bonded abrasion paper against running tyre.
- 4 Working environment: in propose testing artificially can be change heat and humidity comply with [10],[11]. Existing machine also possible to change heat and humidity as required [20].



University of Moratuwa, Sri Lanka.  
Electronic Theses & Dissertations  
[www.lib.mrt.ac.lk](http://www.lib.mrt.ac.lk)

It would be useful in practice to find a quick test of wear, which could be carried out on small samples. Developing a new test machine, which has the primary facility of matching the running surface to actual running surface conditions, would also catalyse the rapid development in tyre wear research.

## 9. CONCLUSION AND FUTURE WORK

The design of the abrasion testing machine presented in this paper is capable of evaluating tyre abrasion accurately based on selected relevant running surfaces. This method is suitable for studying tyre abrasion properties in the absence of an actual vehicle. The apparatus is helpful for early diagnosis of defects, providing information on wear performance of tyres, and reducing expenditure on outdoor tests. conducted proto test had proved wearing of samples give equal results when compare with DIN 53516 standard, also this proto test proved heat buildup of samples when compare with drum test results for that can be refer table 5.5 that is heat buildup is directly related to run time of tyre because when temperature reach to 120 °C tyre will bust even tread is fully available.

In order to advance this concept to the next stage of development, several topics should be further investigated. The machine needs to be designed and tested for its performance and design modifications need to be carried out based on such analysis.


Aesthetic and ergonomics aspects need to be addressed to improve tyre mounting and demounting. Increasing the working load and speed, in order to accommodate more types of tyres such as excavator tyres also can be interesting topics that could be studied.



## 10. REFERENCE

- [1] G. Heinrich and M. Klüppel, "Rubber friction, tread deformation and tire traction," *Wear*, vol. 265, pp. 1052–1060, 2008.
- [2] B. Rodgers and W. Waddell, *Tire Engineering*, Fourth Edi. Elsevier Inc., 2013.
- [3] X. Yang, *Road Load Analysis Techniques in Automotive Engineering*. Elsevier Inc., 2012.
- [4] E. Saibel and C. Tsai, "TIRE WEAR MODEL," 1969.
- [5] E. F. Knuth, D. O. Stalnaker, and J. L. Turner, "Advances in Indoor Tire Tread Wear Simulation," no. 724, 2014.
- [6] C. Liang and G. Wang, "Study on Tire-ground Mechanical-characters of TBR Tires," pp. 5–8, 2011.
- [7] K. Tao, Y. Feng, and F. Tian, "Design and movement simulation of the loading mechanism in high-speed tire testing machine," in *2010 International Conference on Mechanic Automation and Control Engineering, MACE2010*, 2010.
- [8] Tomotsugu SAKAI, H. NAKAMURA, S. KOBAYAKAWA, and Y. OHASHI, "A Study on the Tire Wear Life Test Method," *Japan Soc. Mech. Eng.*, 1997.
- [9] D. Manas, M. Manas, M. Staněk, and V. Pata, "Wear of tyre treads," vol. 37, no. 2, pp. 538–543, 2009.
- [10] "European Tyre and Rim Technical Organisation-Standards Manual," 2015.
- [11] "Technical Data Book." Continental Aktiengesellschaft Hannover, pp. 28–41, 2007.
- [12] D. F. Moore, "Friction and wear in rubbers and tyres\*," vol. 61, pp. 273–282, 1980.
- [13] a. H. Muhr and a. D. Roberts, "Rubber abrasion and wear," *Wear*, vol. 158, pp. 213–228, 1992.
- [14] L. T.-G. Smith, K L, J.W. Hall, "Guide for Pavement Friction," *Contract. Final Rep. NCHRP Proj. 01-43*, no. February, pp. 1–65,75–91, 2009.

- [15] M. Blundell and D. Harty, "Tyre characteristics and modelling," in *The multibody system approach to vehicle dynamics*, 1992.
- [16] J. W. Hall, K. L. Smith, L. T. Glover, J. C. Wambold, T. J. Yager, and Z. Rado, "Guide for Pavement Friction," 2009.
- [17] W. B. Age, C. Bible, K. H. Iii, T. Royal, M. Ages, L. Countries, and I. Revolution, "Combustion 14.1," 1950.
- [18] "DIN\_Type\_Abrasion\_Tester\_for\_Resilient," *Haida Equipment Co., Ltd.* [Online]. Available: [https://www.haida/DIN Type Abrasion Tester.cn](https://www.haida/DIN_Type_Abrasion_Tester.cn).
- [19] T. Round chance Rubber & tyre machinery Co.Ltd, "Tyre Endurance Testing Machine (Solid tyres) model RC-TE-M1 machine operation manual."
- [20] G. J. Heydinger and P. a Grygier, "SAE TECHNICAL Measurement and Modeling of Tire Forces on a Low Coefficient Surface," *Transp. Res.*, vol. 2006, no. 724, 2012.
- [21] L. Blanca, "Vehicle System Dynamics : International Journal of Vehicle A Versatile Flat Track Tire Testing Machine," no. April 2014, pp. 37–41, 2010.
- [22] J. R. Cho, J. H. Choi, and Y. S. Kim, "Tribology International Abrasive wear amount estimate for 3D patterned tire utilizing frictional dynamic rolling analysis," *Tribology Int.*, vol. 44, no. 7–8, pp. 850–858, 2011.
- [23] L. Chen, W. Guolin, A. N. Dengfeng, and M. A. Yinwei, "Tread Wear and Footprint Geometrical Characters of Truck Bus Radial Tires," vol. 26, no. 3, pp. 506–511, 2013.
- [24] "target.pdf." [Online]. Available: [http://www.c-rproducts.com/downloads/pdfs/Industrial\\_vbelt\\_drives\\_design\\_guide.pdf](http://www.c-rproducts.com/downloads/pdfs/Industrial_vbelt_drives_design_guide.pdf).
- [25] "RUD- Cratos Unlimited Power\_(360p)." [Online]. Available: <https://www.youtube.com/watch?v=gL6S92HA-nw>.
- [26] "Industrial\_vbelt\_drives\_design\_guide.pdf." [Online]. Available: [http://www.c-rproducts.com/downloads/pdfs/Industrial\\_vbelt\\_drives\\_design\\_guide.pdf](http://www.c-rproducts.com/downloads/pdfs/Industrial_vbelt_drives_design_guide.pdf). [Accessed: 25-Jan-2015].
- [27] "PI\_2\_12\_Roller\_Kit\_Light\_EN\_web.pdf." [Online]. Available: <http://www.interroll.com/en/interroll-group/downloads/drives-rollers/drives-rollers.php>.

- [28] <https://www.myodesie.com/index.php/wiki/index/returnEntry/id/2985>,  
“INDUSTRIAL PNEUMATICS.” [Online]. Available:  
<https://www.myodesie.com/index.php/wiki/index/returnEntry/id/2985>.
- [29] R. C. Redfield and C. Sutela, “Mountain bike wheel endurance testing and modeling,” vol. 34, pp. 658–663, 2012.
- [30] A. I. Technologies., “AC Motors for Industrial Applications Applied Industrial Technologies Applied.” [Online]. Available:  
[http://www.applied.com/base.cfm?page\\_id=3045](http://www.applied.com/base.cfm?page_id=3045).
- [31] “TRANSMISSION CHAIN - SELECTION PROCEDURE.” [Online].  
Available: [www.gears.com](http://www.gears.com).
- [32] “SPROCKET ENGINEERING DATA.” [Online]. Available: [www.martinsprocket.com](http://www.martinsprocket.com).
- [33] “ROLLER CHAIN PRODUCT CATALOG.”
- [34] Rexnord, “Chain Drive Design.” [Online]. Available:  
[http://www.molenberg.nl/downloads/Chain\\_rexnord\\_Auslegung\\_Kettentrieb  
\(En\).pdf](http://www.molenberg.nl/downloads/Chain_rexnord_Auslegung_Kettentrieb_(En).pdf).
- [35] “TSUBAKIMOTO CHAIN GROUP.” [Online]. Available:  
 [http://www.tsubakimoto.jp/support/download/?code=10\\_10\\_310\\_3\\_1\\_1\\_1#10\\_10\\_310\\_3\\_1\\_1\\_1](http://www.tsubakimoto.jp/support/download/?code=10_10_310_3_1_1_1#10_10_310_3_1_1_1). [Accessed: 22-Dec-2014].  
[www.lib.mrt.ac.lk](http://www.lib.mrt.ac.lk)
- [36] I. Industry, CARLISLE Power Transmission Products, “Industrial V-Belt Drives Design Guide.”
- [37] “Technical Manual V-Belt Drives.” ARNTZ OPTIBELT GROUP GERMANY.
- [38] R. V. Dukkipati, “Mechanics of Machines,” pp. 510–560.
- [39] A. A. Shabana, *Theory of vibration*. Springer-Verlag, 1991.